II-1-3 Magnetic survey

1. Foreword

The rocks, which form earth's crust, have magnetism according to species and amount of the magnetic minerals contained in themselves. Induced magnetization, which is caused by the earth's magnetic field, and residual magnetization, which is proper to rock itself, are created by the magnetism. The magnetic field by such magnetization are very small compared to the earth's normal magnetic field, but it is possible to distingish them by deducting the earth's normal magnetic field from the measured magnetic field.

Generally, magnetic susceptibility of the igneous rocks is higher than that of the sedimentary rocks, and the acidic rocks has higher susceptibility than the basic rocks. Susceptibility is in average in the order of $10^{-4} \sim 10^{-2}$ CGS/CC with the igneous rocks, $10^{-5} \sim 10^{-4}$ CGS/CC with the metamorphic rocks and $10^{-6} \sim 10^{-5}$ CGS/CC with the sedimentary rocks.

Magnetic survey is a method to clarify geological structure and features of rock distribution, by detecting the differences of magnetism. Especially in the geothermal areas, it is expected to detect the distribution of igneous rocks including intrusive rocks, geothermal alteration zones and certain geological structure represented by faults, by this magnetic method. Also, another method based upon the Curie point law to obtain informations on the depth and the location of magmas being seated deep in the underground has been developed.

The process of the works of the magnetic survey, from the field magnetic measurement to the preparation of the final report is shown in the flow sheet (Fig. II.1.3-1).

2. Field survey

2-1 Magnetometer

The magnetometers used in the present magnetic survey are handy type Proton magnetometers made by GEOMETRICS, analogue recorder and susceptibility magnetometer. The specification is shown in the following table.

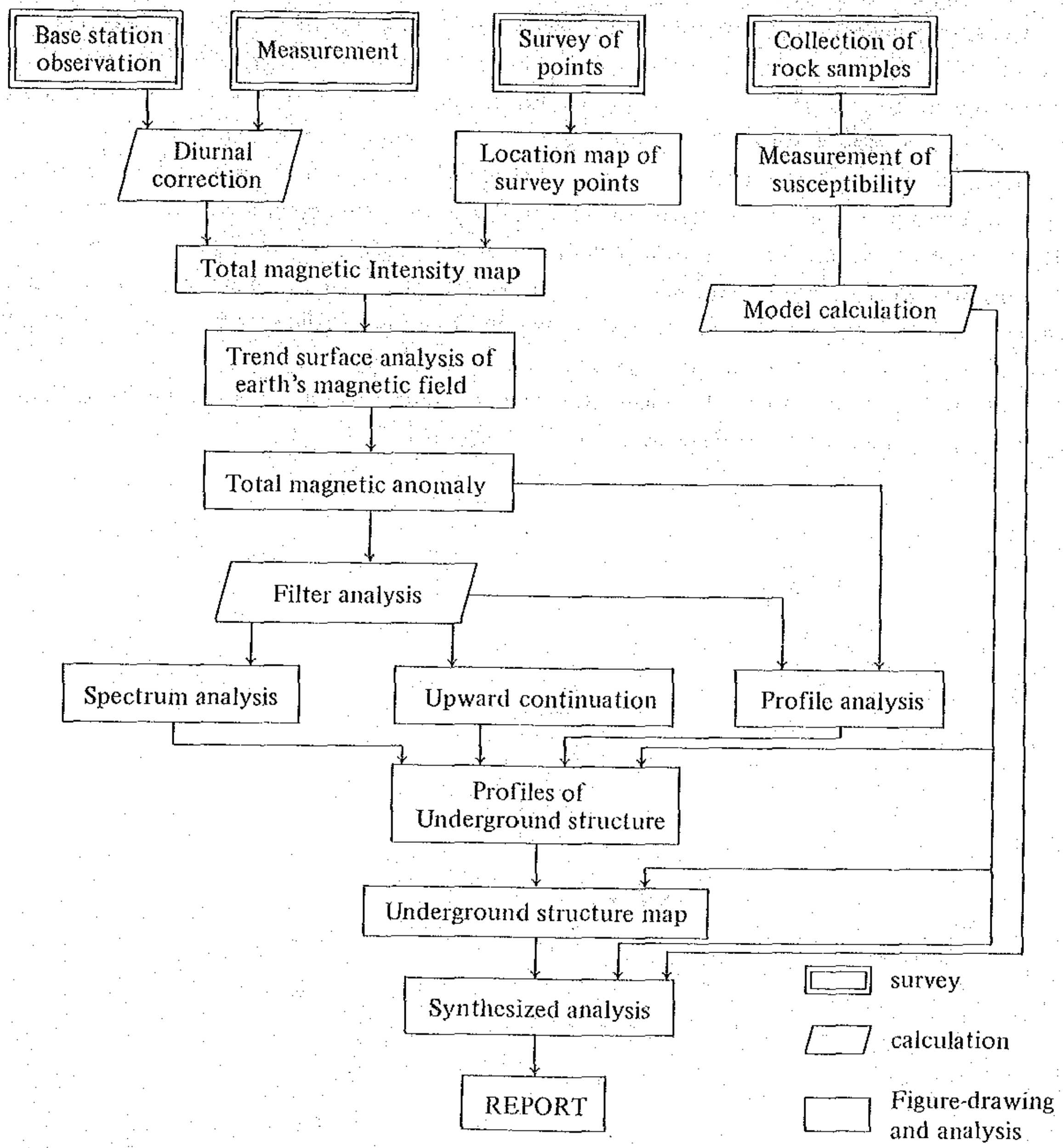

Fig. II.1.3-1 Flow chart of magnetic survey

Table II.1.3-1 Specification of magnetometer

Type	Maker	Precision
Proton magnetometer Model G-806	GEOMETRICS	Sensitivity 1 gamma
Proton magnetometer Model G-846	GEOMETRICS	Sensitivity 1 gamma
Analogue recorder Model ERP-100A	TOA DEMPA	Sensitivity 1 mV/7.5 cm
Susceptibility magnetometer Model 3101	BISON INSTRUMENT	$1 \times 10^{-5} \sim 1 \times 10^{-1}$ CGS/CC

2-2 Principle of Proton magnetometer

Proton magnetometer is often called to be unclear magnetometer. It is a magnetometer by which total magnetism can be measured, employing precession of proton or hydrogen nucleus in liguified hydrocarbon. Hydrocarbon nucleus in water or gasoline is regarded to be small magnetic dipole. Precession is generated in magnetic field and the frequency of the precession is proportional to the intensity of total magnetism T. The magnetic dipoles of hydrogen nuclei stand in a line in the magnetic field formed by temporary current in a coil. When the current is cut, hydrogen nuclei change their position to be in a row in the direction of the earth's magnetic field, and precession is generated. The precession of the magnetic dipoles can be perceived in a detecting coil by electromagnetic induction. Through the measurement of period of voltage in the coil, magnetism can be determined by the following formula.

$$T = \frac{2\pi f}{\gamma}$$

Here γ : magnetic rotation ratio
(in hydrogen nucleus 2.67513×10^{-4} sec^{-1} gauss)

The period of the precession has no relation to the direction of the detecting coil. Accordingly, Proton magnetometer is to measure intensity of total magnetic field, that is, scalar. The frequency of the precession is measured by digital counter in the precision of 1 gamma in the order of 50,000 gamma of the earth's magnetic field.

2-3 Base station and diurnal correction

Earth's magnetic field at a point varies regularly in the period of a day. Therefore, it is required to give diurnal correction to every values measured at different time of a day. In the present magnetic survey, observation of diurnal variation of the magnetic fild was carried out at the base station estabished at the rest house in the west side of the EGAT camp.

The amplitude of the diurnal variation of the magnetic field was approximately 50 gamma. No magnetic storm, which would have caused remarkable magnetic variation, was recognized.

An example of the diurnal variation of the magnetic field is shown in Fig. II.1.3-2,3.

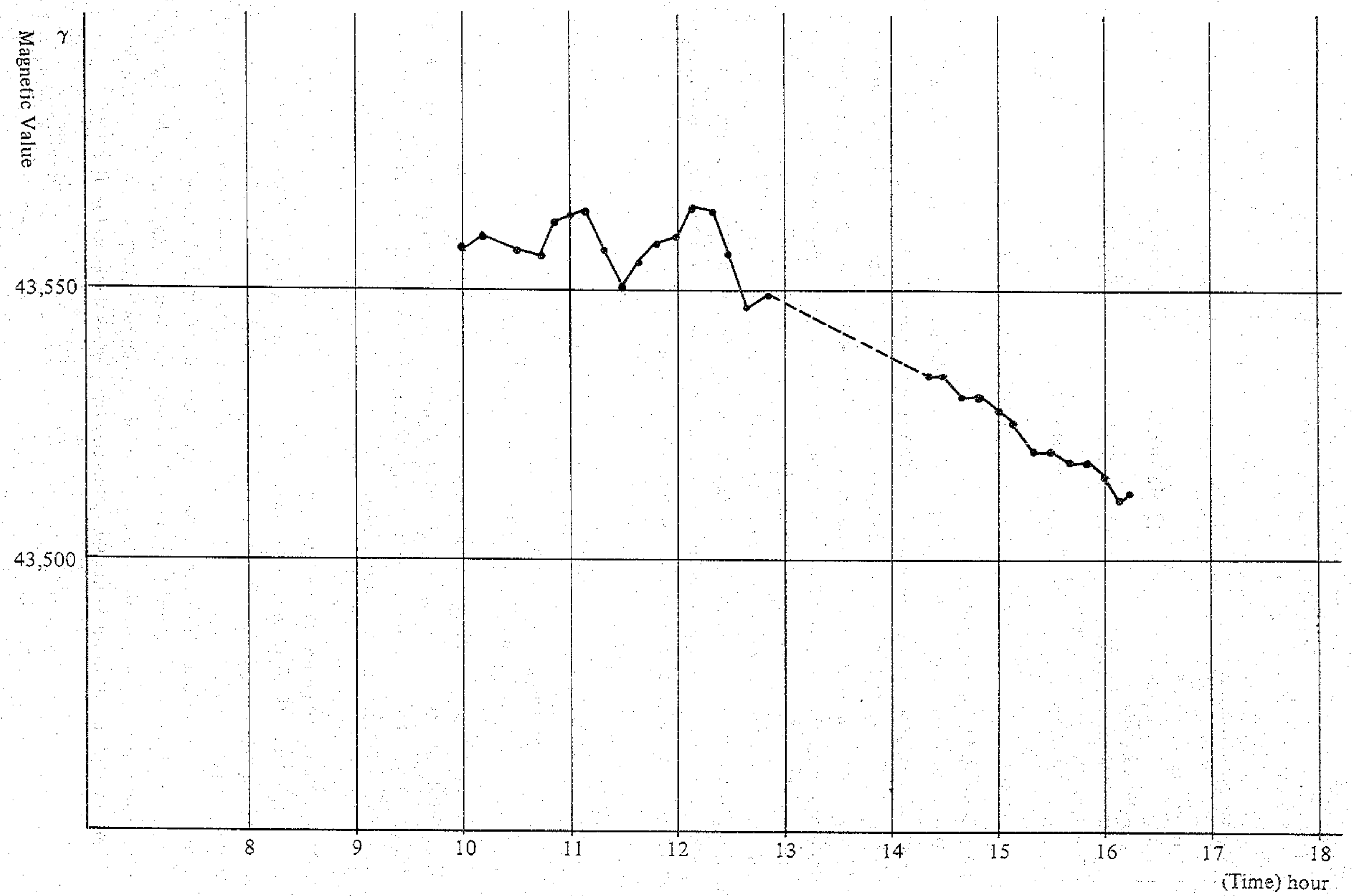

Fig. II.1.3-2 Diural variation of geomagnetic field (Date 11-10)

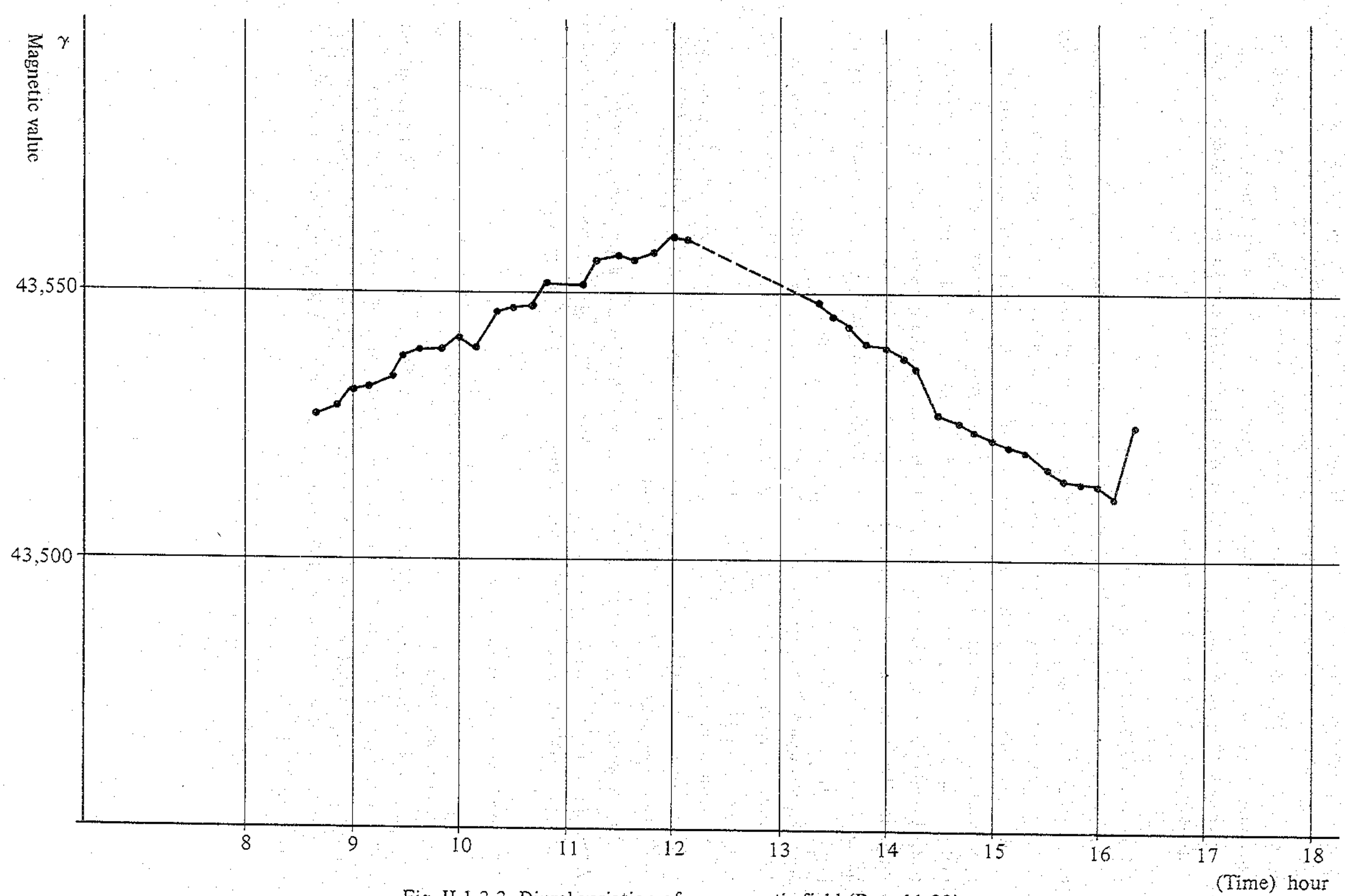

Fig. II.1.3-3 Diural variation of geomagnetic field (Date 11-23)

For the observation of the diurnal variation at the base station, Proton magnetometer Model G-806 and Analogue Recorder Model EPR-100A were employed. Observation at the base station by the Proton magnetometer Model G-846 was also carried out every time at around the beginning of the survey, for the comparative examination of the two magnetometer.

The normal magnetic value at the base station was 43,556 gamma. This magnetic value was that measured at 10°00′ on 10th of November, 1982.

2-4 Survey points and method of survey

In the central part of the surveyed area, the magnetic survey was carried out along the survey lines prepared by bush-cutting by Thailand-side counterpart (EGAT) in the central part of the surveyed area, while in the peripheral zones roads and paths were utilized for survey lines.

By the results of the geological survey completed before the magnetic survey, existence of many faults of N-S trend had been confirmed. It is general for the most effective detection of the faults of N-S trend to carry out magnetic measurement along such survey lines as to cross the faults rectangularly. However, in such low-latitude area as the present surveyed area, things are different. Where magnetic body extends in north and south direction unlimitedly, no magnetic anomaly can be created, whatever high susceptibility the magnetic body has. Magnetic anomaly occurs only in limited cases as the continuation of the magnetic body is intermittent or as the size of the magnetic body varies. In the present survey, survey lines mainly in the direction of N60°E were established with spacing of 100 to 200 meters in the central zone and of 200 to 500 meters in the peripheral zones.

The survey points were located by pegs along the survey lines. The points along the roads were surveyed with simplified transit compass and measuring tape and they were plotted on the topographical map of the scale of 1 to 10,000.

The magnetic measurement was carried out with the Proton magnetometer Model G-846. Although artificial noises are very little in the surveyed area, magnetic variation was recognized to some extent. Therefore, readings were carried out at least 5 times at a point.

2-5 Measurement of susceptibility

2-5-1 In-situ measurement

There were a few outcrops where composing rocks were not weathered so much as to permit In-situ measurement of susceptibility in the surveyed area. Therefore, the measurement of susceptibility was carried out with 84 rock samples including drill cores, after sent back to Japan.

The results of the measurement of susceptibility in the field were shown in the following table (Table II.1.3-2).

Table II.1.3-2 In-situ measurement of susceptibility

No.		Rock	Value
S-1		limestone	2×10^{-6}
S-4	68	sandstone	tr
S-5-1	50	chert	2.5×10^{-6}
S-6	14	tuff breccia	tr
S-7-1	26	andesite	3.2×10^{-6}
S-7-2	4	tuff	13×10^{-6}
S-7-3	15	tuff	2.4×10^{-6}
S-9		chert	13×10^{-6}
G-24	47	sandstone, chert	5×10^{-6}

3. Method of analysis

3-1 Diunal correction

The normal magnetic value at the base station is 43,556 gamma, the measured value at 10°00′ on 10th of November, 1982. Taking the average value of 5 readings at a point at the time of to be $\bar{R}st$ and the magnetic value at the base station at the same time to be Rbt, the diurnal correction value ΔRt and the corrected value Rs are shown as follows.

$$\Delta Rt = 43{,}556 - Rbt$$
$$Rs = \bar{R}st + \Delta Rt$$
$$= \bar{R}st + (43{,}556 - Rbt)$$

In the Table II.1.3-3, are shown the average of measured magnetic values $\bar{R}st$, the duirnal correction values ΔRt and the corrected values Rs at each of the survey points.

Table II.1.3-3 Magnetic values at every survey point (1)
(unit: γ)

Survey point	Average of measured value	Correction Duirnal value	Correction Duirnally value	Survey point	Average of measured value	Correction Duirnal value	Correction Duirnally value
No.	$\overline{R}st$	ΔRt	Rs	No.	$\overline{R}st$	ΔRt	Rs
1	43503	+28	43531	33	43549	+ 5	43554
2	504	+31	535	34	506	+ 8	514
3	491	+39	530	35	560	+13	573
4	498	+39	537	36	533	+14	547
5	504	+38	542	37	551	+16	567
6	495	+33	528	38	538	+18	556
7	512	+30	542	39	488	+20	508
8	500	+31	531	40	505	+21	526
9	499	+34	533	41	526	+22	548
10	506	+30	536	42	377	+26	403
11	521	+30	551	43	526	+22	548
12	514	+32	546	44	572	+22	594
13	513	+29	542	45	553	+16	569
14	519	+28	547	46	531	+ 6	537
15	579	+10	589	47	525	+ 4	529
16	537	+ 6	543	48	575	+ 4	579
17	533	+ 4	537	49	593	+ 4	597
18	539	0	539	50	566	0	566
19	540	+ 1	541	51	535	0	535
20	544	− 2	542	52	547	− 2	545
21	547	− 8	539	53	541	− 4	537
22	556	−10	546	54	547	−10	537
23	552	− 9	543	55	551	− 4	547
24	559	−10	549	56	540	− 8	532
25	556	−12	544	57	573	− 9	564
26	566	−17	549	58	615	−10	605
27	585	−18	567	59	575	−10	565
28	586	−17	569	60	542	− 5	537
29	576	− 7	569	61	550	− 3	547
30	564	− 4	560	62	541	− 2	539
31	562	− 2	560	63	538	+17	555
32	566	+ 1	567	64	532	+20	552

Table II.1.3-3 Magnetic values at every survey point (2)
(unit: γ)

Survey point	Average of measured value	Correction Duirnal value	Correction Duirnally value	Survey point	Average of measured value	Correction Duirnal value	Correction Duirnally value
No.	$\overline{R}st$	ΔRt	Rs	No.	$\overline{R}st$	ΔRt	Rs
65	43532	+22	43554	97	43543	+ 5	43548
66	530	+21	551	98	539	+ 6	545
67	521	+23	544	99	547	+ 3	550
68	524	+25	549	100	553	+ 5	558
69	533	+26	559	101	630	+19	649
70	528	+28	556	102	524	+21	545
71	543	+26	569	103	761	+22	783
72	550	+26	576	104	322	+22	344
73	546	+26	572	105	522	+23	545
74	556	+26	582	106	519	+24	543
75	573	+30	603	107	520	+24	544
76	570	+32	602	108	510	+25	535
77	543	+28	571	109	511	+26	537
78	516	+27	543	110	517	+26	543
79	542	+10	552	111	514	+30	544
80	533	+10	543	112	515	+31	546
81	556	+ 9	565	113	534	+29	563
82	504	+ 8	512	114	504	+32	536
83	564	+ 7	571	115	501	+32	533
84	582	+ 6	588	116	516	+31	547
85	579	+ 2	581	117	531	+33	564
86	564	+ 3	567	118	545	+32	577
87	572	− 1	571	119	529	+16	545
88	424	0	424	120	531	+15	546
89	543	0	543	121	525	+15	540
90	531	0	531	122	531	+14	545
91	550	0	550	123	526	+13	539
92	540	0	540	124	524	+11	535
93	541	0	541	125	524	+11	535
94	536	+ 3	539	126	531	+10	541
95	548	+ 4	552	127	516	+10	526
96	549	+ 3	552	128	514	+ 8	522

Table II.1.3-3 Magnetic values at every survey point (3)
(unit: γ)

Survey point	Average of measured value	Correction Duirnal value	Correction Duirnally value	Survey point	Average of measured value	Correction Duirnal value	Correction Duirnally value
No.	$\bar{R}st$	△Rt	Rs	No.	$\bar{R}st$	△Rt	Rs
129	43531	– 8	43539	161	43408	+96	43504
130	523	+ 6	529	162	412	+95	507
131	544	+ 4	548	163	459	+94	553
132	537	+ 2	539	164	445	+93	538
133	531	+ 2	533	165	443	+84	527
134	532	+ 5	537	166	457	+85	542
135	524	+ 7	531	167	460	+80	540
136	516	+ 7	523	168	451	+85	536
137	538	+ 7	545	169	461	+86	547
138	527	+ 6	533	170	478	+21	499
139	529	+ 5	534	171	540	+24	564
140	535	+ 1	536	172	503	+22	525
141	531	+ 1	532	173	513	+20	533
142	533	0	533	174	509	+19	528
143	533	0	533	175	542	+18	560
144	533	+14	547	176	511	+17	528
145	544	+16	560	177	483	+17	500
146	503	+17	520	178	508	+17	525
147	520	+18	538	179	504	+15	519
148	510	+20	530	180	508	+17	525
149	498	+20	518	181	489	+16	505
150	496	+19	515	182	489	+10	499
151	507	+21	528	183	497	+ 9	506
152	489	+23	512	184	485	+ 9	494
153	490	+24	514	185	500	+ 9	509
154	518	+25	543	186	519	+ 6	525
155	510	+26	536	187	521	+ 4	525
156	503	+28	531	188	531	+ 4	535
157	506	+29	535	189	525	– 1	524
158	425	+102	527	190	533	– 1	532
159	430	+100	530	191	537	0	537
160	433	+98	531	192	530	– 2	528

Table II.1.3-3 Magnetic values at every survey point (4)
(unit: γ)

Survey point	Average of measured value	Correction Duirnal value	Correction Duirnally value	Survey point	Average of measured value	Correction Duirnal value	Correction Duirnally value
No.	$\bar{R}$st	ΔRt	Rs	No.	$\bar{R}$st	ΔRt	Rs
193	43534	– 3	43531	225	43447	–72	43519
194	541	– 3	538	226	447	+72	519
195	520	+12	532	227	448	+72	520
196	503	+14	517	228	444	+74	518
197	481	+15	496	229	439	+78	517
198	562	+18	580	230	457	+81	538
199	507	+20	527	231	466	+85	551
200	506	+22	528	232	467	+85	552
201	504	+33	537	233	482	+79	561
202	508	+34	542	234	404	+80	484
203	492	+35	527	235	368	+81	449
204	470	+35	505	236	361	+153	514
205	487	+36	523	237	372	+150	522
206	466	+38	504	238	394	+143	537
207	484	+39	523	239	401	+130	531
208	471	+41	512	240	387	+129	516
209	484	+42	526	241	414	+127	541
210	479	+42	521	242	386	+126	512
211	444	+74	518	243	413	+121	534
212	462	+65	527	244	412	+111	523
213	441	+77	518	245	419	+135	467
214	435	+81	516	246	332	+135	467
215	460	+54	514	247	332	+135	467
216	490	+54	544	248	357	+142	499
217	441	+55	496	249	376	+143	524
218	451	+48	499	250	362	+146	528
219	472	+46	518	251	494	+35	529
220	473	+47	520	252	504	+28	532
221	478	+45	523	253	501	+29	530
222	478	+45	523	254	492	+30	522
223	447	+63	510	255	537	+31	568
224	452	+70	522	256	503	+33	533

Table II.1.3-3 Magnetic values at every survey point (5)
(unit: γ)

Survey point	Average of measured value	Correction Duirnal value	Correction Duirnally value	Survey point	Average of measured value	Correction Duirnal value	Correction Duirnally value
No.	$\bar{R}st$	ΔRt	Rs	No.	$\bar{R}st$	ΔRt	Rs
257	43498	+25	43523	289	43478	+41	43519
258	504	+24	528	290	550	+38	588
259	486	+22	508	291	502	+37	539
260	508	+19	527	292	499	+37	536
261	510	+17	527	293	498	+37	535
262	511	+15	526	294	495	+36	531
263	514	+13	527	295	492	+34	526
264	516	+11	527	296	496	+31	527
265	507	+11	518	237	504	+30	534
266	512	+12	524	298	503	+30	533
267	495	+30	525	299	467	+52	519
268	485	+31	516	300	476	+52	528
269	486	+32	518	301	467	+51	518
270	505	+30	535	302	469	+53	522
271	500	+30	530	303	466	+54	520
272	497	+35	532	304	471	+55	526
273	515	+36	551	305	460	+55	515
274	504	+37	541	306	472	+56	528
275	493	+38	531	307	462	+57	519
276	499	+40	539	308	459	+57	516
277	482	+21	503	309	454	+58	512
278	526	+19	545	310	459	+61	520
279	549	+25	574	311	464	+61	525
280	483	+35	523	312	462	+60	522
281	468	+43	511	313	458	+61	519
282	440	+46	486	314	465	+63	528
283	467	+45	512	315	458	+65	523
284	486	+47	533	316	477	+65	542
285	440	+48	488	317	469	+65	534
286	513	+46	559	318	382	+65	447
287	476	+46	522	319	346	+66	412
288	499	+46	545	320	401	+67	468

Table II.1.3-3 Magnetic values at every survey point (6)
(unit: γ)

Survey point	Average of measured value	Correction Duirnal value	Correction Duirnally value	Survey point	Average of measured value	Correction Duirnal value	Correction Duirnally value
No.	$\overline{R}$st	ΔRt	Rs	No.	$\overline{R}$st	ΔRt	Rs
321	43447	+67	43514	353	43525	+18	43543
322	466	+66	532	354	521	+17	538
323	464	+65	529	355	519	+16	535
324	514	+23	537	356	527	+16	543
325	517	+22	539	357	517	+15	532
326	518	+22	540	358	520	+14	534
327	513	+21	534	359	523	+14	537
328	514	+21	535	360	520	+14	534
329	520	+21	541	361	517	+14	531
330	509	+21	530	362	521	+13	534
331	516	+21	537	363	522	+12	534
332	516	+21	537	364	520	+12	532
333	514	+21	535	365	516	+11	527
334	496	+23	519	366	518	+11	529
335	518	+23	541	367	523	+11	534
336	512	+23	535	368	505	+ 9	514
337	508	+24	532	369	526	+ 8	534
338	504	+25	529	370	519	+ 7	526
339	549	+26	575	371	515	+ 6	521
340	491	+28	519	372	529	+ 6	535
341	512	+29	541	373	529	+ 3	532
342	521	+31	552	374	532	+ 2	534
343	505	+32	537	375	528	+ 2	530
344	504	+36	540	376	529	+ 2	531
345	395	+28	433	377	525	+ 2	527
346	527	+38	565	378	533	+ 2	535
347	503	+40	543	379	524	+ 2	526
348	483	+42	525	380	514	+ 1	515
349	499	+43	542	381	513	+ 8	521
350	520	+44	564	382	462	+ 8	470
351	583	+45	628	383	485	+ 7	492
352	523	+46	569	384	575	+ 7	582

Table II.1.3-3 Magnetic values at every survey point (7)
(unit: γ)

Survey point	Average of measured value	Correction Duirnal value	Correction Duirnally value	Survey point	Average of measured value	Correction Duirnal value	Correction Duirnally value
No.	R̄st	ΔRt	Rs	No.	R̄st	ΔRt	Rs
385	43553	+ 7	43560	417	43499	+22	43521
386	548	+ 7	555	418	489	+24	513
387	552	+ 7	559	419	506	+24	530
388	525	+ 7	532	420	523	+13	536
389	539	+ 7	546	421	533	+13	546
390	549	+ 7	556	422	522	+12	534
391	538	+ 7	545	423	520	+10	530
392	518	+ 7	525	424	537	+ 8	545
393	536	+ 7	543	425	588	+ 6	594
394	474	+ 7	481	426	533	+ 5	538
395	584	+ 8	592	427	536	+ 3	539
396	528	+ 8	536	428	527	+ 2	529
397	541	+ 7	548	429	527	– 1	526
398	536	+ 8	544	430	528	– 1	527
399	524	+ 8	532	431	534	– 1	533
400	535	+ 8	543	432	544	– 2	542
401	532	+ 9	541	433	539	– 3	536
402	511	+ 9	520	434	548	–10	538
403	526	+11	537	435	538	– 2	536
404	522	+12	534	436	550	– 4	546
405	511	+12	523	437	514	– 5	509
406	502	+11	513	438	530	– 1	529
407	453	+12	465	439	626	– 4	622
408	476	+14	497	440	542	– 3	539
409	502	+16	518	441	545	– 2	543
410	490	+17	507	442	508	0	508
411	500	+18	518	443	527	+ 2	529
412	503	+19	522	444	528	+ 3	531
413	507	+20	527	445	523	+ 4	527
414	520	+21	541	446	507	+ 3	510
415	486	+21	507	447	464	+ 2	466
416	502	+21	523	448	556	+ 2	558

Table II.1.3-3 Magnetic values at every survey point (8)
(unit: γ)

Survey point	Average of measured value	Correction Duirnal value	Correction Duirnally value	Survey point	Average of measured value	Correction Duirnal value	Correction Duirnally value
No.	R̄st	ΔRt	Rs	No.	R̄st	ΔRt	Rs
449	43528	+ 3	43531	481	43513	− 5	43508
450	528	+ 3	531	482	549	− 5	544
451	474	+ 3	477	483	515	− 5	510
452	524	+ 3	527	484	543	− 5	538
453	533	+ 3	536	485	526	− 4	522
454	535	+ 4	539	486	533	− 4	522
455	530	+ 4	534	487	515	− 3	512
456	530	+ 6	536	488	520	− 3	517
457	523	+ 7	530	489	554	− 2	552
458	520	+ 6	526	490	532	− 2	530
459	509	+12	521	491	524	− 1	523
460	504	+11	515	492	521	0	521
461	513	+10	523	493	533	0	533
462	522	+ 8	530	494	530	− 1	529
463	522	+ 8	530	495	535	− 2	533
464	523	+ 7	530	496	541	− 3	538
465	523	+ 5	528	497	542	− 4	538
466	525	+ 3	528	498	551	− 5	546
467	527	+ 2	529	499	536	− 6	530
468	521	+ 3	524	500	542	− 8	534
469	523	+ 4	527	501	533	− 9	524
470	505	+ 6	511	502	547	−14	533
471	526	+ 5	531	503	551	−12	539
472	515	+ 3	518	504	548	−11	537
473	520	+ 2	522	505	541	−10	531
474	520	+ 2	522	506	543	−10	533
475	477	− 1	478	507	540	−10	530
476	474	+ 1	475	508	483	− 9	474
477	528	− 1	527	509	542	− 9	533
478	489	− 6	483	510	540	− 9	531
479	520	− 6	514	511	535	− 9	526
480	487	− 6	481	512	540	− 9	531

Table II.1.3-3 Magnetic values at every survey point (9)

(unit: γ)

Survey point	Average of measured value	Correction Duirnal value	Correction Duirnally value	Survey point	Average of measured value	Correction Duirnal value	Correction Duirnally value
No.	$\bar{R}st$	ΔRt	Rs	No.	$\bar{R}st$	ΔRt	Rs
513	43541	− 9	43532	545	43441	+22	43463
514	539	− 9	530	546	495	+21	516
515	535	−10	525	547	492	+20	512
516	530	−11	519	548	521	+20	541
517	533	− 3	530	549	536	+20	556
518	530	+ 2	532	550	516	+19	535
519	531	+ 3	534	551	513	+19	532
520	526	+ 3	529	552	513	+18	531
521	520	+ 4	524	553	519	+18	537
522	513	+ 4	517	554	544	+16	560
523	538	+ 6	544	555	522	+10	532
524	536	+ 6	542	556	505	+10	515
525	486	+ 7	493	557	518	+10	528
526	499	+ 9	508	558	522	+10	532
527	530	+10	540	559	532	+11	543
528	503	+10	513	560	537	+11	548
529	501	+11	512	561	524	+11	535
530	522	+11	533	562	520	+10	530
531	509	+11	520	563	537	+10	547
532	556	+13	569	564	530	+ 9	539
533	515	+14	529	565	533	+ 8	541
534	497	+15	512	566	528	+ 8	536
535	511	+17	525	567	530	+ 7	537
536	486	+18	504	568	536	+ 7	543
537	551	+38	589	569	523	+ 6	529
538	309	+38	347	570	539	+ 4	543
539	571	+37	608	571	539	+ 1	540
540	271	+36	307	572	533	+ 2	535
541	215	+36	251	573	538	+ 2	540
542	445	+35	480	574	540	+ 2	542
543	522	+35	557	575	536	+ 2	538
544	467	+33	500	576	539	+ 2	541

Table II.1.3-3 Magnetic values at every survey point (10)

(unit: γ)

Survey point	Average of measured value	Correction Duirnal value	Correction Duirnally value	Survey point	Average of measured value	Correction Duirnal value	Correction Duirnally value
No.	$\bar{R}st$	ΔRt	Rs	No.	$\bar{R}st$	ΔRt	Rs
577	43543	+ 8	43551	610	43521	+ 4	43525
578	526	+ 8	534	611	530	+ 4	534
579	519	+ 9	528	612	531	+ 4	535
580	524	+ 9	533	613	532	+ 3	535
581	503	+11	514	614	525	+ 1	526
582	506	+12	518	615	525	+ 1	526
583	499	+13	512	616	540	0	540
584	507	+14	521	617	535	0	535
585	510	+15	525	618	534	0	534
586	510	+17	527	619	539	− 1	538
587	510	+18	528	620	542	− 2	540
588	498	+19	517	621	535	− 2	533
589	489	+22	511	622	537	− 3	534
590	555	+24	579	623	565	−34	531
591	487	+26	513	624	568	−36	531
592	507	+26	533	625	567	−37	530
593	557	+26	548	626	561	−28	533
594	522	+26	548	627	559	−26	533
595	511	+26	537	628	552	−24	528
596	515	+27	542	629	548	−24	524
597	502	+28	530	630	561	−24	537
598	504	+29	533	631	555	−25	530
599	554	+29	583	632	555	−25	530
600	511	+29	540	633	579	−25	554
601	487	+29	516	634	567	−26	541
602	490	+30	520	635	574	−27	547
604	533	+ 6	539	636	562	−22	540
605	529	+ 6	535	637	560	−21	539
606	527	+ 5	532	638	555	−20	535
607	524	+ 4	528	639	552	−17	535
608	528	+ 4	532	640	548	−15	533
609	540	+ 4	544	641	549	−14	535

Table II.1.3-3 Magnetic values at every survey point (11)
(unit: γ)

Survey point	Average of measured value	Correction Duirnal value	Correction Duirnally value	Survey point	Average of measured value	Correction Duirnal value	Correction Duirnally value
No.	R̄st	ΔRt	Rs	No.	R̄st	ΔRt	Rs
642	43551	−12	43539	674	43545	− 2	43543
643	550	−13	537	675	565	−10	556
644	547	−13	534	676	510	−10	500
645	554	−14	540	677	585	−11	574
646	547	−12	535	678	621	−11	610
647	543	−11	532	679	503	−11	492
648	543	− 9	534	680	550	−16	534
649	547	− 8	539	681	583	−19	564
650	543	− 7	536	682	656	−19	637
651	546	− 6	517	683	496	−18	478
652	523	− 6	517	684	505	+32	537
653	502	+26	528	685	507	+34	541
654	511	+24	535	686	504	+35	539
655	558	+22	580	687	506	+35	541
656	534	+20	554	688	504	+35	539
657	525	+19	544	689	515	+36	551
658	505	+18	523	690	505	+37	542
659	500	+16	516	691	508	+39	547
660	516	+15	531	692	494	+40	534
661	513	+15	528	693	493	+43	536
662	509	+16	525	694	498	+46	544
663	520	+ 6	526	695	490	+50	540
664	519	0	519	696	501	+54	555
665	525	− 5	520	697	488	+61	549
666	531	−11	520	698	497	+64	543
667	537	−12	525	699	488	+30	518
668	534	−11	523	700	488	+28	516
669	534	−10	524	701	502	+26	528
670	656	− 6	650	702	493	226	519
671	587	− 2	585	703	502	+25	527
672	549	+ 1	550	704	507	+24	531
673	539	+ 2	541	705	497	+23	520

Table II.1.3-3 Magnetic values at every survey point (12)
(unit: γ)

Survey point	Average of measured value	Correction Duirnal value	Correction Duirnally value	Survey point	Average of measured value	Correction Duirnal value	Correction Duirnally value
No.	$\overline{R}st$	ΔRt	Rs	No.	$\overline{R}st$	ΔRt	Rs
706	43494	+23	43517	738	43494	+45	43539
707	500	+23	523	739	494	+45	539
708	504	+23	527	740	491	+45	536
709	460	+34	494	741	490	+45	535
710	507	+33	533	742	512	+26	538
711	512	+43	544	743	509	+27	536
712	479	+32	511	744	478	+27	505
713	700	+31	731	745	526	+27	553
714	523	+30	553	746	516	+27	543
715	494	+30	524	747	490	+27	517
716	522	+31	553	748	452	+27	479
717	446	+31	477	749	393	+25	418
718	716	+31	747	750	500	+23	523
719	708	+32	740	751	508	+21	529
720	543	+33	576	752	664	+15	679
721	525	+33	558	753	535	+14	549
722	498	+34	532	754	539	+13	552
723	538	+35	573	755	556	+ 8	564
724	509	+36	545	756	449	+10	459
725	495	+37	532	757	546	+12	558
726	494	+38	532	758	526	+14	540
727	505	+38	543	759	522	+16	538
728	494	+38	532	760	525	+16	541
729	486	+37	523	761	510	+16	526
730	510	+36	546	762	517	+15	532
731	500	+35	535	763	530	+15	545
732	498	+36	534	764	413	+ 8	421
733	489	+42	531	765	523	+ 6	529
734	494	+43	537	766	521	+ 4	525
735	467	+44	511	767	502	+ 3	505
736	487	+45	532	768	527	+ 4	531
737	470	+15	535	769	551	+ 4	565

Table II.1.3-3 Magnetic values at every survey point (13)
(unit: γ)

Survey point	Average of measured value	Correction Duirnal value	Correction Duirnally value	Survey point	Average of measured value	Correction Duirnal value	Correction Duirnally value
No.	R̄st	ΔRt	Rs	No.	R̄st	ΔRt	Rs
770	43485	+ 3	43488	802	43545	+ 1	43546
771	519	+13	532	803	539	+ 2	541
772	508	+12	520	804	532	+ 3	535
773	523	+12	535	805	535	+ 4	539
774	524	+11	535	806	534	+ 5	539
775	528	+11	539	807	525	+ 6	531
776	573	+ 8	581	808	518	+ 6	524
777	534	+ 6	540	809	524	+ 7	531
778	534	+ 6	540	810	527	+ 8	535
779	537	+ 5	542	811	460	+16	476
780	534	+ 4	538	812	473	+16	489
481	530	+ 3	533	813	519	+16	535
482	521	+ 1	522	814	494	+17	511
483	550	0	550	815	513	+17	530
784	539	− 1	538	816	512	+17	529
785	539	− 2	537	817	493	+17	510
786	498	− 4	494	818	498	+17	515
787	553	− 6	547	819	391	+17	408
788	550	− 7	543	820	506	+18	524
789	534	− 8	526	821	512	+19	531
790	539	− 6	533	822	471	+21	492
791	542	− 6	536	823	494	+24	517
792	541	− 7	534	824	479	+24	503
793	540	− 7	533	825	464	+25	489
794	527	− 4	523	826	473	+27	500
795	540	0	540	827	493	+30	523
796	543	0	543	828	526	+19	545
797	535	− 1	534	829	525	+18	543
798	533	− 1	532	830	520	+17	537
799	529	− 1	528	831	521	+16	537
800	534	0	534	832	528	+16	544
801	539	+ 1	540	833	486	+15	501

Table II.1.3-3 Magnetic values at every survey point (14)

(unit: γ)

Survey point	Average of measured value	Correction Duirnal value	Correction Duirnally value	Survey point	Average of measured value	Correction Duirnal value	Correction Duirnally value
No.	$\bar{R}st$	ΔRt	Rs	No.	$\bar{R}st$	ΔRt	Rs
834	43546	+13	43559	866	43531	− 6	43525
835	532	+16	548	867	536	−12	524
836	521	+15	536	868	534	−14	520
837	536	+17	553	869	548	−20	528
838	564	+22	586	870	529	−17	512
839	569	+28	597	871	528	−15	513
840	523	+29	552	872	523	−11	512
841	537	+41	568	873	534	−12	522
842	496	+32	528	874	545	−11	534
843	499	+34	533	875	534	− 8	526
844	496	+33	529	876	546	− 3	543
845	514	+10	524	877	537	− 1	536
846	513	+11	524	878	524	0	524
847	529	+ 8	537	879	541	+ 2	543
848	489	+ 6	495	880	520	+ 9	520
849	494	+ 4	498	881	511	+11	522
850	497	+ 1	498	882	516	+13	529
851	512	− 1	511	883	510	+15	525
852	513	− 1	512	884	508	+17	525
853	500	0	500	885	505	+18	523
854	485	0	485	886	489	+19	508
855	513	− 1	512	887	507	+20	527
856	570	− 2	568	888	502	+22	524
857	498	− 3	495	889	506	+22	528
858	530	− 4	526	890	521	+ 6	527
859	635	− 5	630	891	508	+ 8	516
860	551	− 6	545	892	521	+ 7	528
861	483	− 6	477	893	533	+ 7	540
862	538	− 4	534	894	512	+ 6	518
863	538	− 4	534	895	513	+ 5	518
864	523	− 4	519	896	524	+ 2	526
865	538	− 5	533	897	527	+ 3	530

Table II.1.3-3 Magnetic values at every survey point (15)

(unit; γ)

Survey point	Average of measured value	Correction Duirnal value	Correction Duirnally value	Survey point	Average of measured value	Correction Duirnal value	Correction Duirnally value
No.	$\overline{R}st$	ΔRt	Rs	No.	$\overline{R}st$	ΔRt	Rs
898	43515	+ 3	43518				
899	513	+ 3	516				
900	531	− 1	530				
901	524	− 5	519				
902	623	− 3	620				

3-2 Magnetic maps

By inputting the location of the survey points and the diurnally corrected values into computer, maps stated hereunder were drawn up.

3-2-1 Total magnetic intensity map (PL. III.1.3-1)

The total magnetic intensity map was drawn up based upon the total magnetic values R̄s obtained after diurnal correction of the measured magnetic values at each survey point.

In the first place, mesh grid of 150 m x 150 m was established in all over the surveyed area. A fan with the interior angle of 170° is drawn around each grid point. The radius of the fan is determined so that the fan could in clude more than 6 magnetic survey points, in whichever direction the fan may turn. The average of the total magnetic values of every survey point by weighing the reciprocal of square of the distance from each survey point to the grid point is taken to be the magnetic value of the grid point. By this method, anomalous values and the wave length of extremely short period are made rather smooth. Total magnetic intensity map was drawn by tying such points as to have equal grid magnetic value. Values of the iso-magnetic contours on the map, PL. II.1.3-1, are expressed as the values after deduction of the average total magnetic value, 43,536 gamma, to make it easy to read the map.

3-2-2 Total magnetic anomaly (PL. II.1.3-2)

Value of magnetic anomaly is calculated by reducing earth's magnetic field from total magnetic value, and the map of total magnetic anomaly was drawn by tyiing the above values by iso-value contour.

The earth's magnetic field in whole of the surveyed area is obtained by a trend surface in first order polynomial of the total magnetic intensity map. By deducting the grid data of this trend surface from the lattice data of the total magnetic intensity map, total magnetic anomaly map has been drawn up.

The trend surface in first order polynomial (Fig. II.1.3-4) is a plane expressed by the following formula, which gentle dipping in the direction of north and south. Accordingly, shape and form expressed by the iso-value contours on the magnetic anomaly map are almost same as those shown on the total magnetic intensity map.

$$Z(X.Y) = 43{,}556 - 0.647\,X + 0 \cdot Y\,\gamma$$

3-2-3 Upward continuation map (PL. II.1.3-3)

As the influence of magnetism near the surface is significant in the magnetic survey, the upward comtinuation map is usually employed for the analysis of underground structure. The upward continuation map has an effect as if the magnetism had been measured in the air above the survey point. It is useful to extract anomalies of long wave length caused by large scaled underground structure at depth, eliminating anomalies of short wave length owing to decrement of such wave caused by small scaled underground structure in the shallow part below surface.

The upward continuation map was drawn with the values obtained by multiplying the magnetic value of each grid point on the magnetic intensity map by the continuation coefficient, according to continuation law. As the 49 grid data of 7 lines by 7 rows around the grid point are required for an upward value at a grid point, some shortage of data occurs in the peripheral zone of the surveyed area. In case the number of data is less than 25 against 49, treatment was suspended.

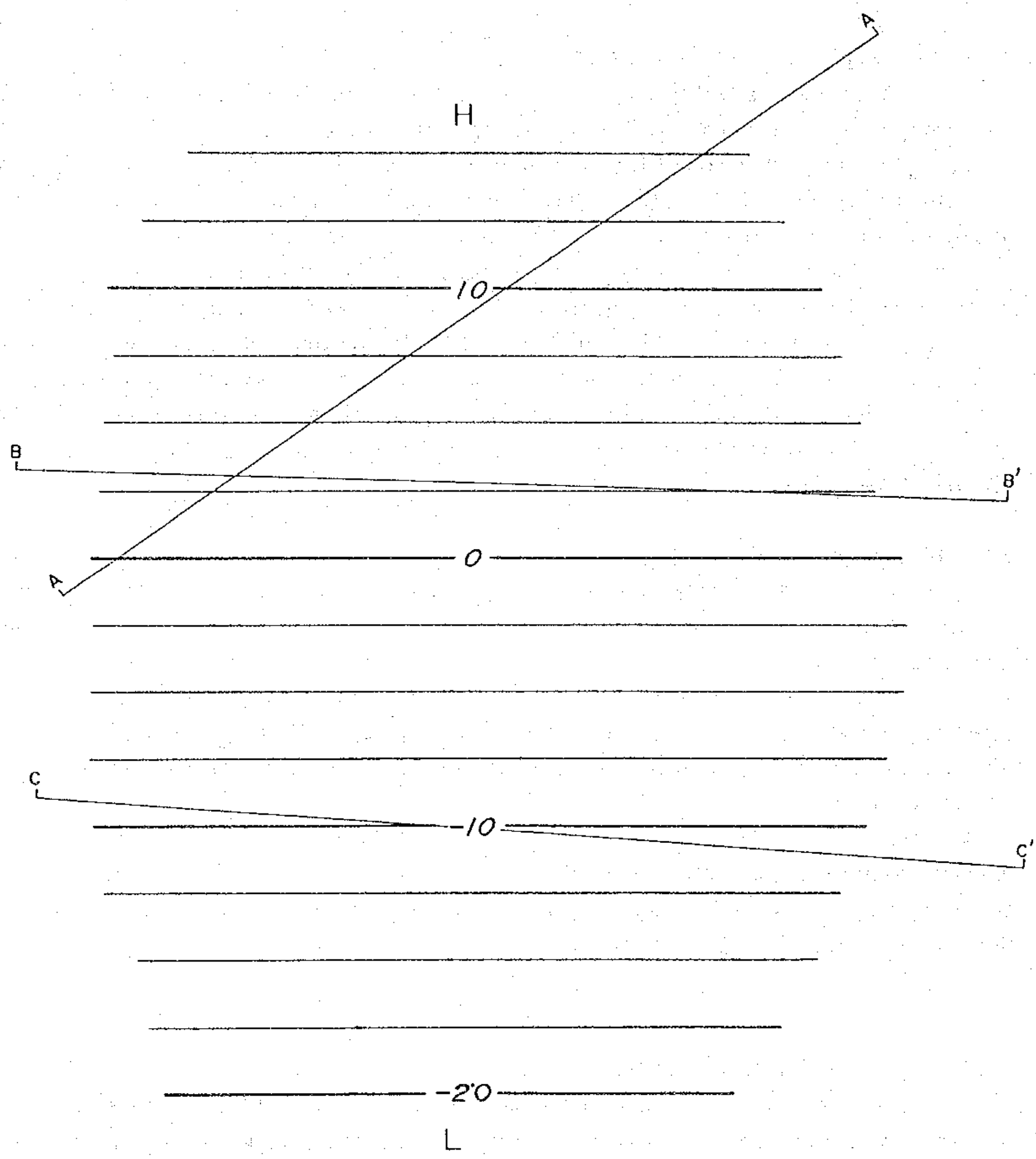

Fig. II.1.3-4 Magnetic trend (First order polynomial)

3-2-4 Spectrum analysis

Various wave lengths are contained in the total magnetic anomaly map. The spectrum analysis is a method to distinguish shallow underground structure from deep underground structure according to the sizes of the wave length.

The spectrum analysis map is expressed by logargythm of energy spectrum Log E at various frequency f (Fig. II.1.3-5).

The energy spectrum E can be obtained as a function of the following factors on the magnetic anomaly map; the frequency in X direction: fx, that in Y direction; fy, and complex number spectrum concerning amplitude and phase: S (fx, fy).

Viewing the distribution of the logargythm values of energy spectrum against frequency f (cycle/km) in the spectrum analysis shown in Fig. II.1.3-5, two straight lines are approximated. From the gradients of these regression lines, average depth of the source of the anomalies causing the magnetic bodies in the surveyed area can be known by the following formula.

$$H = -\frac{1}{4\pi} \cdot \frac{\Delta \log E}{\Delta f}$$

By the above, the magnetic structure in this surveyed area is divided, on the whole, into the Regional Component (HR) at the average depth of 760 meters and the Near Surface Component (HN) at the average depth of 65 meters. Based on this result, the deep magnetic component map (PL. II.1.3-4) and the shallow magnetic component map (PL. II.1.3-5) were drawn up. The deep and the shallow magnetic component map were prepared by convolution of the magnetic data and the weighted function calculated from the elements on the spectrum analysis.

The relation of the Deep Magnetic Component HR (X, Y), the Shallow Magnetic Component HN (X, Y) and the magnetic anomaly G (X, Y) is shown as follows.

$$G (X, Y) = HR (X, Y) + HN (X, Y)$$

3-3 Model calculation

The response by the magnetic bodies changes variously by three elements of the magnetism (total magnetic intensity, declination, inclination). Therefore, it is necessary to get information of the specific character is each survey area. Hence three dimensional calculation was carried out with prism model, which is most widely applicable as a shape of magnetic body, while two dimensional calculation was performed with dyke model and step model, by having declinations and inclinations varied.

The results of these model calculation are exhibited in Fig. II.1.3-6,7 and 8.

By the result of the caluculation with prism model, it is shown that positive and negative magnetic anomalies appear in pair, with the distribution of magnetic anomalies varied according to the forms of the surface of the magnetic body. In case of step model or dyke model, magnetic anomalies expressed on the profiles perpendicular to the strikes of the structure are varying according to the direction of the strikes.

The expression of $\alpha = 0°$ displays, along the section, the anomaly in N-S direction which is created when a magnetic body lies in east and west direction.

The expression of $\alpha = 90°$ displays, along the section, the anomaly in the direction which is created when a magnetic body lies in north and south direction.

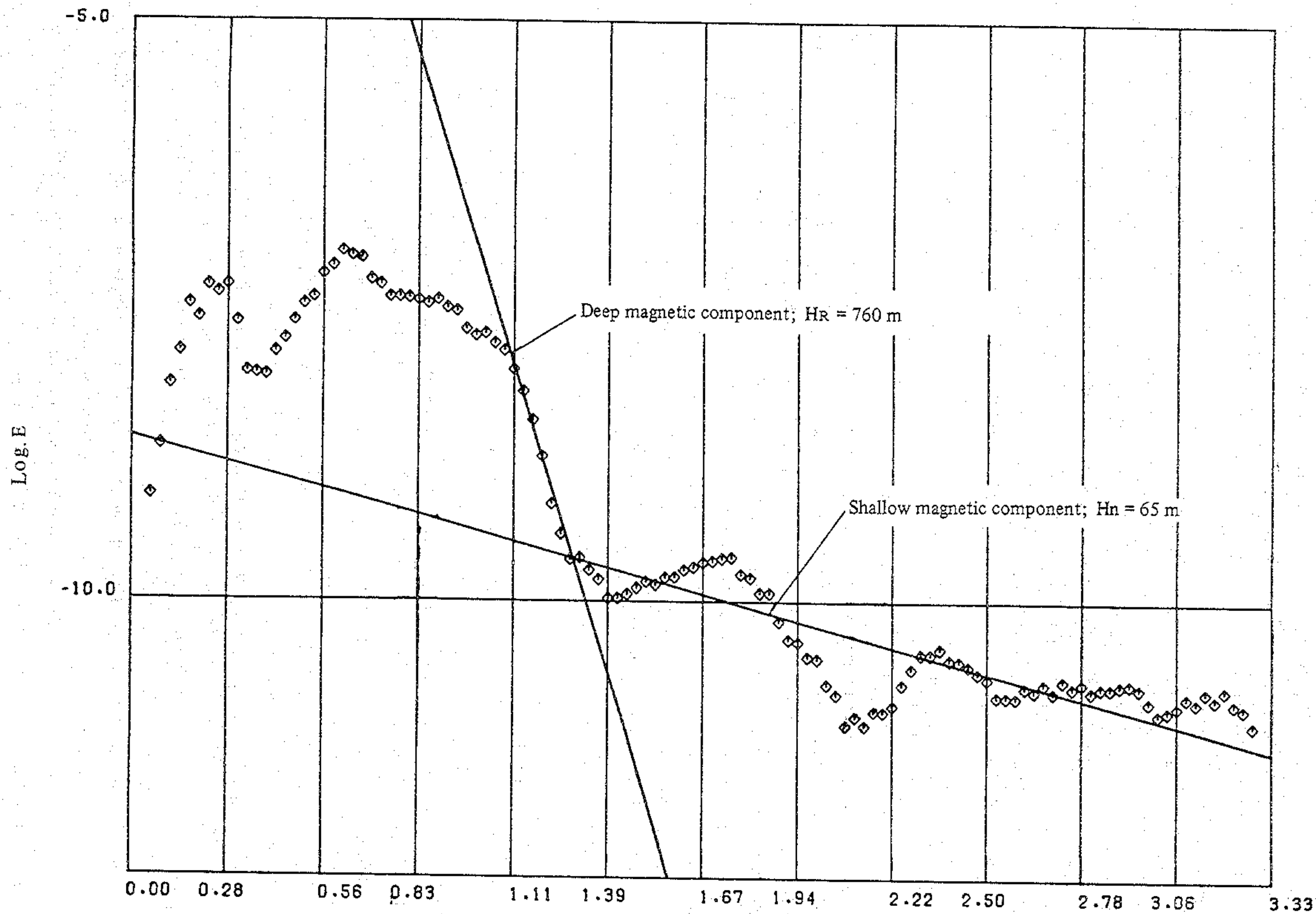

Fig. II.1.3-5 Spector analysis

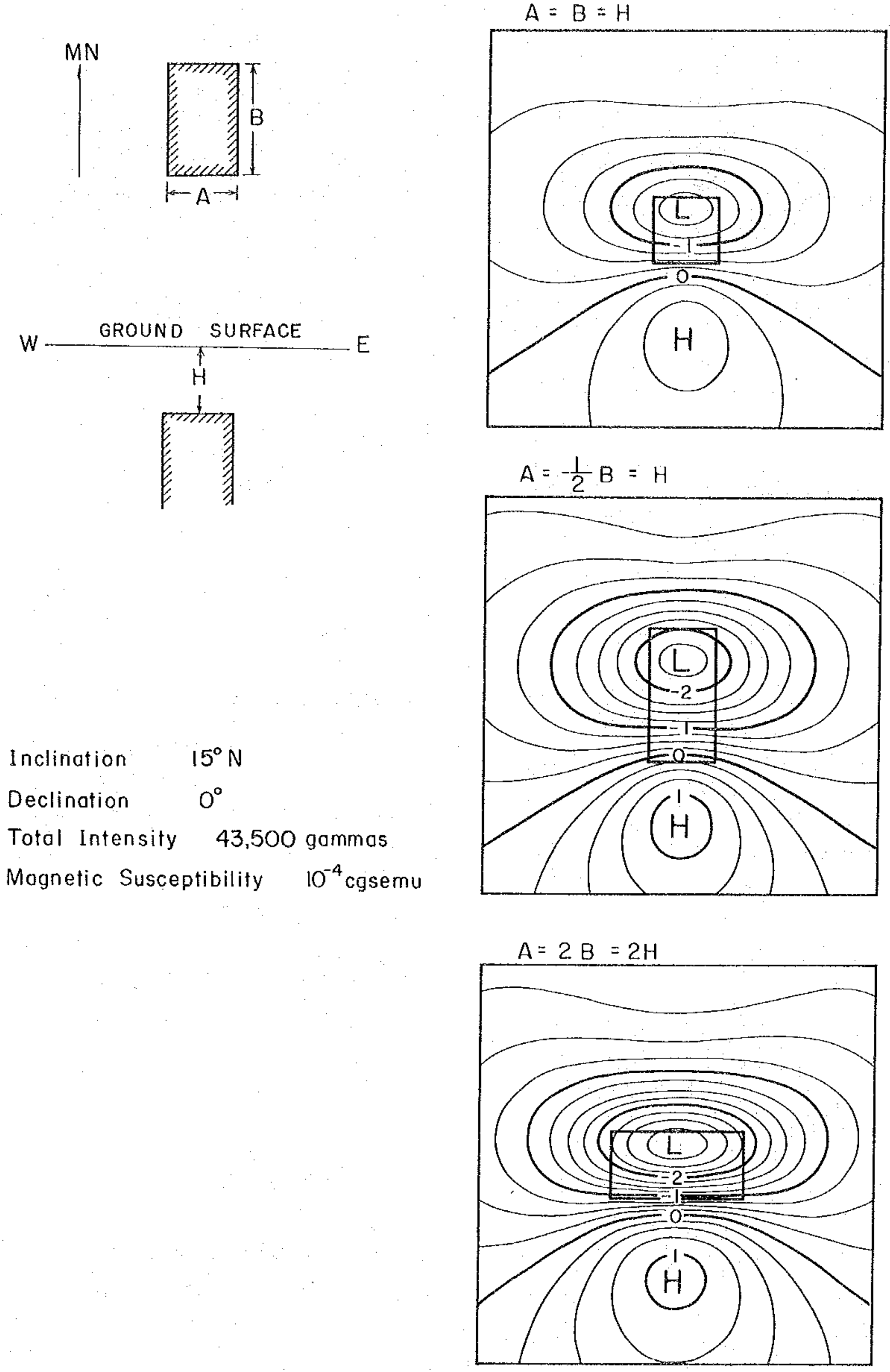

Fig. II.1.3-6 Magnetic response of prism model

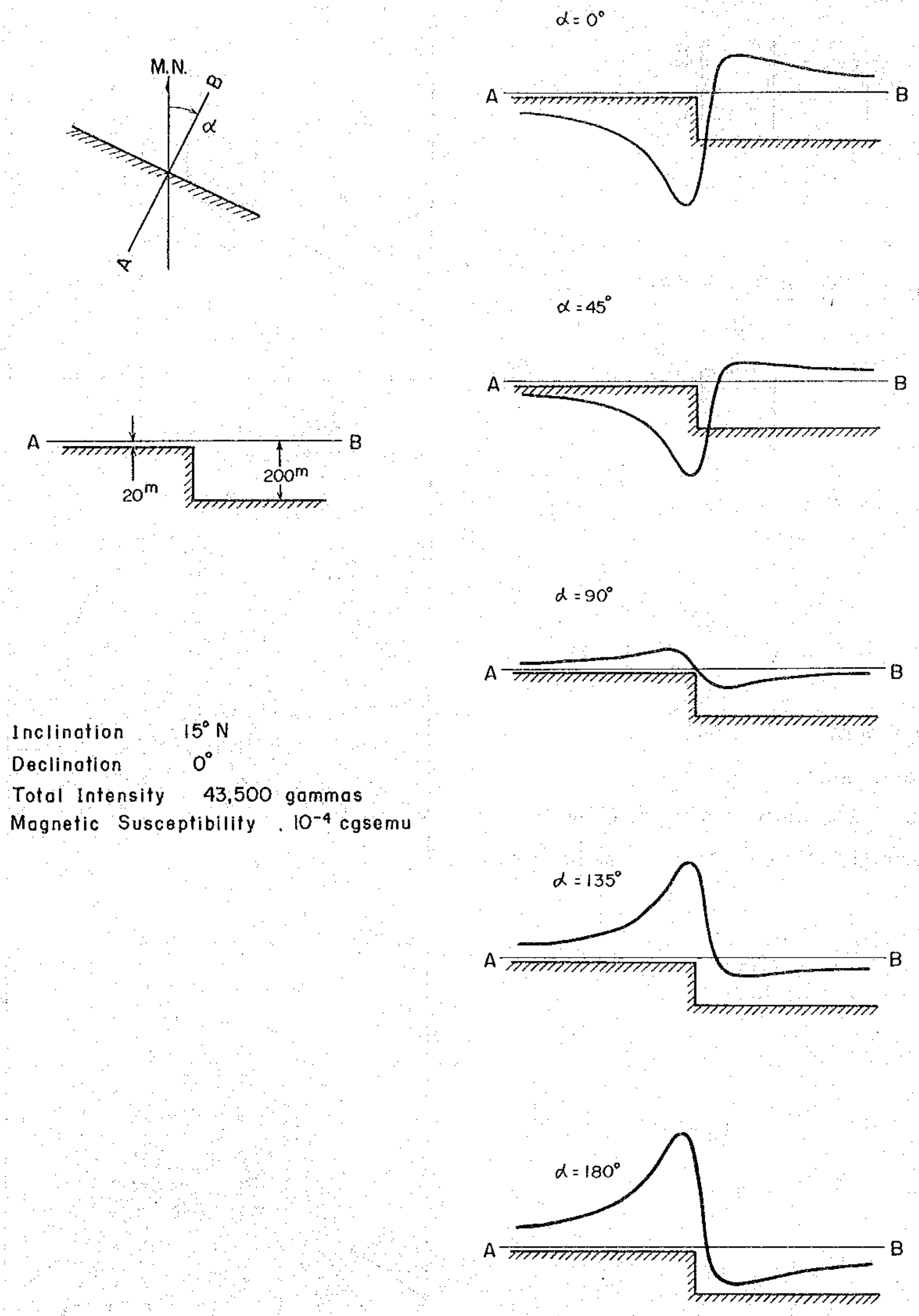

Fig. II.1.3-7 Magnetic response of step model

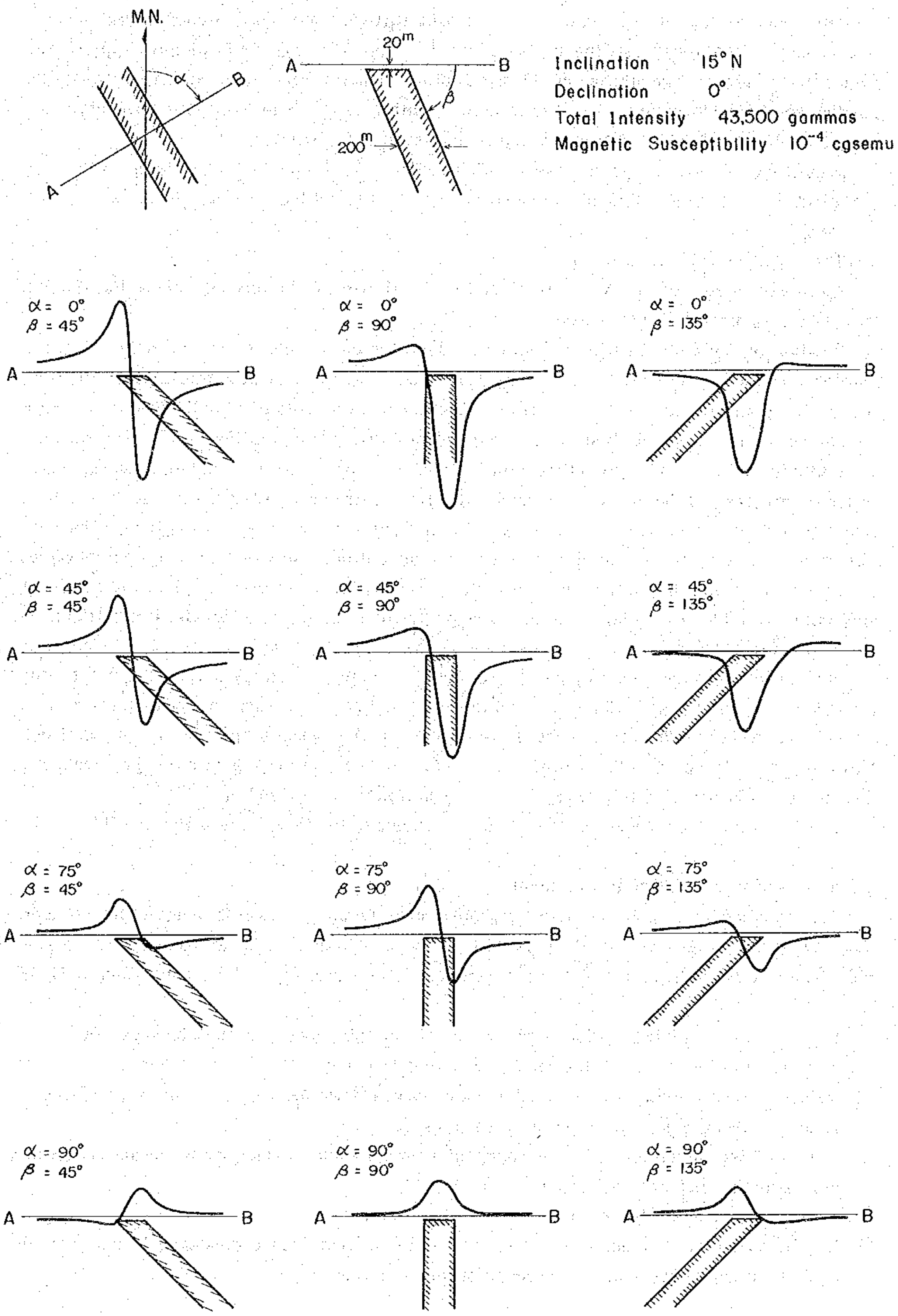

Fig. II.1.3-8 Magnetic response of dyke model

The main geological structures in the present surveyed area have trend of N-S system. Accordingly, it is thought that the models of $\alpha = 90° \sim \alpha = 45°$ or $\alpha = 135°$ are most appropriate. From the results of the above model calculation, comparatively small positive anomaly or positive anomaly accompanying negative anomaly with deep gradient with short wave length are thought to be distributed in this surveyed area, in case of dyke structure.

Meanwhile, in case of step structure, it is thought that anomaly in smallest with $\alpha = 90°$ and that positive and negative anomalies are associated each other with $\alpha = 45°$ or $\alpha = 135°$.

3-4 Prfile analysis (PL. II.1.2-6,7,8)

Along the three profiles (A–A', B–B' and C–C') shown on the magnetic plans (PL. II.1.3-1 etc.), two dimensional profile analysis was completed.

Reading the magnetic distribution along the lines for the profiles on the magnetic plans, the magnetic profiles are prepared in the first place. Considering the geological information, the rock susceptibility and the results of the various model calculation, a model of underground structure containing plural magnetic bodies is composed. Inputting the location, the form and the susceptibility of the underground structure model into the electronic computer, it calculates magnetic response on the surface with given underground structure. At such point as the result of calculation does not coincide the value on the magnetic profile, renewed magnetic values are distributed on revised underground structures by the automatical variation of the input values which are expressing the underground structure (location, form and susceptibility), and the most approximated underground structure model is obtained as the output. Usually, it is difficult to get high coincidence in the above process by a single operation. Therefore, considering the results of the calculation, the analyst would give revised model of underground structure to the electronic computer, again. But the repetition of this operation, such model of underground structure as to have high coincidence to the values on the magnetic profile can be expressed. However, as there would be numerous underground structure models to have the same magnetic distribution, it is necessary to give careful consideration for the elucidation.

The method of the magnetic profile analysis is shown in the flow chart of Fig. II.1.3-9.

3-5 Result of susceptibility measurement

After the collected rock samples were ground and screened with sieves to homogeneous grain size, susceptibility was measured by enclosing the powdered material in non-magnetic plastic pipe. The results of the susceptibility measurement is shown in Fig. II.1.3-10 and Table II.1.3-4.

By the results of the susceptibility measurement, the following items have been clarified.

(1) The suceptibility of the basaltic rocks is scattered as widely as $10^{-4} \sim 10^{-6}$ emu.

(2) Values of susceptibility are scattered in wide range, as a whole. The variation of susceptibility is fairly wide even in a single species of the rocks.

(3) Values of the susceptibility of the sedimentary rocks such as shale, sandstone and limestone are mostly as small as less than 10^{-5} emu.

(4) The susceptibility of the granite is as low as 10^{-5} emu.

(5) It is basaltic rocks belonging to the upper part of the Kiu Lom Formation which are revealing high susceptibility among the rocks distributed in this surveyed area.

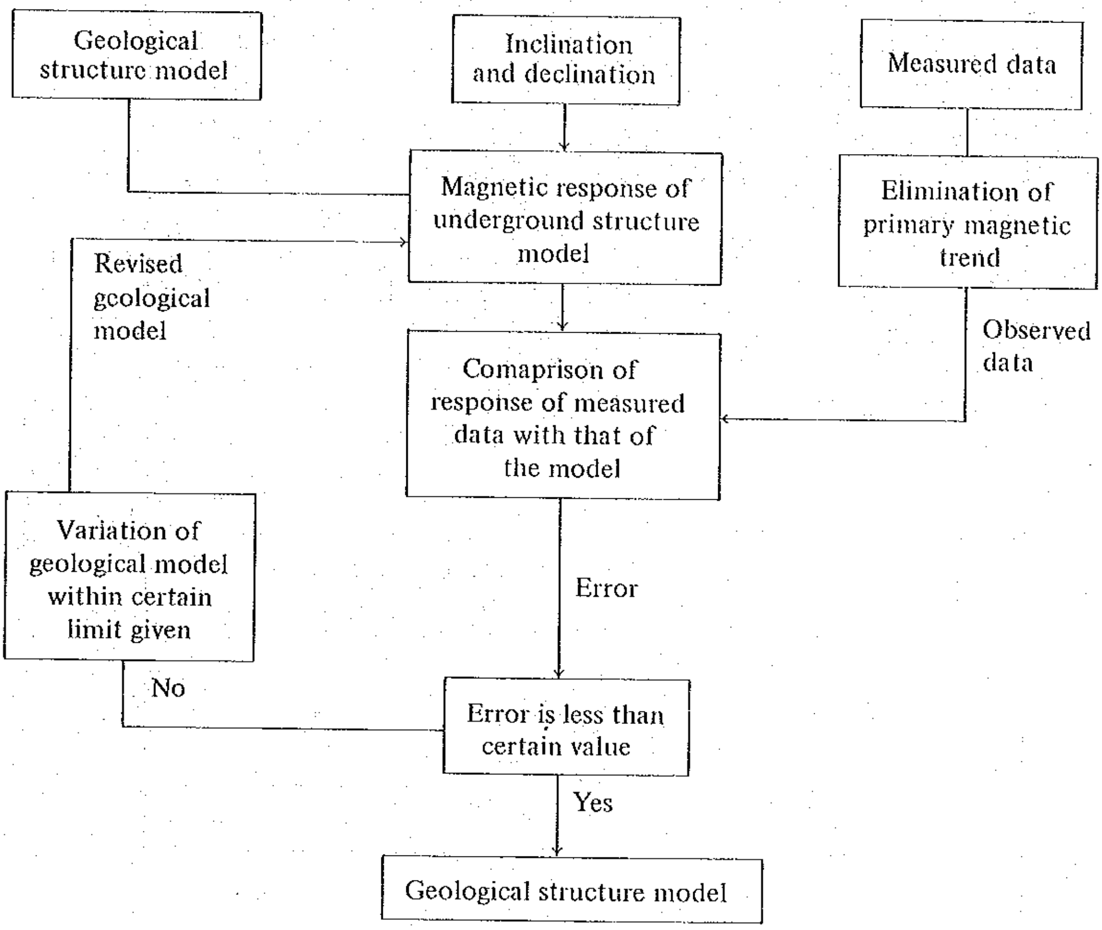

Fig. II.1.3-9 Flow chart of magnetic profile analysis

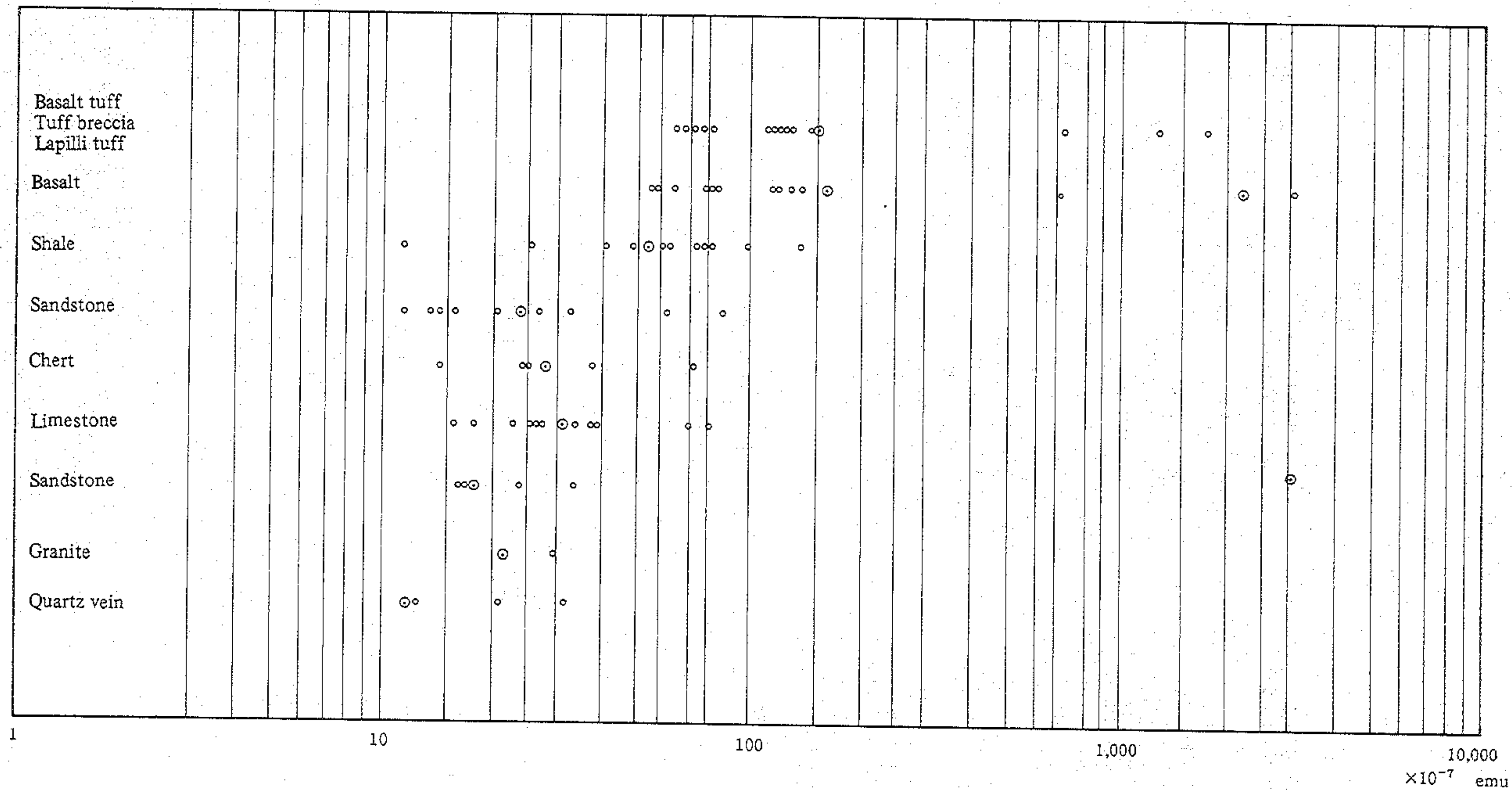

Fig. II.1.3-10 Magnetic susceptibility distribution

Table II.1.3-4 Results of susceptibility measurement (1)

Rock	Resived No.	Apparent susceptibility (cgs/cc)	Correction coefficient		True susceptibility (cgs/cc)
Bosalt	20	6.2×10^{-6}	0.984	2.03	1.24×10^{-6}
〃	21	4.0×10^{-6}	0.984	1.97	7.75×10^{-6}
〃	22	4.3×10^{-6}	0.984	1.96	8.29×10^{-6}
〃	23	3.88×10^{-6}	0.984	1.85	7.06×10^{-6}
〃	24	2.8×10^{-6}	0.984	1.99	5.48×10^{-6}
〃	25	3.0×10^{-6}	0.984	1.93	5.70×10^{-6}
〃	26	4.1×10^{-6}	0.984	2.01	8.11×10^{-6}
〃	27	6.8×10^{-6}	0.984	1.99	1.33×10^{-6}
〃	28	1.62×10^{-6}	0.984	1.99	3.17×10^{-6}
〃	29	6.0×10^{-6}	0.984	1.98	1.17×10^{-6}
〃	30	5.8×10^{-6}	0.984	1.99	1.14×10^{-6}
〃	81	3.3×10^{-6}	0.984	2.00	6.49×10^{-6}
〃	82	1.21×10^{-6}	0.984	1.96	2.33×10^{-6}
Tuff	1	4.3×10^{-6}	0.984	1.87	7.91×10^{-6}
〃	2	5.1×10^{-6}	0.984	2.07	1.04×10^{-6}
〃	3	3.3×10^{-6}	0.984	1.88	6.10×10^{-6}
〃	4	3.6×10^{-6}	0.984	1.77	6.98×10^{-6}
Basaltic tuff	5	3.5×10^{-6}	0.984	2.06	7.09×10^{-6}
Tuff	6	6.0×10^{-6}	0.984	1.86	1.10×10^{-6}
〃	7	3.4×10^{-6}	0.984	2.00	6.69×10^{-6}
〃	8	3.7×10^{-6}	0.984	1.97	7.17×10^{-6}
〃	9	7.0×10^{-6}	0.984	2.00	1.38×10^{-6}
〃	10	3.9×10^{-6}	0.984	1.93	7.41×10^{-6}
〃	11	6.4×10^{-6}	0.984	1.98	1.25×10^{-6}
〃		1.3×10^{-6}	0.984	1.85	2.37×10^{-6}
Tuff breccia	12	8.75×10^{-6}	0.984	2.04	1.76×10^{-6}
〃	13	7.21×10^{-6}	0.984	1.88	1.33×10^{-6}
〃	14	2.5×10^{-6}	0.984	1.94	4.77×10^{-6}
〃	15	3.2×10^{-6}	0.984	1.99	6.27×10^{-6}
〃	16	7.0×10^{-6}	0.984	2.09	1.44×10^{-6}
〃	17	5.9×10^{-6}	0.984	1.92	1.11×10^{-6}
〃	18	6.1×10^{-6}	0.984	1.90	1.14×10^{-6}
Limestone	52	1.4×10^{-6}	0.984	2.48	3.42×10^{-6}
〃	53	1.3×10^{-6}	0.984	2.05	2.62×10^{-6}
〃	54	0.8×10^{-6}	0.984	1.94	1.53×10^{-6}
〃	55	0.9×10^{-6}	0.984	2.01	1.78×10^{-6}
〃	56	1.4×10^{-6}	0.984	1.96	2.70×10^{-6}
Limestone	57	2.1×10^{-6}	0.984	1.92	3.97×10^{-6}
〃	58	1.4×10^{-6}	0.984	1.99	2.74×10^{-6}
Silicified limestone	83	2.0×10^{-6}	0.984	1.95	3.84×10^{-6}
Limestone	59	4.3×10^{-6}	0.984	1.93	8.17×10^{-6}
〃	60	1.3×10^{-6}	0.984	1.97	2.52×10^{-6}
〃	61	1.2×10^{-6}	0.984	1.91	2.26×10^{-6}
〃	62	3.3×10^{-6}	0.984	2.10	6.82×10^{-6}
〃	63	1.9×10^{-6}	0.984	2.01	3.76×10^{-6}

Table II.1.3-4 Results of susceptibility measurement (2)

Rock	Revised No.	Apparent susceptibility (cgs/cc)	Correction coefficient		True susceptibility (cgs/cc)
Chert (weathered)	47	1.2×10^{-6}	0.984	2.08	2.46×10^{-6}
〃	48	1.9×10^{-6}	0.984	1.95	3.65×10^{-6}
Chert	49	0.8×10^{-6}	0.984	1.83	1.44×10^{-6}
〃	50	1.4×10^{-6}	0.984	1.86	2.56×10^{-6}
〃	51	3.9×10^{-6}	0.984	1.88	7.21×10^{-6}
Calcareous shale	31	2.1×10^{-6}	0.984	1.91	2.63×10^{-6}
Black shale	32	1.4×10^{-6}	0.984	2.15	5.71×10^{-6}
Shale	33	4.6×10^{-6}	0.984	2.17	9.82×10^{-6}
Calcareous shale (fresh)	34	2.2×10^{-6}	0.984	1.90	4.11×10^{-6}
〃 (weathered)	35	4.3×10^{-6}	0.984	1.91	8.08×10^{-6}
Shale	36	7.1×10^{-6}	0.984	1.91	1.33×10^{-6}
Brocky shale	79	2.6×10^{-6}	0.984	1.88	4.81×10^{-6}
Shale	84	3.0×10^{-6}	0.984	2.07	6.11×10^{-6}
〃	37	3.6×10^{-6}	0.984	2.15	7.62×10^{-6}
〃	38	3.8×10^{-6}	0.984	1.93	7.22×10^{-6}
〃 (weathered)	39	0.6×10^{-6}	0.984	1.98	1.17×10^{-6}
Sand stone	40	3.0×10^{-6}	0.984	1.98	5.84×10^{-6}
〃	41	0.7×10^{-6}	0.984	1.93	1.33×10^{-6}
〃	42	1.6×10^{-6}	0.984	2.06	3.24×10^{-6}
〃	64	0.5×10^{-6}	0.984	1.93	9.50×10^{-6}
〃	65	0.9×10^{-6}	0.984	1.95	1.73×10^{-6}
〃	66	1.7×10^{-6}	0.984	2.04	3.41×10^{-6}
〃	67				
〃	43	1.1×10^{-6}	0.984	2.04	2.21×10^{-6}
〃	68	0.9×10^{-6}	0.984	1.99	1.76×10^{-6}
〃	78	0.7×10^{-6}	0.984	2.07	1.43×10^{-6}
〃		0.4×10^{-6}	0.984	1.92	7.56×10^{-6}
〃	80	0.6×10^{-6}	0.984	2.00	1.18×10^{-6}
〃	44	0.8×10^{-6}	0.984	2.12	1.67×10^{-6}
〃	45	4.1×10^{-6}	0.984	2.12	8.55×10^{-6}
〃	46	1.4×10^{-6}	0.984	2.01	2.77×10^{-6}
〃	69	1.2×10^{-6}	0.984	2.01	2.37×10^{-6}
Granite	70	1.5×10^{-6}	0.984	2.04	3.01×10^{-6}
〃	71	0.8×10^{-6}	0.984	1.95	1.53×10^{-6}
〃	72	0.8×10^{-6}	0.984	2.03	1.53×10^{-6}
Quartz vein	73	0.7×10^{-6}	0.984	1.85	2.40×10^{-6}
〃	74	0.2×10^{-6}	0.984	2.05	4.03×10^{-6}
〃	75	1.8×10^{-6}	0.984	1.93	3.42×10^{-6}
〃	76	0.3×10^{-6}	0.984	1.99	5.87×10^{-6}
〃	77	1.1×10	0.984	2.03	2.20×10^{-6}

4. Results of the analysis

4-1 Plans and profiles of analysis

The following plans and profiles were drawn up by the results of the analysis.

PL. II.1.3-1 Total magnetic intensity
PL. II.1.3-2 Total magnetic anomaly
PL. II.1.3-3 Upward continuation
PL. II.1.3-4 Deep magnetic component
PL. II.1.3-5 Shallow magnetic component
PL. II.1.3-6 Result of magnetic modelling
PL. II.1.2-6 Underground structure profile (A–A')
PL. II.1.2-7 Underground structure profile (B–B')
PL. II.1.2-8 Underground structure profile (C–C')
PL. II.1.3-7 Underground structure

Fig. II.1.3-4 Magnetic trend (First order polynomial)
Fig. II.1.3-5 Spectrum analysis
Fig. II.1.3-6,7,8 Magnetic response (prims, dyke, step)

4-1-1 Total magnetic intensity (PL. II.1.3-1

Forms of iso-magnetic conters are almost same as those of the magnetic anomaly map (PL. II.1.3-2).

4-1-2 Magnetic trend of first order polynomial (Fig. II.1.3-4)

This plan expresses roughly the earth's magnetic field in the surveyed area. There is a gentle slope southward from the north, but no variation is found in the direction of east and west.

4-1-3 Magnetic anomaly map (PL. II.1.3-2)

The magnetic variation on the Magnetic intensity map is from the highest value of +112.5 (+43,556) gamma to the lowest of −184.6 (+43,556) gamma, while on the magnetic anomaly map the highest value is +113 (43,556) gamma and the lowest value is −175 (+43,556) gamma, taking 0 as the base.

Positive and negative anomalies are expressed as small closed circle of iso-magnetic contours, which are widely distributed in whole of the surveyed area. The individual areas occupied by such closed circles are as small as 200 to 800 meters in major axis. The closed circles of iso-magnetic conters are found predominantly in the area where basaltic rocks are distributed, but they are not always correspondent to the distribution of the basaltic rocks. It can be said that they are distributed along the Ban Mae Khu Ha fault and along the Huai Mae Khuha fault as well as in the area surrounded by these faults. The closed iso-magnetic contours are also found along the Hual Wai fault. Negative anomalies which have rather large area are distributed along the above faults or along the faults oblique to the above faults. In the areas where shale, chert and sandstone are distributed, almost no magnetic anomaly has been found.

As for the distribution of negative anomalies, an anomaly surrounded by the iso-magnetic contour of 10 gamma of the approximate length of 1,000 meters in major axis is found about

800 meters west of the EGAT camp. Also, about 700 m north of the site of the geothermal exploration well GTE-4 and along the upstream of the Huai Ko Pong River in the eastern part, are distributed negative anomalies of the approximate size of 1,500 maters in major axis.

4-1-4 Upward continuation map (75 m above the surface) (PL. II.1.3-3)

As the upward continuation treatment has filtering character to extract deep component, the pattern of the upward continuation map is similar to that on the deep component map (PL. II.1.3-4). It is thought that this upward continuation map would show the structure in shallower part than the deep component map, because waves with rather smaller wave-length appear on the former, although they are basicaly of the same character.

4-1-5 Deep component map (PL. II.1.3-4)

This map has the following characteristics compared to the total magnetic intensity map.

Variation of the magnetic anomalies is from the highest of 47 gamma to the lowest of −55 gamma. The individual areas expressed by the closed iso-magnetic conters are rather wide, though number of the anomalies is smaller.

Locations of positive anomalies and negative ones on this map are almost coincident with those on the total magnetic intensity map. The anomalies are distributed along the Huai Mae Khu Ha fault, along the Ban Mae Khu Ha fault, along the Huai Wai fault and along the Huai Mae Koen fault.

A negative magnetic anomaly whose major axis is approximately 1,000 meters is distributed about 800 m west of the EGAT camp and about 700 meters north of the geothermal exploration well of GTE-4.

4-1-6 Shallow component map (PL. II.1.3-5)

There are many small closed circles of crowded iso-magnetic conter lines, with approximate distance of 200 meters in minor axis. They are distributed especially along the Ban Mae Khu Ha fault, the Huai Mae Khu Ha fault and the Huai Pong faults oblique to the former two faults. Also, they are found along the Huai Wai fault.

4-1-7 Result of magnetic modelling profile

It is necessary to consider the direction of the anomalies for the analysis of magnetic anomalies. With the remarkable anomalies shown on the total magnetic intensity map (PL. II.1.3-1), model analysis was completed. By the results of this model analysis and by the results of model calculation, plan of underground structure (PL. II.1.3-7) was drawn up.

4-1-8 Underground structure profiles (PL. II.1.2-6,7,8)

Locations of the three profiles, along which the analysis has been completed (A–A', B–B' and C–C') are shown on PL. II.1.3-1. They are the same profiles as were employed for the analysis in the gravity survey.

Along these profiles, the magnetic anomaly map, the filtering profiles and the underground structure map have been displayed, as shown below.

Magnetic anomaly map.

Filtering prifiles are expressing profiles of the spectrum analysis deep component and shallow component) and the upward continuation.

Underground structure profiles are expressing the8tructure model obtained by the results of the simulation.

The magnetic bodies analysed are distributed in the shape of dykes in the shallow to deep part below surface, seated in the Kiu Lom Formation.

The calculated susceptibility is 3 ~ 37 x 10^{-4} cgsemu, which is in the range of the susceptibility of the basaltic rocks in the Kiu Lom Formation.

4-2 Magnetic distribution and underground structure

Viewing from the analysis results of the magnetic survey, the underground structure in this surveyed area is divided into three blocks (PL. II.1.3-7).

[I] block ; the area east of the Huai Mae Khu Ha fault and the Huai Wai fault

[II] block ; the area from the Huai Mae Khu Ha fault and the Huai Wai fault to the Ban Mae Khu Ha fault

[III] block ; the area west of the Ban Mae Khu Ha fault

In the [I] block, the upper part of the Kiu Lom Formation is distributed widely.

Number of the magnetic bodies analysed in this block is comparatively small and the regularity of the distribution is uncertain.

In the [II] block1the upper part of the Kiu Lom Formation is distributed in the eastern part, bordered by the limestone bed of the middle part of the Kiu Lom Formation, while the middle to lower part of the Kiu Lom Formation is distributed in the western part of the limestone bed. There are faults of N-S trend such1as the Huai Wai fault, the Huai Mae Khu Ha fault and the Ban Mae Khu Ha fault, in addition to the other faults crossing the above faults in the NW-SE direction.

The magnetic bodies analysed are numberous, and most of them are distributed along the around the above-stated faults. Other than those found along the faults, there are magnetic bodies located in a row in the direction of north and south, near Ban Mae Khu Ha.

The [III] block is the area where the sedimentary rocks of the middle to lower part of the Kiu Lom Formation are distributed. By the results of the susceptibility measurement, the susceptibility values of the sedimentary rocks are small, and no remarkable magnetic body is recognized in this block. The things are same in the area east of the Huai Mae Koen fault in the eastern part of the surveyed area.

It has been clarified that the magnetic bodies in this block are distributed, as afore-mentioned, in the area where the middle part of the Kiu Lom Formation is found, and that most of them are found in the area south of the Huai Wai fault, along the Huai Mae Khu Ha fault and along the Ban Mae Khu Ha fault. As there is intimate relation between the distribution of magnetic bodies and that of the faults, it is possible that some subsurface faults would exist in the vicinity of the area around Ban Mae Khu Ha where magnetic bodies are distributed.

By the results of the measurement of the susceptibility, the susceptibility of the upper part of the Kiu Lom Formation is higher than that of the other beds, and the values are scattered in fairly wide range. However, no relation has been recognized between the distribution of the magnetic bodies and distribution and its shape of the upper part of the Kiu Lom Formation, but the distribution of the magnetic bodies is thought to be related intimately with the locations of the faults.

As the magnetic bodies, certain layers in which magnetic minerals are concentrated, certain parts in basaltic rocks where magnetism is specially strong and certain high magnetic intrusive rocks are thought to exist in this area. In case the magnetic bodies are the former two, distribution of the magnetic bodies would correspond to the strike and distribution of certain beds. However, the distribution of the magnetic bodies is corresponding to the location of the faults actually. Therefore the magnetic bodies are thought to represent existency of some magnetic intrusive rocks along the faults, or to represent difference of the geological components like beds, bounded by the faults.

5. Summary

(1) The magnetic survey was carried out with the cooperation of Thailand side counterpart (EGAT, DMR) and with the joint of students of the Khon Khaen University as a part of their field practice. Number of the total survey points was 901 in the present magnetic survey. The in-situ measurement of rock susceptibility was completed at 9 localities, while the measurement of rock piece susceptibility was completed with 84 rock samples collected in the field.

(2) The survey points were located by the land survey with simplified transit compasses and by the bush-cutted survey lines prepared by EGAT.

(3) After the diurnal correction for the measured magnetic values, the total magnetic intensity map was drawn up. That is, by reducing the values of earth's magnetic fields which were caught as the trend surface of the first order polynomial from the total magnetic intensity, the magnetic anomaly map was figured up. This map is to express magnetic anomalies due to the underground structure. Based on this magnetic anormaly map, various filtering plans and profiles were drawn up.

(4) In order to get information on the character of the magnetic anomalies in this surveyed area, the modelling calculations were performed with various models applicable to possible forms of the structures, and the results of the calculation were illustrated. Refering to the modelling calculation, profile analyses were executed on the representative magnetic anomalies. Based on the results of these analyses, the three profiles and the underground structure map were figured up.

(5) By the results of the above-mentioned analyses, the following items have been clarified.

1. The magnetic bodies analysed are found in the area where the middle part of the Kiu Lom Formation is distributed.
2. Viewing from the distribution of the magnetic bodies, the surveyed area is divided into three blocks of [I], [II] and [III], as is displayed on the plan of the underground structure (PL. II.1.3-7).
3. No direct relation has been recognized between the distribution of the magnetic bodies and the strikes of the layers or the distributing shapes of the Kiu Lom Formation, but it has been recognized that they are found distributed rather densely along the Ban Mae

Khu Ha fault, along the Huai Mae Khu Ha fault and around the south of the Huai Wai fault.

4. According to the results of the measurement of susceptibility, the basaltic rocks of the upper part of the Kiu Lom Formation have high values of magnetism though they are scattering, while other rocks in the surveyed area have low magnetism.
5. It is difficult to extract demagnetization zone due to geothermal activity, because the sedimentary rocks, distributed in the area where the geothermal indications are located, have very small values of magnetism.
6. From the fact that the distribution of the magnetic bodies has intimate relation to the locations of the faults, it is thought that these magnetic bodies thus delineated would be representing existence of certain magnetic intrusive rocks along the faults, or difference of the geological components such as beddings bounded by the faults. Therefore, it is possible that such faults along which the magnetic bodies are concentrated are composing tectonical fractured zones.

II-2 Secondary Investigation

II-2-1 Deep Electric Survey

1. Introduction

The deep electric survey was carried out for the purpose to obtain informations on the geothermal reservoirs through the distribution of resistivity (or conductance) in the surveyed area by measuring ratios of electric field to magnetic field, by the execution of magnetotelluric method (MT method) and vertical electromagnetic sounding method (CSAMT method: Controlled Source Audiofrequency Magnetotelluric method).

The components measured in the MT method are two components of underground natural electric field (Ex, Ey) and three components of natural magnetic field (Hx, Hy, Hz). Number of total sounding points in this survey by MT method was 33.

The components measured in the CSAMT method are two components of magnetic field (Hx, Hz) and a component of electric field (Ey), which are induced by loop. Five loops were prepared from A to E. Total number of the sounding points is 33. The same points as used for the survey by MT method were employed for the sounding points of the deep electric survey.

2. Field Survey

2-1 Method of measurement of MT survey

2-1-1 Apparatus for measurement

The specification of the apparatus employed in the present MT survey is as follows.

Table II.2.1-1 Apparatus for measurement of MT survey

Apparatus	Amount	Specification
Amplifier unit for electric field	2	(1st Stage) Input Level 1 micro V Max. Gain 2×10^2 1.00 Hz High Cut Filter (2nd Stage) Max. Gain 10^4 0.33 Hz High Cut Filter
Amplifier unit for magnetic field	3	Max. Gain 2×10^4 0.33 Hz High Cut Filter
Wave form Recorder	1	Full Scale ± 5 V Chart Speed 0.085 cm/s, 0.17 cm/s (2 Stage Variable)
Data Logger (Double cassette)	1	Full Scale ± 5 V Sampling Rate 100 ms/1 DATA 5 Sample Multiplexer
Battery	2	12 V, 100 A
Magnetic sensor (Induction type coil)	3	115 mm ϕ X 1050 mmL ab. 10 kg

(Accessory) M.T. cable a suit, Electrode a suit
Tools a suit, Others a set

2-1-2 Method of measurement

The method of measurement in this MT survey is as shown in the following Fig.II.2.1-1.

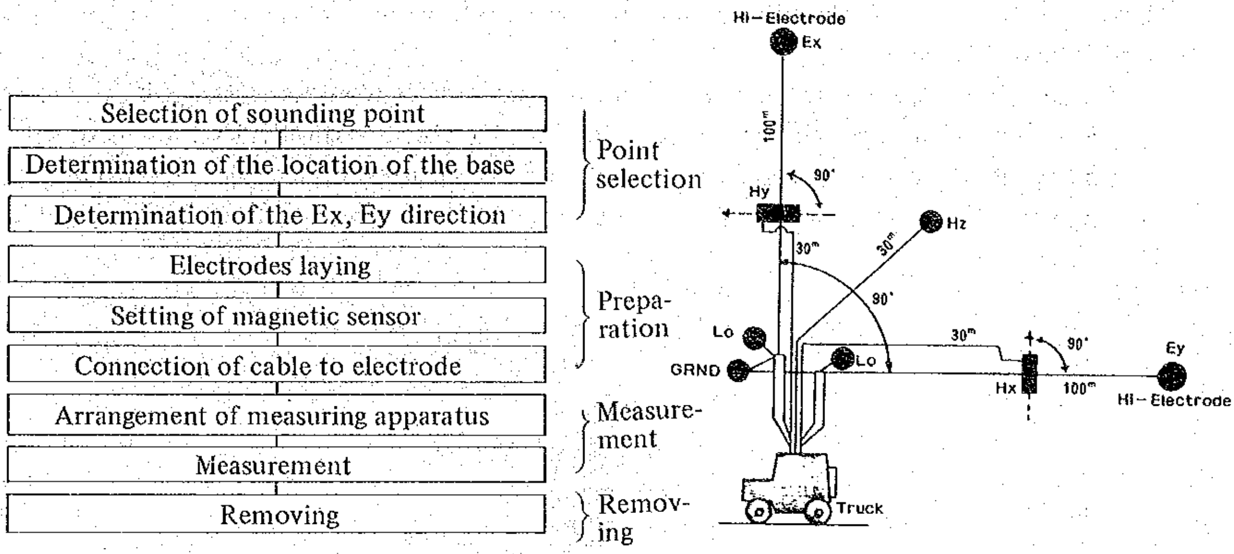

Fig. II.2.1-1 Measurement of MT survey

(1) Selection of sounding points

Measurable point were selected around the programmed point, avoiding steep slopes and confining the bushcutting to weeding. Also, the base points were selected in most appropriate sites in the actual field condition, where it is possible to establish survey lines. Two survey lines of the length of 100 meters were lated out in a L shape array. Directions, topographical undulation and conditions of surrounding area were recorded on the field note at each point.

Relation of the locations of Ex base and Ey base is as shown in the following figure (Fig. II. 2.1-2). In the left-hand side from the base is Ex line and in the right hand side is Ey line.

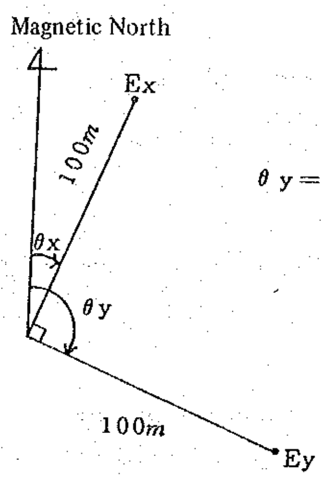

$$\theta y = \theta x + 90°$$

Fig. II.2.1-2 Distribution of survey lines

(2) Preparation

Sensor was placed in a way as shown in Fig. II.2.1-2. The electrodes were placed at 5 sites; 3 at the base and one each at the sites of Ex and Ey. The way of laying these electrodes is shown in Fig. II.2.1-4. A hole 30 cm deep with diameter of 20 cm was sunk, in which water and soil were thrown in to make mud. After laying non-polarized electrode of $CuSO_4$ – Cu system, soil was piled as high as 20 cm.

Hx and Hy coils were placed on the wooden stand with the coil axes. Also, coil for Hz was buried as deep as about 60 cm with its head upward. To stand it vertically, level was used. After confirming the directions of coils, levelling and perpendicularity, wooden box or polyethylene bucket was put on them and fixed with soil cover to avoid direct sunbeam and wind. (Fig. II.2.1-5,6).

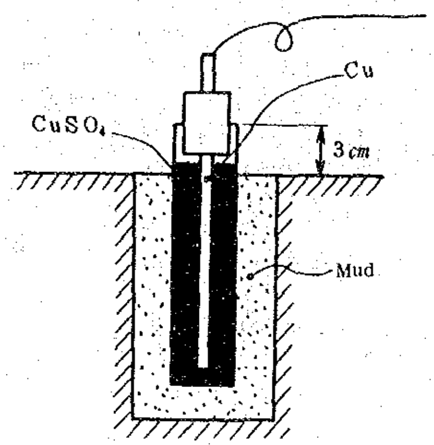

Fig. II.2.1-4 Way of laying electrode

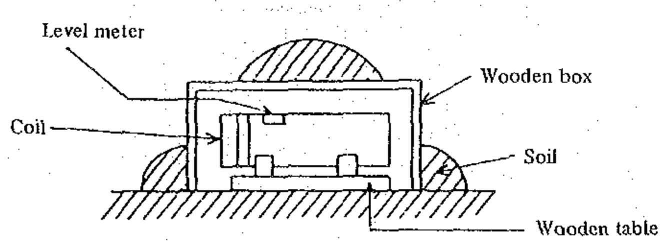

Fig. II.2.1-5 Way of setting Hx, Hy coils

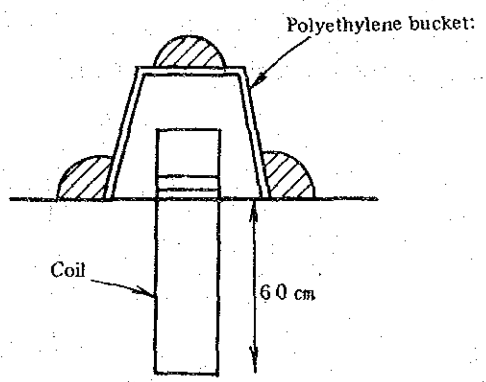

Fig. II.2.1-6 Way of setting Hz coil

The connection of cables to the electrode was by wire-nuts. To avoid direct sun beam, bucket was put on connection box as a covering and weight like soil or stone was placed on it (Fig. II.2.1-7).

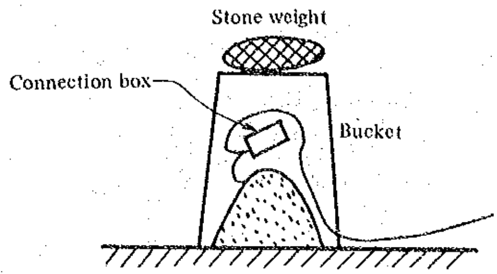

Fig. II.2.1-7 Way of connecting electrode to cable

(3) Measurement

As the process of the measurement, apparatus were connected in the first place, followed by the measurement of coil resistance and earthing resistance. After connection of the cables to the pannel, adjustment of the amplifier and setting the cassette tape to the data logger, signals were checked for a while. Then recording began by starting the data logger.

In the course of the measurement, the graphic paper was being watched to check noises. For the analysis of electromagnetic field of the period up to 200 second, recording of data was continued for more than 2 hours, and for more than 4 files of noiseless data, taking 21 minutes' record to be one file in case of single measurement.

2-2 Measurement of CSAMT method

2-2-1 Apparatus for measurement

For the measurement of CSAMT method, the following apparatus were employed.

Table II.2.1-2. Apparatus for the measurement by CSAMT method

Apparatus	Amount	Specification
Transmitter	1	Frequency 280, 140, 70, 35, 17.5, 8.75 4.38 2.19 1.09 Hz Power 1 kW
Receiver	2	Input level 10 micro V Output Display Digital 4 figures Band Pass Filter, Notch Filter 50 Hz/60 Hz
Sensor	1 set	Telluric Current Sensor x 1 Magnetic Field Sensor x 2

(Accessory)

Tools a set

Others a set

2-2-2 **Method of measurement**

Method of measurement by CSAMT survey is shown in Fig. II.2.1-8, roughly.

After generating power by 1 kw generator, electric current of 9 steps of 280, 140, 70, 35, 17.5, 8.75, 4.38, 2.19 and 1.09 Hz were input into a square loop of a side of the approximate length of 300 meters, to generate artificial magnetic field.

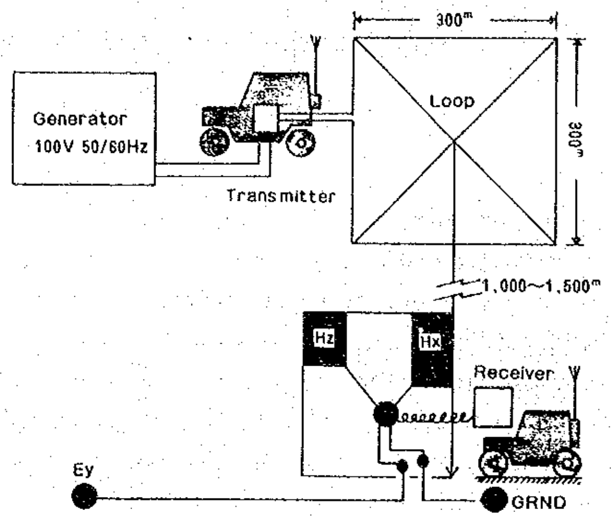

Fig. II.2.1-8 Method of measurement of CSAMT survey

Setting the receiver alow 700 to 1,500 meters from the loop, the signals were received by sensors of Hx, Hz and Ey. As the signals were as small as 10 micro V to 20 micro V, they were amplified by the amplifier. After passing the band pass filter, which was tuned to the same frequency of the loop current, and passing the knotch filter of 50 Hz, they were finally read on the display as the digitalized value averaged.

3. **Method of analysis**

The processes of the analysis are exhibited in the following figure (Fig. II.2.1-9).

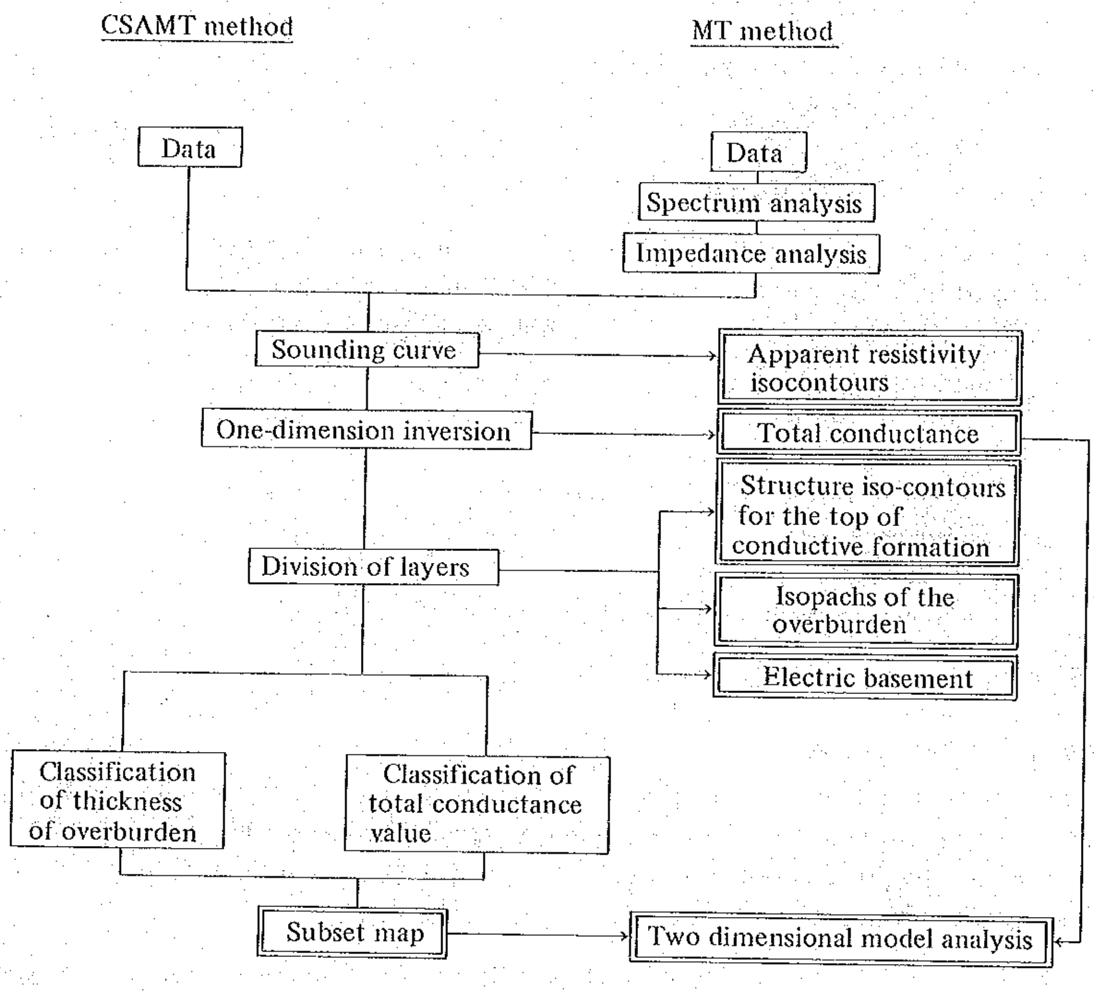

Fig. II.2.1-9 Analysis process of CSAM method and MT method

The results of the data processing of the measured values recorded in the field and the digital data obtained by the analysis of the results are shown on Fig. II.2.1-10 ~ 42.

In the above figures, the apparent resistivity values actually measured at every sounding point are expressed with the apparent resistivity curves which were obtained by the execution of inversion program based on the horizontal multi-layered models.

The apparent resistivity values are those after the axes of the coordinate are rotated to the main axes or to the main trend. The average of the rotation angles was also noted by the unit of degree.

The results of the CSAMT method were also plotted on the same plan of the MT method.

3-1 Results of the CSAMT method

The apparent resistivity was calculated from the field records of the measured values, according to the following formula.

$$\rho a = (K/\mu_o f)\,[Ey/Hx]^2$$

Here ρa : apparent resistivity (ohm-m)
μ_o : magnetic permeability
f : frequency (Hz)
K : correction coefficient

This formula is similar to that used as the base for the MT method. However, in this case of the formula for CSAMT method, correction coefficient K which is a function of (Hx/Hz) is included. The apparent resistivity is obtained according to the following formula, too.

$$\rho_a = K''\mu_o r^2\ 2\pi f/(9Hx/Hz)$$

Here ρ_a : apparent resistivity (ohm-m)
μ_o : magnetic permeability
f : frequency (Hz)
K″ : correction coefficient
r : distance between the receiver and the center of the loop (m)

In this formula, K″ is also a function of Hx/Hz.

3-2 Results of MT method

The results of the digital calculation on the measured values recorded in the field are summarized respectively at every survey point and are exhibited in the Fig. II.2.1-10 ~ 42. It is only the most appropriate values of the outputs from the computer that are listed there.

Details of the items listed are as follows.

(1) Plot of the frequency (with error bar displayed) against the measured values of apparent resistivity, after rotation of the coordinate system.
(2) Apparent resistivity curve by the calculation based on the columnar distribution of the resistivity obtained from the inversion analysis.
(3) Average angle of rotation
(4) Total conductance value
(5) Columnar distribution of the resistivity obtained from the inversion analysis (horizontal multi-layered model).
(6) Digital list of the above (2)
(7) Digital list of the above (1)

In some cases, (1) and (2) are not coincident in the area where the periods are rather long (near T = 100 sec). The reason is that the resistivity distribution at the extreme depth (40 to 60 km) was not considered.

3-2-1 Rotation angle

$$\theta z = \frac{1}{4} \arctan \frac{2Re[(Zyy - Zxx)(Zxy* + Zyx*)]}{|Zxy + Zyx|^2 - |Zyy - Zxx|^2}$$

According to the above formula, the angle θz is determined, so that the diagonal elements of the impedance tensor Zxy and Zyx could take the maximum values (note 1). This angle represents the angle between the X axis actually measured and the direction in which the greatest earth's current is flow (in the axis directions). The values of the rotation angles entered on the digital lists are the average values of the rotation angles in each period. This direction is called to be main direction.

(note 1) The basic formula for the MT analysis is given as below.

$$\begin{vmatrix} Ex \\ Ey \end{vmatrix} = \begin{vmatrix} Zxx \\ Zyx \end{vmatrix}\begin{vmatrix} Zxy \\ Zyy \end{vmatrix} \cdot \begin{vmatrix} Hx \\ Hy \end{vmatrix}$$

The matrix of the coefficients connecting electric field and magnetic field is called impedance tensor.

3-2-2 Apparent resistivity

$$\rho_{ax} = 0.2\ T\ |Zxy|^2$$

The apparent resistivities are the values calculated from the diagonal elements (Zxy and Zyx) of the impedance tensor after the rotation of the coordinate system by such angle as equal to the rotation angle. The parameters were obtained after the impedance tensor was calculated in two ways.

The first way is to solve the following equations of impedance employing power spectrum against magnetic field.

$$\langle Ex\ Hx* \rangle = Zxx \langle Hx\ Hx* \rangle + Zxy \langle Hy\ Hx* \rangle$$
$$\langle Ex\ Hy* \rangle = Zxx \langle Hx\ Hy* \rangle + Zxy \langle Hy\ Hy* \rangle$$
$$\langle Ey\ Hx* \rangle = Zyx \langle Hx\ Hx* \rangle + Zyy \langle Hy\ Hx* \rangle$$
$$\langle Ey\ Hy* \rangle = Zyx \langle Hx\ Hy* \rangle + Zyy \langle Hy\ Hy* \rangle$$

Here $\langle\ \ \rangle$ stands for power spectrum and (*) means paired complex number.

The other way is to solve the following equations using power spectrum against electric field.

$$\langle Ex\ Ex* \rangle = Zxx \langle Hx\ Ex* \rangle + Zxy \langle Hy\ Ex* \rangle$$
$$\langle Ex\ Ey* \rangle = Zxx \langle Hx\ Ey* \rangle + Zxy \langle Hy\ Ey* \rangle$$
$$\langle Ey\ Ex* \rangle = Zyx \langle Hx\ Ex* \rangle + Zyy \langle Hy\ Ex* \rangle$$
$$\langle Ey\ Ey* \rangle = Zyx \langle Hx\ Ey* \rangle + Zyy \langle Hy\ Ey* \rangle$$

If the values of the impedance obtained by the above two ways are close each other, it can be said that noise was small or none in the field of the measurement. If these two values are different, they were affected by fair amount of noise. Here, it is a condition that, in the magnetic and electric fields, the noise has no correlation to them.

In case there is big discrepancy in the results obtained by the above two ways, such values were not employed as the data. Reversely, if they were very close each other, both values were

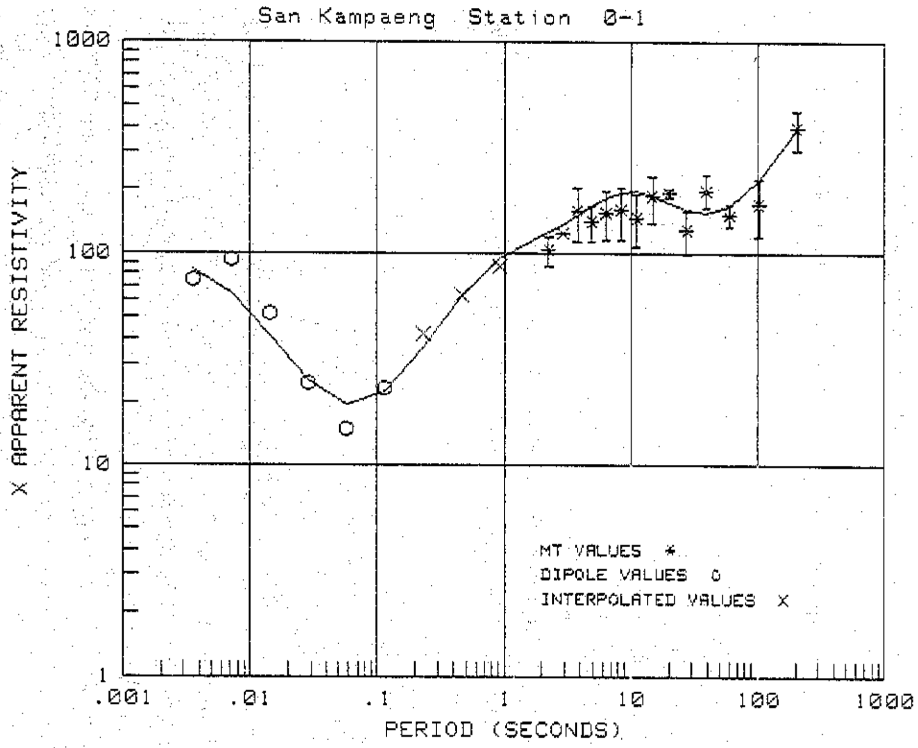

AVERAGE ROTATION ANGLE= 37.0(DEGREES)
TOTAL CONDUCTANCE = 77.0 (MHOS) (FOR TOP 6 LAYERS)

LAYERED MODEL

RESISTIVITY	DEPTH(KM)	ALTITUDE(M)
		560.0 (SURFACE)
12.1	.013	547.0
201.0	.257	303.0
3.0	.310	250.0
32.9	.628	-68.0
3288.5	8.376	-7816.0
5.0	8.601	-8041.0
3545.0	27.000	-26440.0
45.0	35.000	-34440.0

San Kampaeng Station 0-1

MODEL DATA

PERIOD (SECONDS)	APPARENT RESISTIVITY
.0036	84.12
.0071	64.80
.0143	41.06
.0286	25.52
.0570	19.55
.1143	22.64
.2286	36.21
.4571	62.63
.9143	95.40
2.2605	126.45
2.9257	137.27
3.7926	151.07
4.9230	166.92
6.4000	182.01
8.3934	192.46
11.1304	194.13
14.8406	186.21
20.0787	172.27
27.6755	158.83
39.3840	153.25
60.2373	166.55
102.4003	224.01
204.7921	399.99

X-AXIS FIELD DATA

PERIOD (SECONDS)	APPARENT RESISTIVITY
.0036	74.57
.0071	92.70
.0143	51.72
.0286	24.57
.0570	14.84
.1143	23.64
.2286	41.56
.4571	63.06
.9143	86.42
2.2605	103.54 ± 16.781
2.9257	124.68 ± .426
3.7926	158.77 ± 45.662
4.9230	139.90 ± 25.564
6.4000	154.53 ± 39.867
8.3934	160.39 ± 43.946
11.1304	147.23 ± 39.731
14.8406	184.26 ± 46.646
20.0787	190.55 ± 9.868
27.6755	127.92 ± 29.112
39.3840	197.32 ± 35.570
60.2373	150.38 ± 17.707
102.4003	170.22 ± 49.882
204.7921	393.21 ± 86.284

Fig. II.1-10

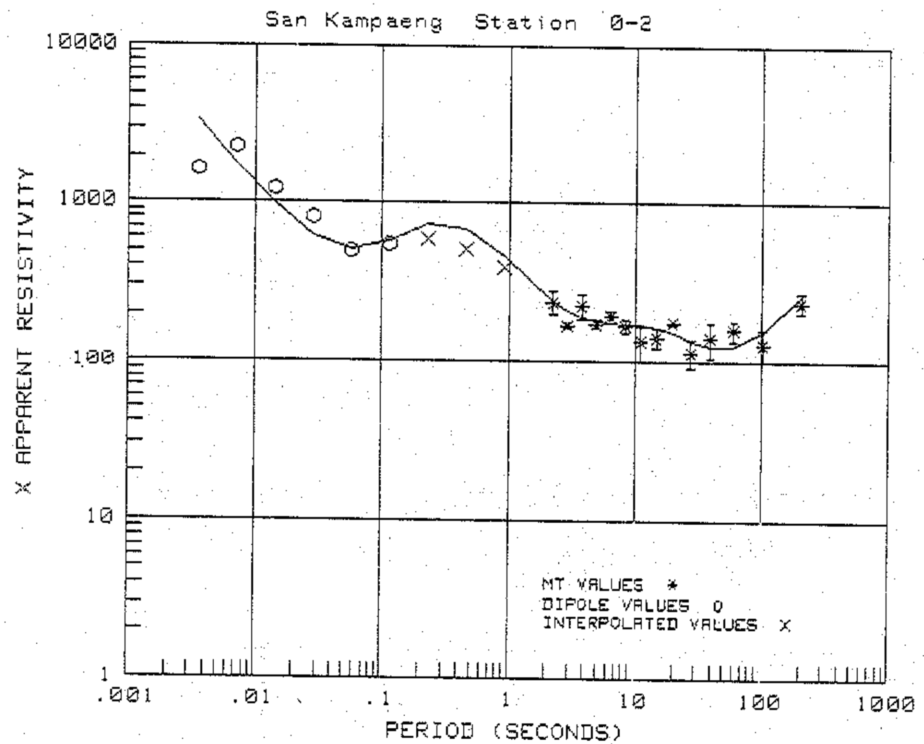

AVERAGE ROTATION ANGLE= -69.0(DEGREES)
TOTAL CONDUCTANCE = 102.0 (MHOS) (FOR TOP 6 LAYERS)
LAYERED MODEL

RESISTIVITY	DEPTH(KM)	ALTITUDE(M)
		630.0 (SURFACE)
20600.0	.450	180.0
5000.0	1.259	-629.0
3.0	1.272	-642.0
1461.8	5.109	-4479.0
1000.0	8.000	-7370.0
5.0	8.460	-7830.0
3460.0	27.000	-26370.0
42.0	36.000	-35370.0

San Kampaeng Station 0-2

MODEL DATA

PERIOD (SECONDS)	APPARENT RESISTIVITY
.0036	3378.26
.0071	1775.07
.0143	980.63
.0286	620.88
.0570	509.64
.1143	583.78
.2286	731.48
.4571	688.04
.9143	460.20
2.2605	240.96
2.9257	209.74
3.7926	189.91
4.9230	179.38
6.4000	175.34
8.3934	174.10
11.1304	171.38
14.8406	163.88
20.0787	151.21
27.6755	136.71
39.3840	125.87
60.2373	126.77
102.4003	157.24
204.7921	266.76

X-AXIS FIELD DATA

PERIOD (SECONDS)	APPARENT RESISTIVITY
.0036	1625.74
.0071	2269.35
.0143	1232.36
.0286	812.39
.0570	504.49
.1143	550.90
.2286	585.24
.4571	510.84
.9143	387.93
2.2605	237.42 ± 38.960
2.9257	169.02 ± 5.581
3.7926	225.65 ± 41.254
4.9230	174.16 ± 9.713
6.4000	196.02 ± 11.922
8.3934	168.83 ± 15.291
11.1304	135.22 ± 34.133
14.8406	142.31 ± 19.865
20.0787	175.25 ± 3.105
27.6755	114.17 ± 23.377
39.3840	142.64 ± 35.992
60.2373	158.44 ± 23.204
102.4003	130.01 ± 29.105
204.7921	237.81 ± 33.697

Fig. II.1-11

San Kampaeng Station 0-3

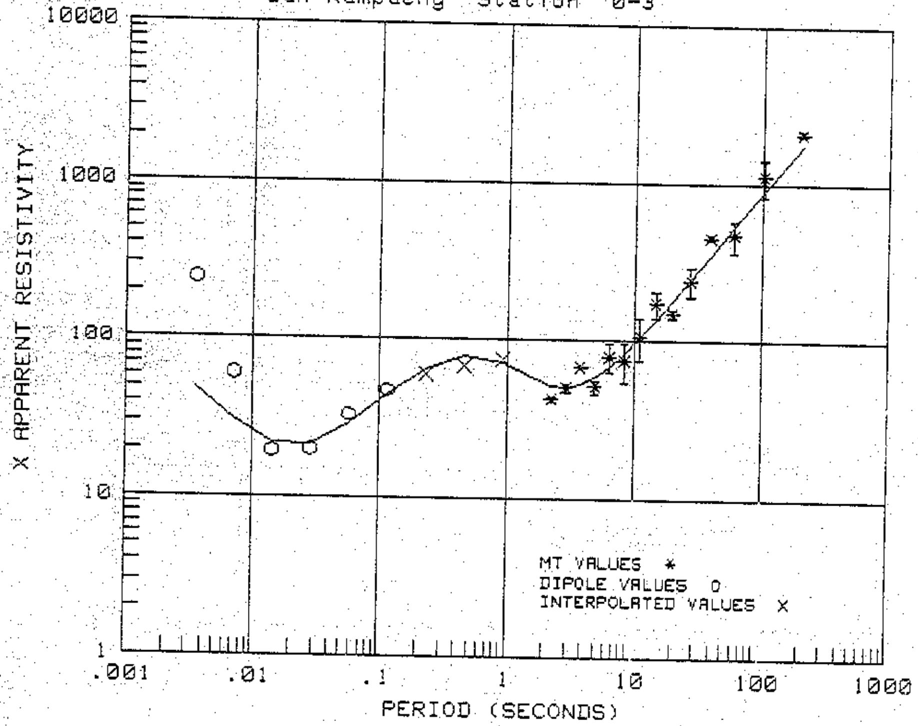

AVERAGE ROTATION ANGLE= 16.0(DEGREES)
TOTAL CONDUCTANCE = 119.8 (MHOS) (FOR TOP 6 LAYERS)

LAYERED MODEL

RESISTIVITY	DEPTH(KM)	ALTITUDE(M)
		710.0 (SURFACE)
930.5	.068	642.0
18.6	.205	505.0
3.0	.234	476.0
2791.4	2.046	-1336.0
50.0	5.000	-4290.0
5.0	5.215	-4505.0

MODEL DATA

PERIOD (SECONDS)	APPARENT RESISTIVITY
.0036	48.76
.0071	31.32
.0143	21.81
.0286	21.37
.0570	29.58
.1143	45.81
.2286	65.28
.4571	79.10
.9143	72.07
2.2605	52.81
2.9257	51.77
3.7926	53.75
4.9230	59.19
6.4000	68.63
8.3934	83.35
11.1304	105.21
14.8406	136.17
20.0787	181.00
27.6755	246.92
39.3840	349.34
60.2373	532.57
102.4003	903.89
204.7921	1806.56

San Kampaeng Station 0-3

X-AXIS FIELD DATA

PERIOD (SECONDS)	APPARENT RESISTIVITY
.0036	240.17
.0071	60.49
.0143	19.69
.0286	20.22
.0570	33.69
.1143	48.42
.2286	60.58
.4571	69.51
.9143	75.11
2.2605	43.19 ± 1.569
2.9257	50.97 ± 3.393
3.7926	69.03 ± .507
4.9230	52.24 ± 5.104
6.4000	79.98 ± 16.657
8.3934	76.52 ± 20.716
11.1304	106.60 ± 30.986
14.8406	172.14 ± 32.371
20.0787	147.49 ± 9.847
27.6755	242.82 ± 51.645
39.3840	454.25 ± 16.822
60.2373	473.08 ± 108.888
102.4003	1139.38 ± 307.718
204.7921	2144.23 ± 80.168

Fig. II.1-12

San Kampaeng Station 1-0

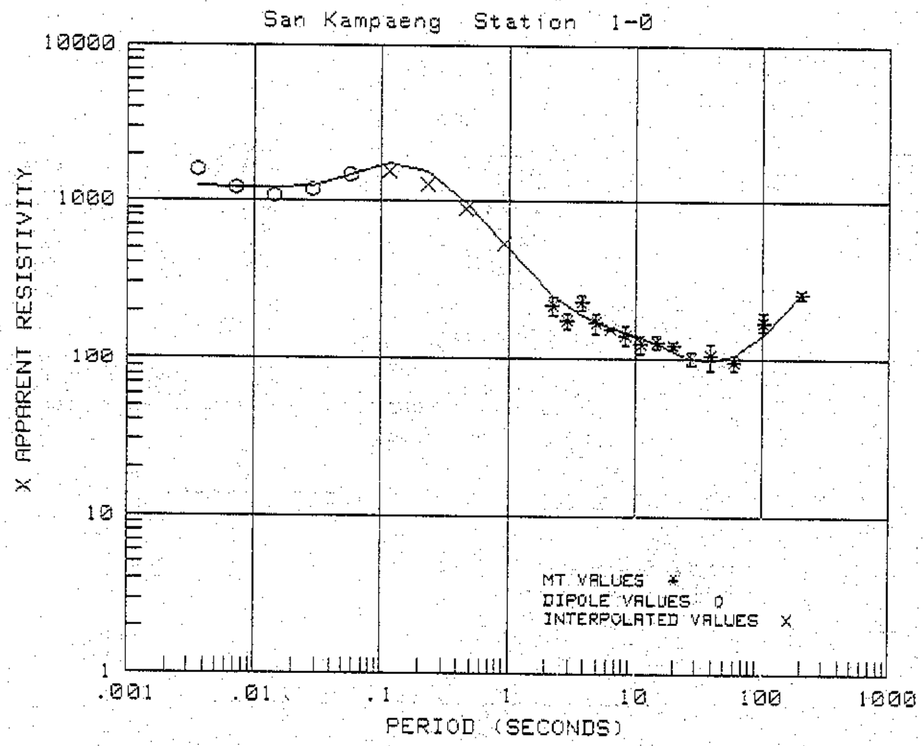

AVERAGE ROTATION ANGLE= 66.0(DEGREES)
TOTAL CONDUCTANCE = 115.4 (MHOS) (FOR TOP 6 LAYERS)

LAYERED MODEL

RESISTIVITY	DEPTH(KM)	ALTITUDE(M)
		362.0 (SURFACE)
3612.3	.439	-77.0
3.0	.440	-78.0
1422.4	3.566	-3204.0
1682.1	7.757	-7395.0
60.2	7.943	-7581.0
5.0	8.479	-8117.0
3200.0	22.000	-21638.0
30.0	28.000	-27638.0

MODEL DATA

PERIOD (SECONDS)	APPARENT RESISTIVITY
.0036	1261.70
.0071	1218.95
.0143	1222.67
.0286	1254.25
.0570	1465.56
.1143	1743.81
.2286	1542.81
.4571	977.91
.9143	536.77
2.2605	255.62
2.9257	217.38
3.7926	191.13
4.9230	173.68
6.4000	161.49
8.3934	150.77
11.1304	138.83
14.8406	125.38
20.0787	111.90
27.6755	101.53
39.3840	97.91
60.2373	107.50
102.4003	146.46
204.7921	263.65

San Kampaeng Station 1-0

X-AXIS FIELD DATA

PERIOD (SECONDS)	APPARENT RESISTIVITY
.0036	1574.32
.0071	1232.37
.0143	1090.09
.0286	1184.21
.0570	1492.02
.1143	1550.20
.2286	1276.58
.4571	882.95
.9143	542.14
2.2605	218.31 ± 28.971
2.9257	175.40 ± 18.061
3.7926	228.59 ± 24.813
4.9230	170.23 ± 23.213
6.4000	156.62 ± 3.925
8.3934	142.82 ± 20.490
11.1304	125.90 ± 16.155
14.8406	129.14 ± 11.232
20.0787	122.80 ± 5.300
27.6755	101.91 ± 9.566
39.3840	105.25 ± 20.079
60.2373	96.05 ± 10.370
102.4003	174.13 ± 23.249
204.7921	258.11 ± 15.981

Fig. II.1-13

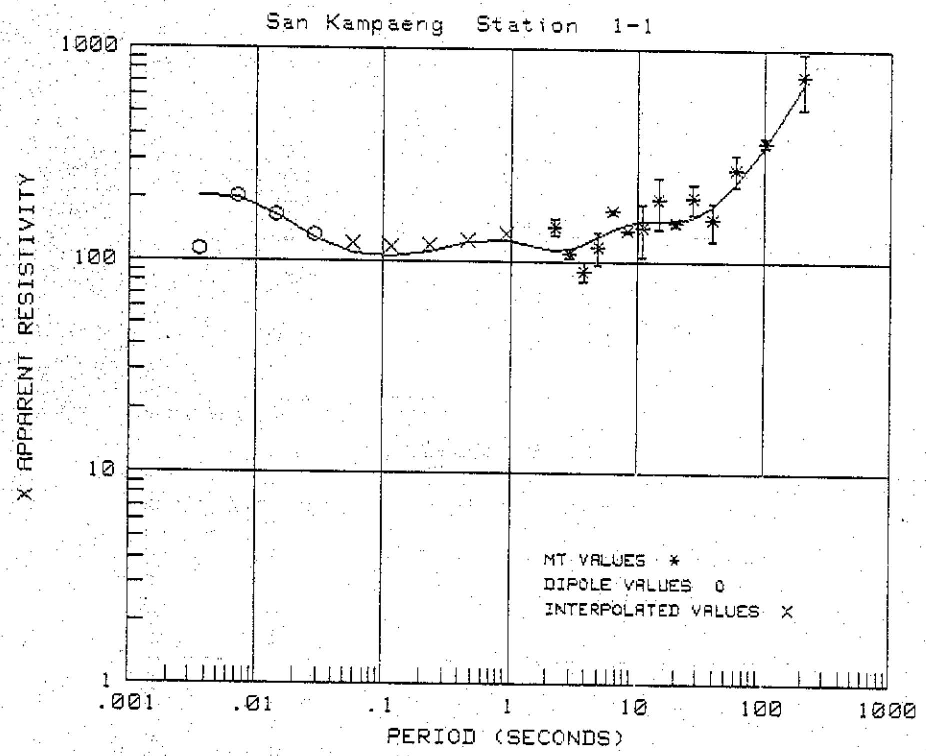

AVERAGE ROTATION ANGLE= -60.0(DEGREES)
TOTAL CONDUCTANCE = 86.7 (MHOS) (FOR TOP 6 LAYERS)

LAYERED MODEL

RESISTIVITY	DEPTH(KM)	ALTITUDE(M)
		395.0 (SURFACE)
206.7	.177	218.0
159.3	.536	-141.0
106.2	.726	-331.0
3.0	.739	-344.0
159.3	7.500	-7105.0
5.0	7.675	-7280.0
3950.0	31.000	-30605.0
29.5	34.000	-33605.0

San Kampaeng Station 1-1

MODEL DATA

PERIOD (SECONDS)	APPARENT RESISTIVITY
.0036	203.18
.0071	199.16
.0143	165.35
.0286	129.13
.0570	110.04
.1143	105.83
.2286	110.66
.4571	124.54
.9143	126.88
2.2605	113.72
2.9257	116.28
3.7926	122.88
4.9230	132.43
6.4000	142.78
8.3934	151.39
11.1304	155.98
14.8406	156.77
20.0787	157.40
27.6755	163.90
39.3840	184.69
60.2373	237.52
102.4003	364.75
204.7921	697.84

X-AXIS FIELD DATA

PERIOD (SECONDS)	APPARENT RESISTIVITY
.0036	113.03
.0071	202.18
.0143	166.50
.0286	134.61
.0570	121.98
.1143	117.87
.2286	119.79
.4571	126.27
.9143	136.23
2.2605	146.40 ± 13.599
2.9257	109.70 ± 5.794
3.7926	90.07 ± 9.135
4.9230	116.75 ± 20.652
6.4000	174.63 ± 5.381
8.3934	140.32 ± 1.672
11.1304	146.35 ± 41.552
14.8406	197.75 ± 55.196
20.0787	155.00 ± 5.301
27.6755	201.55 ± 30.936
39.3840	159.81 ± 33.736
60.2373	277.53 ± 48.265
102.4003	371.69 ± 18.378
204.7921	744.87 ± 212.853

Fig. II.1-14

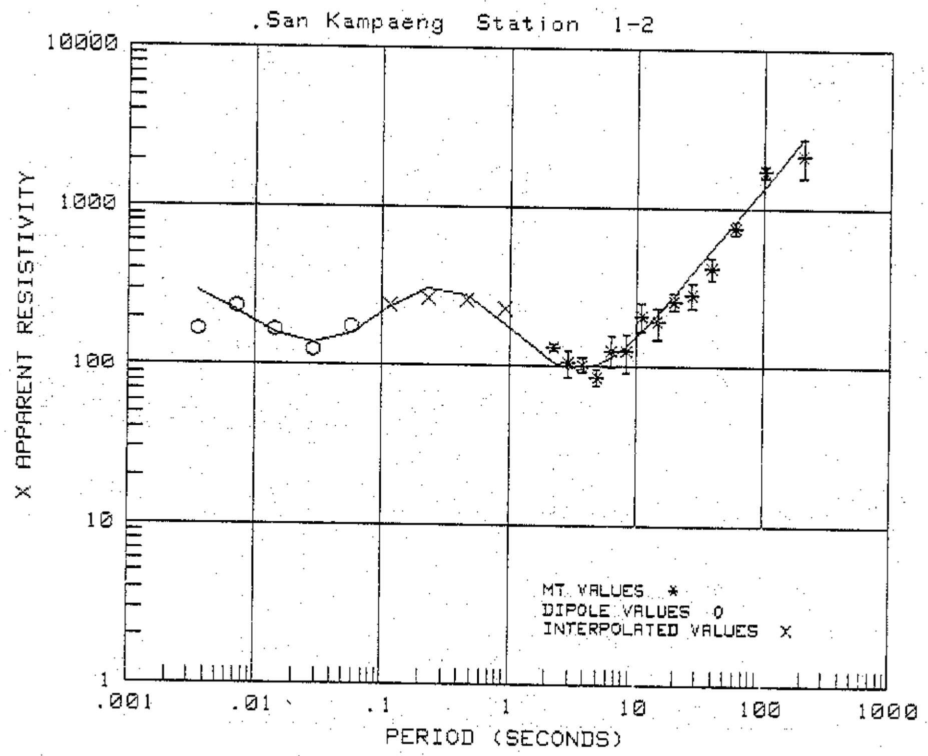

AVERAGE ROTATION ANGLE= -14.0(DEGREES)
TOTAL CONDUCTANCE = 95.7 (MHOS) (FOR TOP 6 LAYERS)

LAYERED MODEL

RESISTIVITY	DEPTH(KM)	ALTITUDE(M)
		388.0 (SURFACE)
268.2	.137	251.0
273.3	.413	-25.0
140.1	.559	-171.0
3.0	.570	-182.0
700.0	5.100	-4712.0
5.0	5.515	-5127.0

San Kampaeng Station 1-2

MODEL DATA

PERIOD (SECONDS)	APPARENT RESISTIVITY
.0036	289.95
.0071	219.17
.0143	160.06
.0286	139.76
.0570	162.00
.1143	233.69
.2286	308.15
.4571	279.75
.9143	184.11
2.2605	105.93
2.9257	98.50
3.7926	97.39
4.9230	102.78
6.4000	115.23
8.3934	136.46
11.1304	169.31
14.8406	216.77
20.0787	286.19
27.6755	388.91
39.3840	548.98
60.2373	835.84
102.4003	1417.73
204.7921	2832.83

X-AXIS FIELD DATA

PERIOD (SECONDS)	APPARENT RESISTIVITY
.0036	169.44
.0071	233.54
.0143	168.93
.0286	125.02
.0570	175.54
.1143	239.57
.2286	268.78
.4571	260.53
.9143	228.90
2.2605	132.71 ± 7.539
2.9257	105.47 ± 19.123
3.7926	102.18 ± 11.029
4.9230	85.87 ± 10.369
6.4000	127.30 ± 29.683
8.3934	125.78 ± 33.584
11.1304	211.50 ± 44.242
14.8406	192.42 ± 42.559
20.0787	260.64 ± 31.069
27.6755	286.65 ± 51.639
39.3840	419.96 ± 65.621
60.2373	753.40 ± 77.990
102.4003	1751.71 ± 142.939
204.7921	2181.06 ± 595.882

Fig. II.1-15

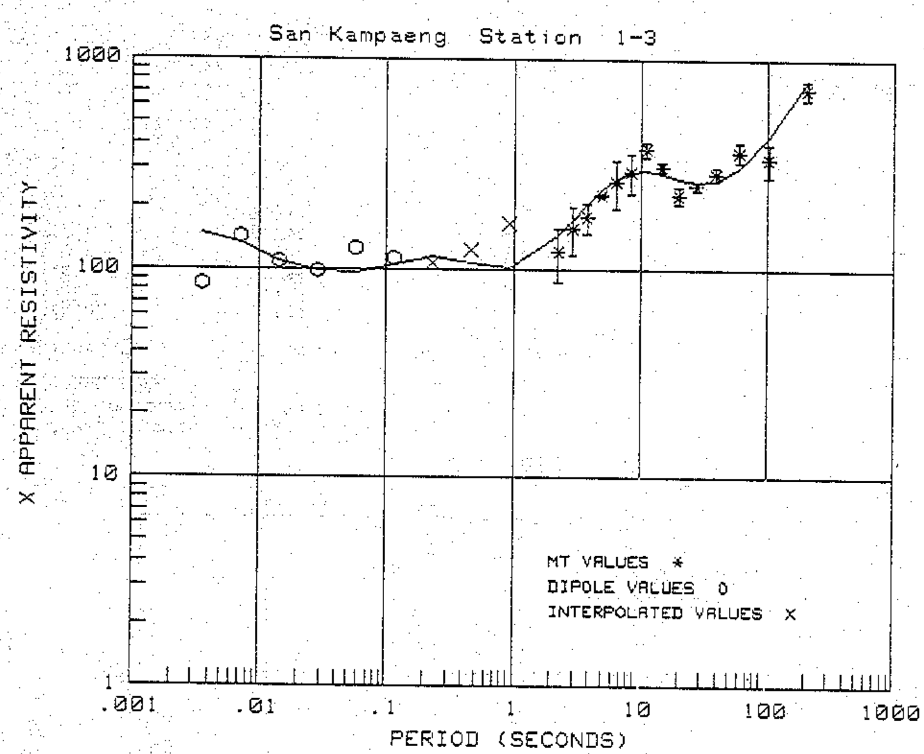

AVERAGE ROTATION ANGLE= -64.0(DEGREES)
TOTAL CONDUCTANCE = 49.3 (MHOS) (FOR TOP 6 LAYERS)

LAYERED MODEL

RESISTIVITY	DEPTH(KM)	ALTITUDE(M)
		383.0 (SURFACE)
80.0	.050	333.0
187.1	.342	41.0
95.9	.463	-80.0
3.0	.472	-89.0
150.0	4.500	-4117.0
5.0	4.580	-4197.0
3845.0	34.000	-33617.0
48.0	40.000	-39617.0

San Kampaeng Station 1-3

MODEL DATA

PERIOD (SECONDS)	APPARENT RESISTIVITY
.0036	148.64
.0071	132.69
.0143	109.49
.0286	97.71
.0570	96.86
.1143	104.80
.2286	114.63
.4571	107.35
.9143	101.78
2.2605	146.42
2.9257	173.10
3.7926	204.90
4.9230	238.67
6.4000	269.11
8.3934	290.17
11.1304	296.30
14.8406	287.90
20.0787	272.22
27.6755	260.36
39.3840	265.00
60.2373	307.49
102.4003	437.75
204.7921	806.59

X-AXIS FIELD DATA

PERIOD (SECONDS)	APPARENT RESISTIVITY		
.0036	85.21		
.0071	144.13		
.0143	110.29		
.0286	97.96		
.0570	125.52		
.1143	112.60		
.2286	108.07		
.4571	124.96		
.9143	164.90		
2.2605	121.61	+	35.892
2.9257	158.08	+	41.125
3.7926	177.71	+	29.187
4.9230	225.15	+	4.855
6.4000	261.58	+	67.211
8.3934	292.28	+	60.675
11.1304	374.68	+	30.155
14.8406	308.79	+	17.979
20.0787	226.54	+	20.723
27.6755	250.27	+	13.269
39.3840	286.50	+	20.318
60.2373	364.49	+	36.810
102.4003	336.91	+	61.811
204.7921	715.57	+	70.738

Fig. II.1-16

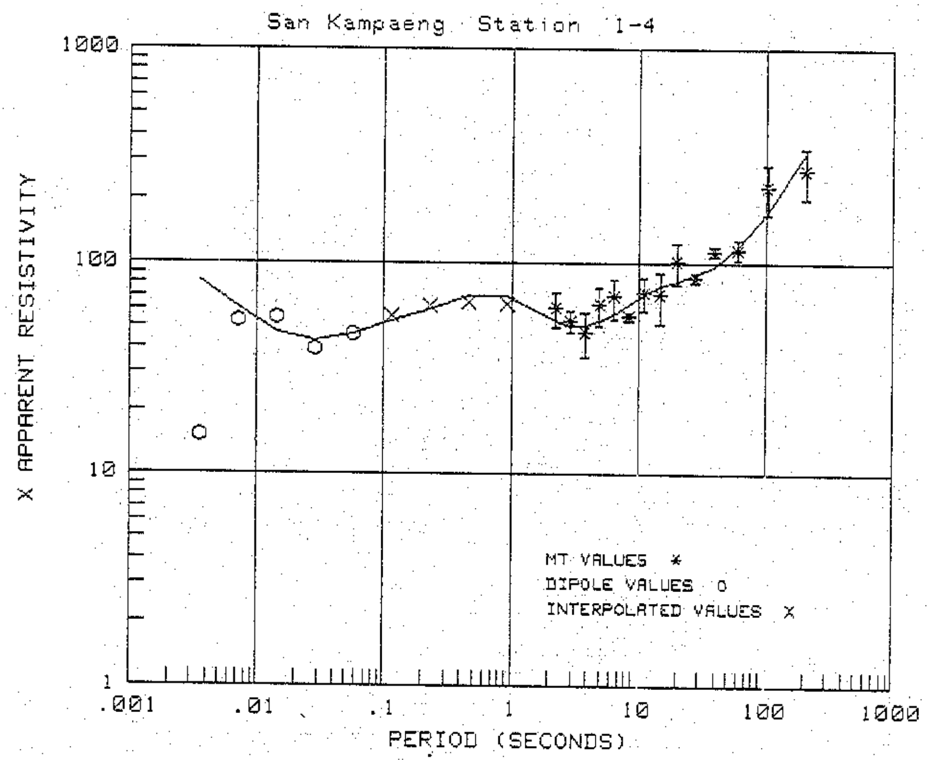

AVERAGE ROTATION ANGLE= 14.0(DEGREES)
TOTAL CONDUCTANCE = 147.4 (MHOS) (FOR TOP 7 LAYERS)

LAYERED MODEL

RESISTIVITY	DEPTH(KM)	ALTITUDE(M)
		380.0 (SURFACE)
75.1	.073	307.0
76.6	.219	161.0
39.2	.296	84.0
3.0	.319	61.0
622.0	.800	-420.0
75.0	4.800	-4420.0
5.0	5.204	-4824.0
4150.0	31.000	-30620.0
46.0	37.000	-36620.0

San Kampaeng Station 1-4

MODEL DATA

PERIOD (SECONDS)	APPARENT RESISTIVITY
.0036	81.36
.0071	61.82
.0143	46.29
.0286	42.30
.0570	46.20
.1143	52.88
.2286	59.83
.4571	69.57
.9143	69.46
2.2605	52.60
2.9257	50.27
3.7926	50.24
4.9230	52.60
6.4000	57.14
8.3934	63.45
11.1304	70.55
14.8406	77.00
20.0787	82.30
27.6755	87.61
39.3840	96.88
60.2373	119.29
102.4003	175.86
204.7921	329.12

X-AXIS FIELD DATA

PERIOD (SECONDS)	APPARENT RESISTIVITY
.0036	15.10
.0071	52.66
.0143	54.97
.0286	39.01
.0570	45.90
.1143	56.46
.2286	62.83
.4571	64.89
.9143	63.77
2.2605	61.06 ± 11.551
2.9257	52.97 ± 6.455
3.7926	46.75 ± 11.379
4.9230	63.06 ± 12.587
6.4000	69.13 ± 14.811
8.3934	55.51 ± 2.690
11.1304	72.02 ± 13.444
14.8406	70.33 ± 19.133
20.0787	101.89 ± 22.994
27.6755	84.51 ± 4.511
39.3840	113.90 ± 5.831
60.2373	116.48 ± 12.692
102.4003	226.73 ± 58.574
204.7921	271.34 ± 72.789

Fig. II.1-17

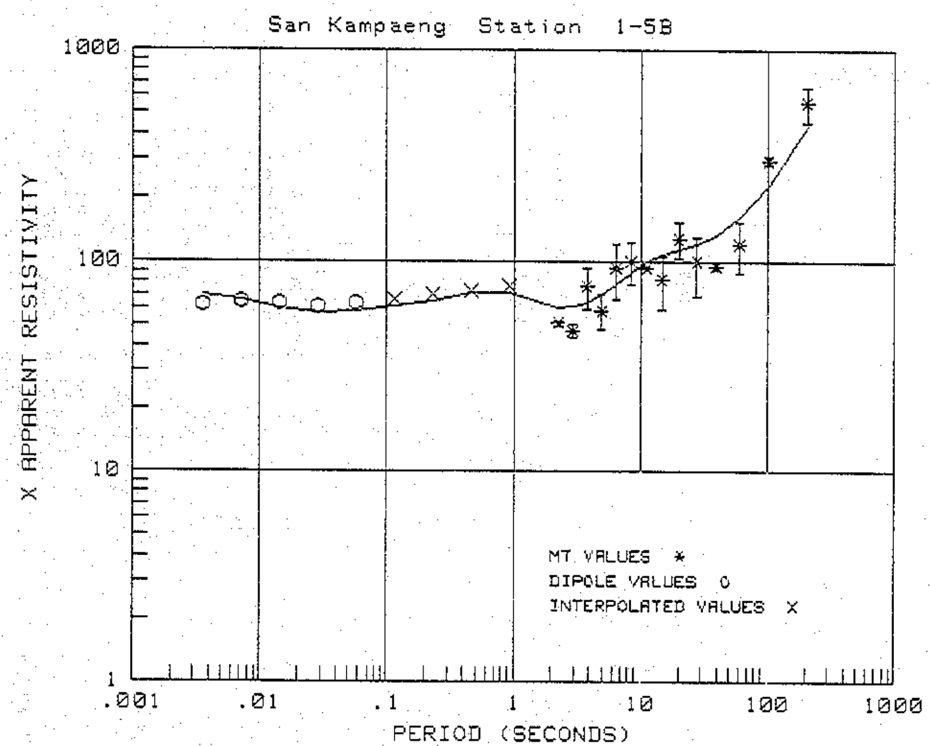

AVERAGE ROTATION ANGLE= 19.0(DEGREES)
TOTAL CONDUCTANCE = 120.2 (MHOS) (FOR TOP 6 LAYERS)

LAYERED MODEL

RESISTIVITY	DEPTH(KM)	ALTITUDE(M)
		390.0 (SURFACE)
65.0	.091	299.0
70.0	.273	117.0
61.4	.370	20.0
3.0	.377	13.0
80.0	6.000	-5610.0
5.0	6.210	-5820.0
4235.0	35.000	-34610.0
33.0	39.000	-38610.0

San Kampaeng Station 1-5B

MODEL DATA

PERIOD (SECONDS)	APPARENT RESISTIVITY
.0036	69.99
.0071	66.15
.0143	59.90
.0286	56.97
.0570	57.83
.1143	60.91
.2286	64.53
.4571	70.38
.9143	71.00
2.2605	60.66
2.9257	60.90
3.7926	63.90
4.9230	69.79
6.4000	78.21
8.3934	88.50
11.1304	99.13
14.8406	107.88
20.0787	114.20
27.6755	119.97
39.3840	130.75
60.2373	158.82
102.4003	231.87
204.7921	431.85

X-AXIS FIELD DATA

PERIOD (SECONDS)	APPARENT RESISTIVITY
.0036	62.43
.0071	65.24
.0143	63.03
.0286	61.05
.0570	63.18
.1143	66.30
.2286	69.41
.4571	72.54
.9143	75.76
2.2605	50.76 ± 1.471
2.9257	46.66 ± 3.263
3.7926	76.17 ± 17.310
4.9230	58.16 ± 11.016
6.4000	92.51 ± 26.918
8.3934	99.63 ± 21.623
11.1304	93.73 ± .326
14.8406	82.46 ± 23.178
20.0787	127.67 ± 23.378
27.6755	99.19 ± 30.612
39.3840	94.89 ± 3.254
60.2373	119.46 ± 31.451
102.4003	298.51 ± 13.852
204.7921	557.09 ± 107.263

Fig. II.1-18

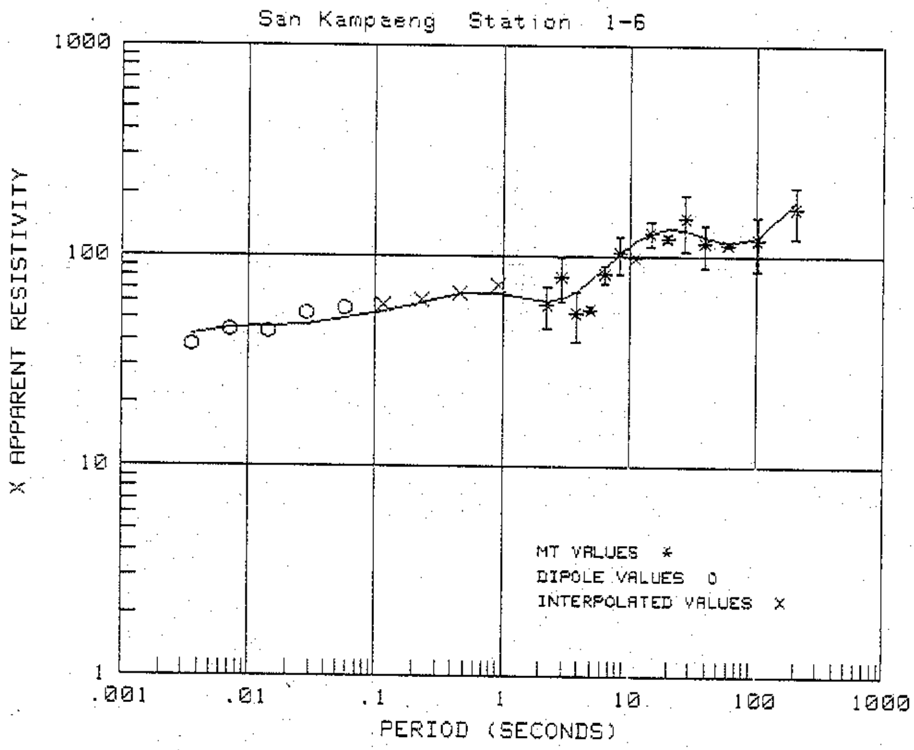

AVERAGE ROTATION ANGLE= -72.0(DEGREES)
TOTAL CONDUCTANCE = 112.4 (MHOS) (FOR TOP 6 LAYERS)

LAYERED MODEL

RESISTIVITY	DEPTH(KM)	ALTITUDE(M)
		405.0 (SURFACE)
35.0	.090	315.0
70.0	.273	132.0
61.4	.370	35.0
3.0	.377	28.0
80.0	6.000	-5595.0
5.0	6.165	-5760.0
4230.0	32.000	-31595.0
25.0	39.000	-38595.0

MODEL DATA

PERIOD (SECONDS)	APPARENT RESISTIVITY
.0036	41.77
.0071	45.27
.0143	45.68
.0286	46.66
.0570	49.79
.1143	54.47
.2286	59.50
.4571	65.95
.9143	66.31
2.2605	59.87
2.9257	62.01
3.7926	67.23
4.9230	75.77
6.4000	87.48
8.3934	101.95
11.1304	117.34
14.8406	129.83
20.0787	135.72
27.6755	132.93
39.3840	123.85
60.2373	115.56
102.4003	123.80
204.7921	184.93

San Kampaeng Station 1-6

X-AXIS FIELD DATA

PERIOD (SECONDS)	APPARENT RESISTIVITY
.0036	37.73
.0071	44.01
.0143	43.12
.0286	53.12
.0570	56.17
.1143	57.56
.2286	60.84
.4571	65.84
.9143	72.40
2.2605	57.96 ± 13.003
2.9257	78.66 ± 18.859
3.7926	52.62 ± 13.890
4.9230	55.26 ± 1.387
6.4000	81.67 ± 8.289
8.3934	103.56 ± 21.287
11.1304	98.71 ± .298
14.8406	127.97 ± 17.408
20.0787	121.94 ± 5.034
27.6755	151.76 ± 45.223
39.3840	114.68 ± 26.243
60.2373	114.37 ± 2.711
102.4003	119.25 ± 34.727
204.7921	168.36 ± 45.764

Fig. II.1-19

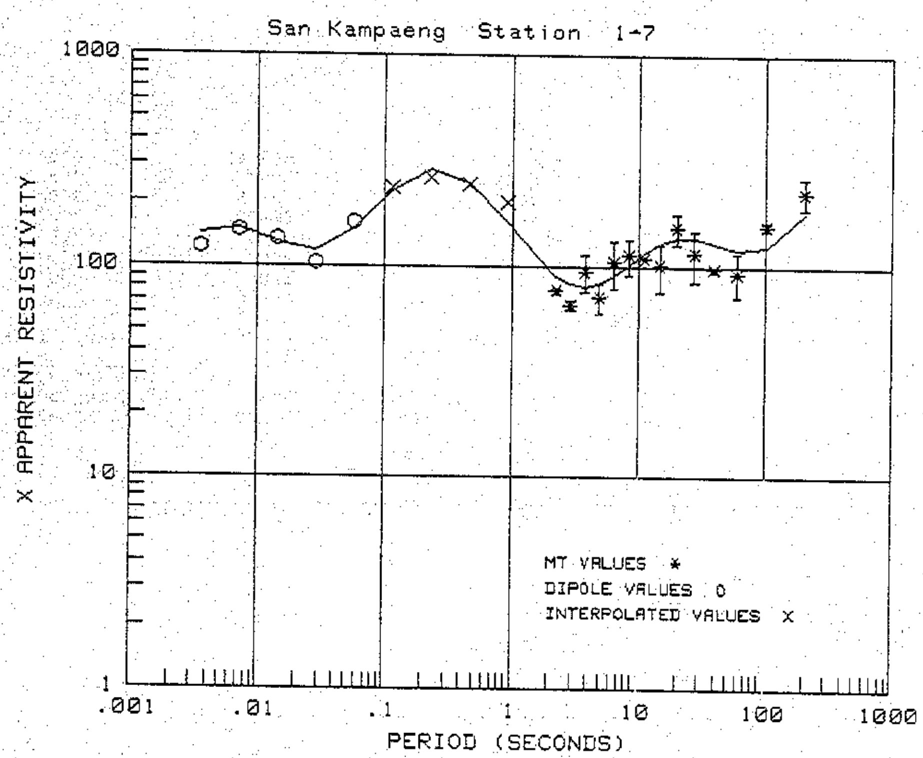

AVERAGE ROTATION ANGLE= -77.0(DEGREES)
TOTAL CONDUCTANCE = 117.3 (MHOS) (FOR TOP 6 LAYERS)

LAYERED MODEL

RESISTIVITY	DEPTH(KM)	ALTITUDE(M)
		390.0 (SURFACE)
112.4	.161	229.0
224.9	.490	-100.0
197.2	.664	-274.0
3.0	.676	-286.0
1500.0	4.500	-4110.0
5.0	5.035	-4645.0
4352.0	34.000	-33610.0
28.0	42.000	-41610.0

MODEL DATA

PERIOD (SECONDS)	APPARENT RESISTIVITY
.0036	140.24
.0071	149.60
.0143	128.87
.0286	118.67
.0570	149.48
.1143	224.71
.2286	288.61
.4571	249.02
.9143	159.11
2.2605	89.94
2.9257	82.97
3.7926	81.00
4.9230	83.75
6.4000	90.84
8.3934	101.85
11.1304	115.43
14.8406	128.24
20.0787	136.38
27.6755	136.40
39.3840	128.79
60.2373	119.46
102.4003	124.08
204.7921	178.66

San Kampaeng Station 1-7

X-AXIS FIELD DATA

PERIOD (SECONDS)	APPARENT RESISTIVITY
.0036	121.93
.0071	145.60
.0143	133.73
.0286	104.24
.0570	160.01
.1143	232.67
.2286	261.82
.4571	243.29
.9143	198.75
2.2605	77.10 ± 1.954
2.9257	65.99 ± 4.038
3.7926	94.60 ± 18.810
4.9230	71.54 ± 11.856
6.4000	105.38 ± 26.830
8.3934	113.06 ± 21.471
11.1304	109.93 ± .334
14.8406	101.80 ± 25.036
20.0787	150.47 ± 24.108
27.6755	115.74 ± 31.253
39.3840	97.80 ± 2.937
60.2373	93.55 ± 21.552
102.4003	155.28 ± 6.305
204.7921	224.00 ± 37.738

Fig. II.1-20

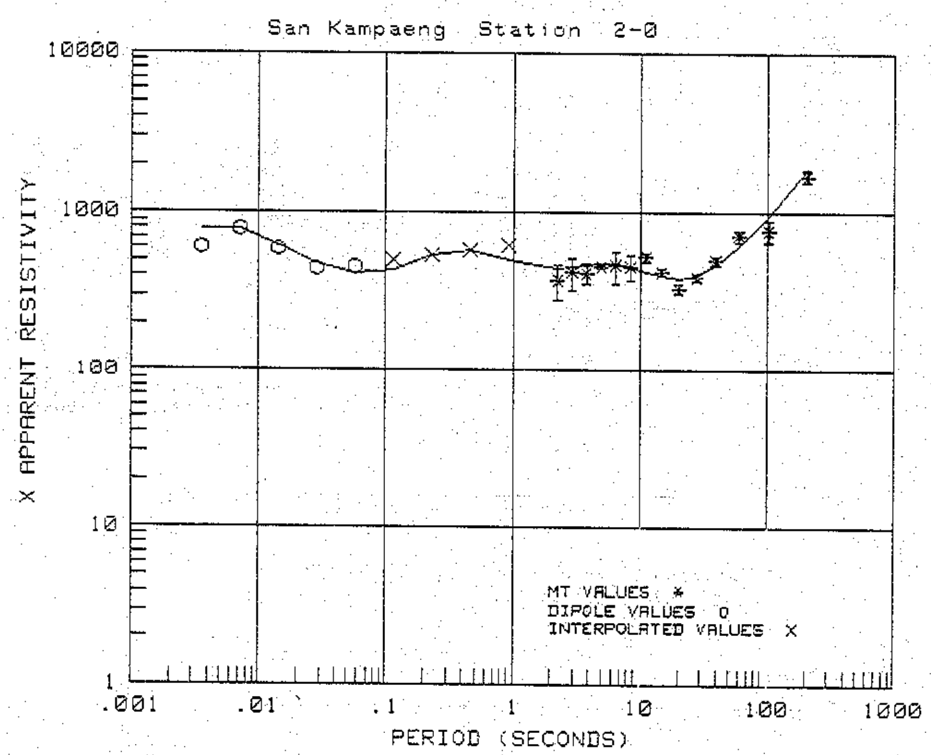

AVERAGE ROTATION ANGLE= 23.0(DEGREES)
TOTAL CONDUCTANCE = 39.4 (MHOS) (FOR TOP 6 LAYERS)

LAYERED MODEL

RESISTIVITY	DEPTH(KM)	ALTITUDE(M)
		383.0 (SURFACE)
650.0	.313	70.0
845.1	.950	-567.0
741.1	1.287	-904.0
3.0	1.296	-913.0
900.0	10.000	-9617.0
5.0	10.125	-9742.0
4280.0	36.000	-35617.0
41.0	39.000	-38617.0

MODEL DATA

PERIOD (SECONDS)	APPARENT RESISTIVITY
.0036	798.99
.0071	794.03
.0143	622.21
.0286	470.64
.0570	407.31
.1143	428.42
.2286	531.88
.4571	583.86
.9143	496.68
2.2605	437.71
2.9257	450.28
3.7926	456.26
4.9230	475.93
6.4000	471.72
8.3934	452.09
11.1304	423.14
14.8406	397.30
20.0787	386.51
27.6755	403.41
39.3840	465.11
60.2373	615.52
102.4003	965.50
204.7921	1866.28

San Kampaeng Station 2-0

X-AXIS FIELD DATA

PERIOD (SECONDS)	APPARENT RESISTIVITY
.0036	602.81
.0071	799.48
.0143	590.02
.0286	444.69
.0570	454.42
.1143	493.93
.2286	533.28
.4571	572.99
.9143	613.91
2.2605	373.42 ± 95.515
2.9257	416.42 ± 93.886
3.7926	412.65 ± 58.736
4.9230	452.55 ± 8.458
6.4000	460.16 ± 102.580
8.3934	454.94 ± 81.849
11.1304	520.14 ± 36.281
14.8406	422.28 ± 21.308
20.0787	330.30 ± 26.186
27.6755	389.86 ± 17.915
39.3840	497.82 ± 30.598
60.2373	714.41 ± 62.530
102.4003	772.75 ± 122.868
204.7921	1683.76 ± 144.256

Fig. II.1-21

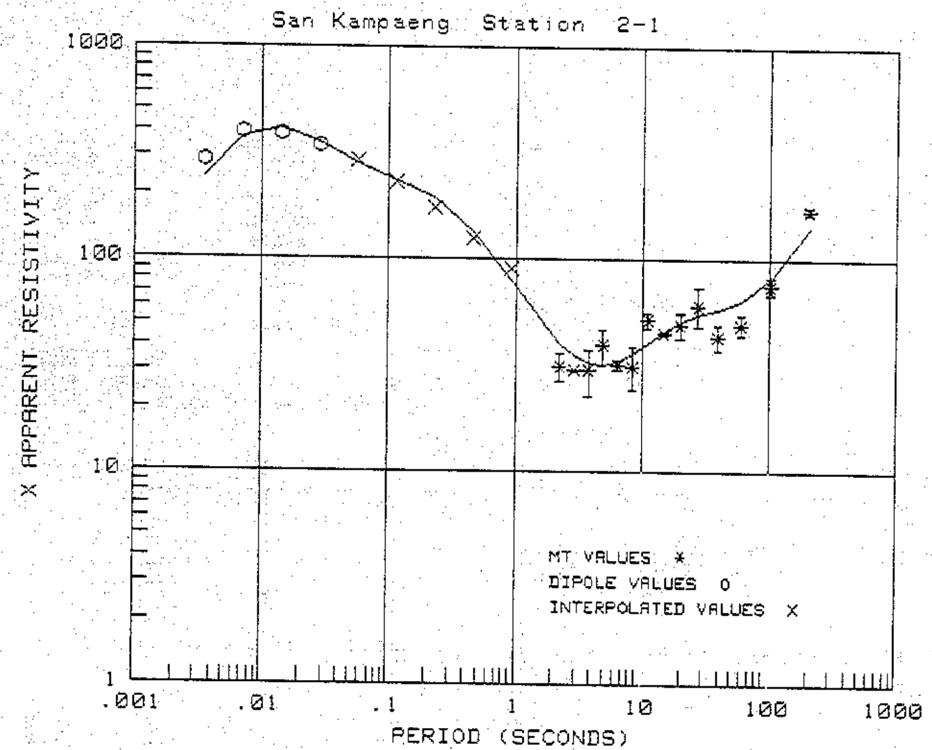

AVERAGE ROTATION ANGLE= 5.0(DEGREES)
TOTAL CONDUCTANCE = 208.8 (MHOS) (FOR TOP 6 LAYERS)

LAYERED MODEL

RESISTIVITY	DEPTH(KM)	ALTITUDE(M)
		355.0 (SURFACE)
240.0	.296	59.0
746.2	.893	-538.0
654.4	1.211	-856.0
3.0	1.217	-862.0
80.0	3.000	-2645.0
5.0	3.910	-3555.0
3720.0	29.000	-28645.0
22.0	34.000	-33645.0

San Kampaeng Station 2-1

MODEL DATA

PERIOD (SECONDS)	APPARENT RESISTIVITY
.0036	240.00
.0071	367.47
.0143	402.45
.0286	351.58
.0570	276.34
.1143	229.29
.2286	191.73
.4571	134.78
.9143	79.21
2.2605	40.16
2.9257	35.29
3.7926	32.63
4.9230	31.99
6.4000	33.21
8.3934	36.19
11.1304	40.69
14.8406	45.93
20.0787	50.96
27.6755	54.80
39.3840	57.85
60.2373	63.62
102.4003	81.98
204.7921	140.48

X-AXIS FIELD DATA

PERIOD (SECONDS)	APPARENT RESISTIVITY		
.0036	286.48		
.0071	386.89		
.0143	380.97		
.0286	338.70		
.0570	284.49		
.1143	225.47		
.2286	170.83		
.4571	125.16		
.9143	89.65		
2.2605	31.34	±	4.885
2.9257	30.11	±	.375
3.7926	30.05	±	7.353
4.9230	39.47	±	7.364
6.4000	31.79	±	1.664
8.3934	31.55	±	7.352
11.1304	51.79	±	4.526
14.8406	44.38	±	1.038
20.0787	49.43	±	6.923
27.6755	60.61	±	12.473
39.3840	43.25	±	5.963
60.2373	49.34	±	5.295
102.4003	75.31	±	6.616
204.7921	169.07	±	7.178

Fig. II.1-22

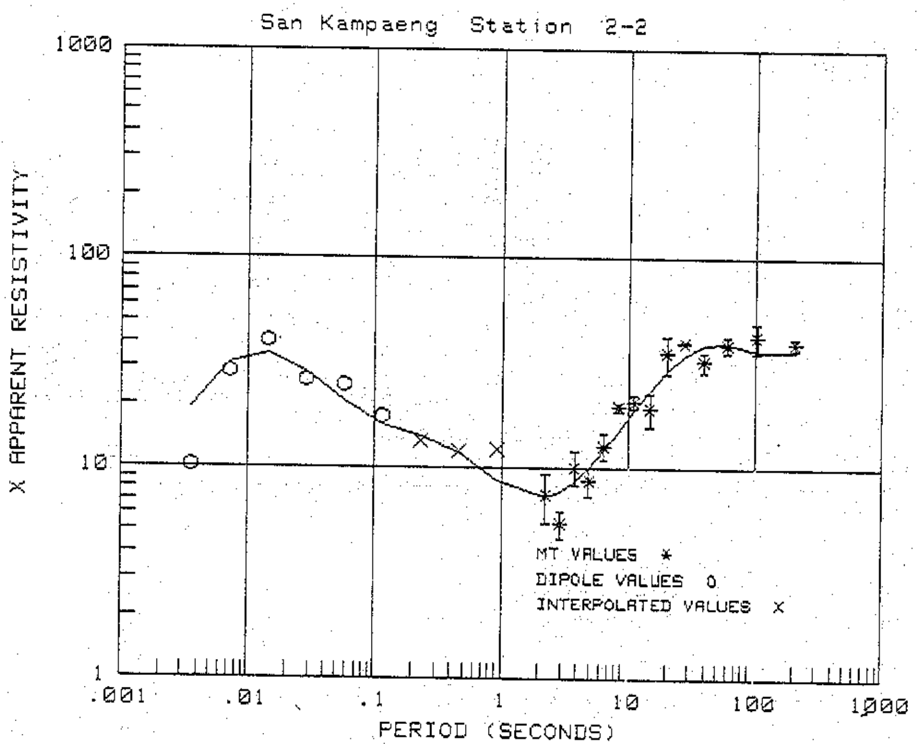

AVERAGE ROTATION ANGLE= 6.0(DEGREES)
TOTAL CONDUCTANCE = 278.8 (MHOS) (FOR TOP 6 LAYERS)

LAYERED MODEL

RESISTIVITY	DEPTH(KM)	ALTITUDE(M)
		358.0 (SURFACE)
19.3	.084	274.0
70.0	.253	105.0
52.7	.343	15.0
3.0	.456	-98.0
16.3	.851	-493.0
5.0	1.893	-1535.0
3542.0	22.000	-21642.0
20.0	38.000	-37642.0

San Kampaeng Station 2-2

MODEL DATA

PERIOD (SECONDS)	APPARENT RESISTIVITY
.0036	19.30
.0071	31.23
.0143	34.78
.0286	28.57
.0570	20.70
.1143	16.16
.2286	14.00
.4571	11.74
.9143	8.63
2.2605	7.17
2.9257	7.65
3.7926	8.61
4.9230	10.09
6.4000	12.17
8.3934	15.00
11.1304	18.76
14.8406	23.42
20.0787	28.93
27.6755	34.61
39.3840	38.94
60.2373	39.68
102.4003	36.30
204.7921	36.37

X-AXIS FIELD DATA

PERIOD (SECONDS)	APPARENT RESISTIVITY		
.0036	10.22		
.0071	28.67		
.0143	40.28		
.0286	25.93		
.0570	24.84		
.1143	17.64		
.2286	13.27		
.4571	11.97		
.9143	12.25		
2.2605	7.37	±	1.965
2.9257	5.36	±	.789
3.7926	10.05	±	1.912
4.9230	8.61	±	1.353
6.4000	12.71	±	1.814
8.3934	19.43	±	1.009
11.1304	20.64	±	1.570
14.8406	19.04	±	3.382
20.0787	35.29	±	7.412
27.6755	39.88	±	.430
39.3840	32.27	±	3.482
60.2373	38.91	±	3.523
102.4003	42.52	±	6.881
204.7921	39.35	±	2.615

Fig. II.1-23

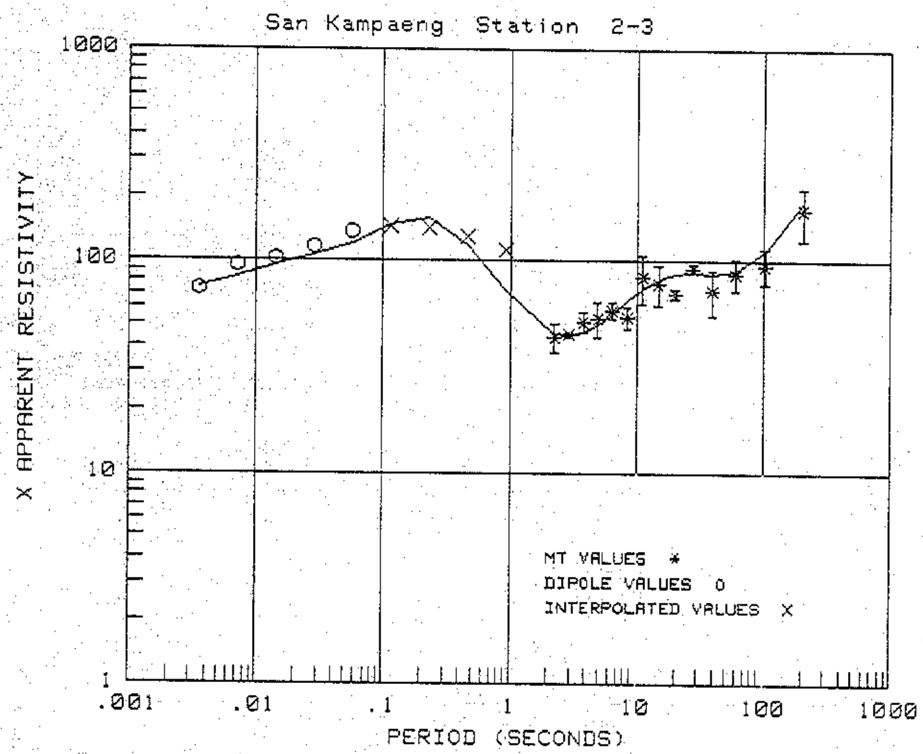

AVERAGE ROTATION ANGLE= -71.0(DEGREES)
TOTAL CONDUCTANCE = 138.3 (MHOS) (FOR TOP 6 LAYERS)
LAYERED MODEL

RESISTIVITY	DEPTH(KM)	ALTITUDE(M)
		364.0 (SURFACE)
43.0	.044	320.0
177.9	.134	230.0
118.6	.182	182.0
3.0	.184	180.0
154.5	2.948	-2584.0
5.0	3.537	-3173.0
3654.0	28.000	-27636.0
25.0	34.000	-33636.0

San Kampaeng Station 2-3

MODEL DATA

PERIOD (SECONDS)	APPARENT RESISTIVITY
.0036	75.44
.0071	83.94
.0143	94.83
.0286	105.64
.0570	120.50
.1143	147.53
.2286	156.20
.4571	117.29
.9143	72.18
2.2605	45.23
2.9257	44.13
3.7926	45.67
4.9230	49.75
6.4000	56.13
8.3934	64.50
11.1304	73.82
14.8406	81.93
20.0787	86.89
27.6755	87.88
39.3840	87.01
60.2373	90.34
102.4003	111.73
204.7921	187.40

X-AXIS FIELD DATA

PERIOD (SECONDS)	APPARENT RESISTIVITY
.0036	74.03
.0071	94.70
.0143	102.52
.0286	116.61
.0570	135.80
.1143	144.90
.2286	141.06
.4571	128.22
.9143	111.24
2.2605	43.48 ± 6.471
2.9257	44.74 ± 1.045
3.7926	51.53 ± 5.917
4.9230	53.36 ± 9.895
6.4000	58.14 ± 4.932
8.3934	53.98 ± 6.529
11.1304	83.94 ± 21.354
14.8406	78.05 ± 16.718
20.0787	69.97 ± 3.472
27.6755	91.92 ± 4.049
39.3840	72.56 ± 17.621
60.2373	86.58 ± 15.072
102.4003	94.88 ± 17.861
204.7921	170.86 ± 46.043

Fig. II.1-24

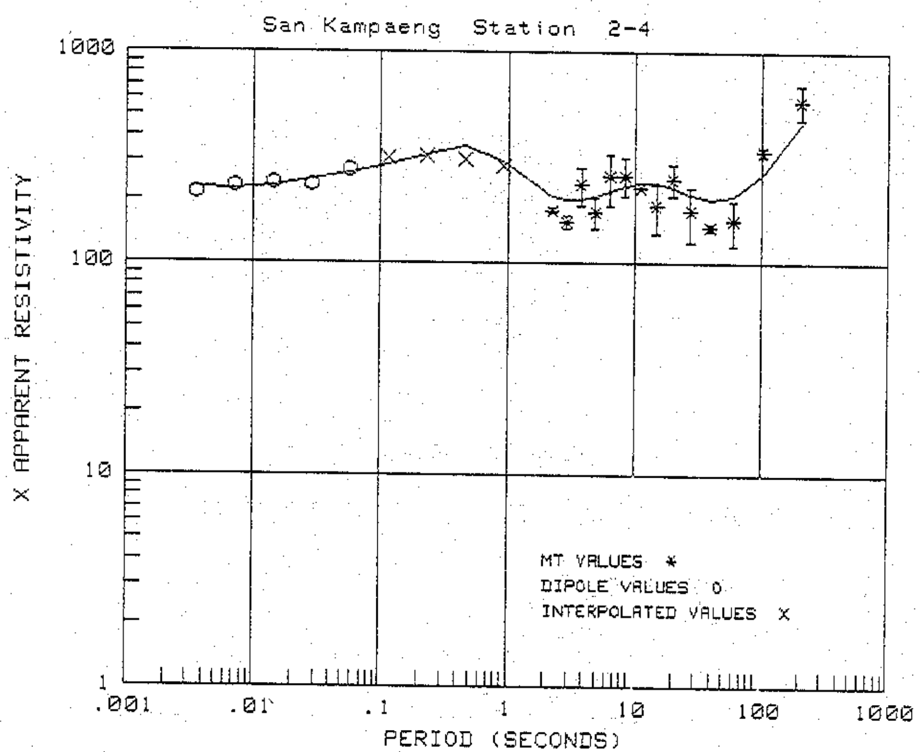

AVERAGE ROTATION ANGLE= -55.0(DEGREES)
TOTAL CONDUCTANCE = 77.4 (MHOS) (FOR TOP 7 LAYERS)

LAYERED MODEL

RESISTIVITY	DEPTH(KM)	ALTITUDE(M)
		390.0 (SURFACE)
200.0	.096	294.0
312.6	.288	102.0
274.2	.391	-1.0
3.0	.393	-3.0
357.3	6.340	-5950.0
100.0	9.000	-8610.0
5.0	9.160	-8770.0
4520.0	36.000	-35610.0
28.0	40.500	-40110.0

San Kampaeng Station 2-4

MODEL DATA

PERIOD (SECONDS)	APPARENT RESISTIVITY
.0036	227.31
.0071	220.35
.0143	228.18
.0286	245.99
.0570	266.36
.1143	291.18
.2286	327.67
.4571	353.59
.9143	301.56
2.2605	207.48
2.9257	198.04
3.7926	197.79
4.9230	205.40
6.4000	217.98
8.3934	231.24
11.1304	239.18
14.8406	236.97
20.0787	224.81
27.6755	208.53
39.3840	197.59
60.2373	206.16
102.4003	264.82
204.7921	459.29

X-AXIS FIELD DATA

PERIOD (SECONDS)	APPARENT RESISTIVITY
.0036	213.84
.0071	228.95
.0143	240.66
.0286	235.77
.0570	275.27
.1143	311.01
.2286	321.31
.4571	310.49
.9143	286.82
2.2605	175.74 ± 4.773
2.9257	154.63 ± 10.138
3.7926	233.38 ± 49.722
4.9230	173.32 ± 30.777
6.4000	255.36 ± 69.659
8.3934	258.49 ± 52.596
11.1304	226.99 ± .739
14.8406	184.63 ± 40.649
20.0787	249.68 ± 42.861
27.6755	174.68 ± 50.539
39.3840	146.79 ± 4.718
60.2373	158.26 ± 39.063
102.4003	336.16 ± 14.624
204.7921	504.17 ± 105.447

Fig. II.1-25

San Kampaeng Station 2-5

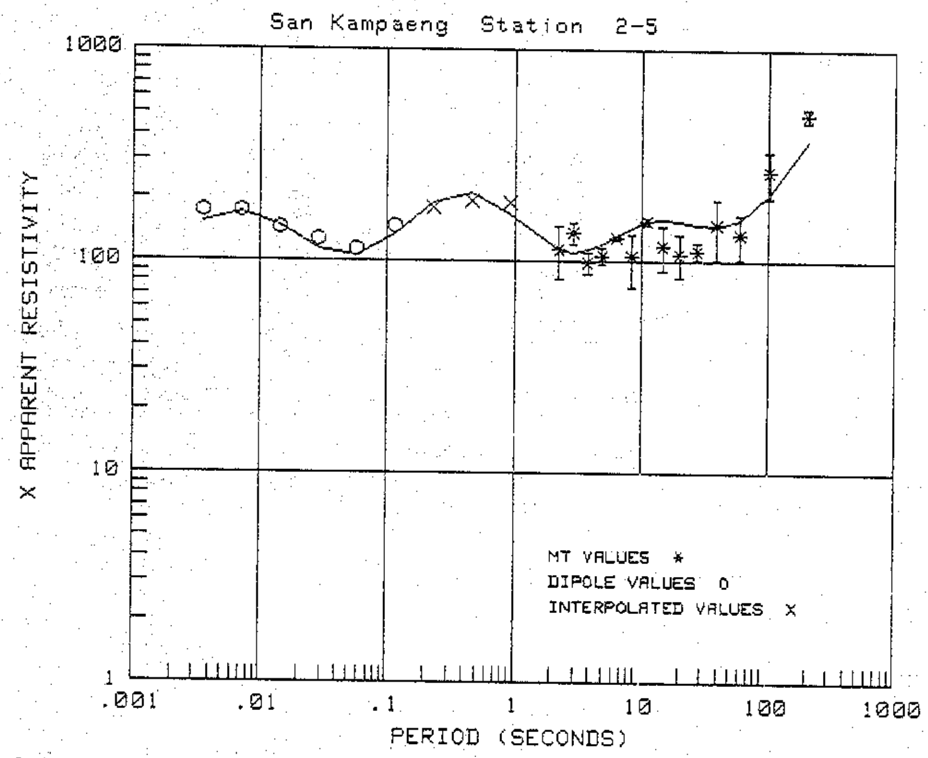

AVERAGE ROTATION ANGLE= 27.0(DEGREES)
TOTAL CONDUCTANCE = 92.3 (MHOS) (FOR TOP 6 LAYERS)

LAYERED MODEL

RESISTIVITY	DEPTH(KM)	ALTITUDE(M)
		385.0 (SURFACE)
120.0	.166	219.0
236.3	.503	-118.0
207.2	.681	-296.0
3.0	.700	-315.0
600.0	5.294	-4909.0
5.0	5.667	-5282.0
4431.0	31.000	-30615.0
35.0	37.000	-36615.0

MODEL DATA

PERIOD (SECONDS)	APPARENT RESISTIVITY
.0036	152.32
.0071	170.39
.0143	145.52
.0286	113.39
.0570	105.12
.1143	132.87
.2286	188.73
.4571	212.11
.9143	166.90
2.2605	113.46
2.9257	110.40
3.7926	112.95
4.9230	120.43
6.4000	131.36
8.3934	143.55
11.1304	153.41
14.9406	157.29
20.0787	154.57
27.6755	148.57
39.3840	146.10
60.2373	158.66
102.4003	211.12
204.7921	373.77

San Kampaeng Station 2-5

X-AXIS FIELD DATA

PERIOD (SECONDS)	APPARENT RESISTIVITY
.0036	173.11
.0071	172.48
.0143	143.55
.0286	126.66
.0570	113.92
.1143	145.59
.2286	179.08
.4571	192.36
.9143	187.84
2.2605	114.27 ± 31.064
2.9257	136.09 ± 16.482
3.7926	97.64 ± 11.565
4.9230	105.74 ± 9.715
6.4000	128.42 ± 2.740
8.3934	104.70 ± 29.382
11.1304	154.07 ± 5.165
14.8406	118.30 ± 28.494
20.0787	108.13 ± 24.980
27.6755	111.69 ± 9.330
39.3840	149.71 ± 47.638
60.2373	133.70 ± 32.197
102.4003	265.47 ± 67.879
204.7921	492.87 ± 32.688

Fig. II.1-26

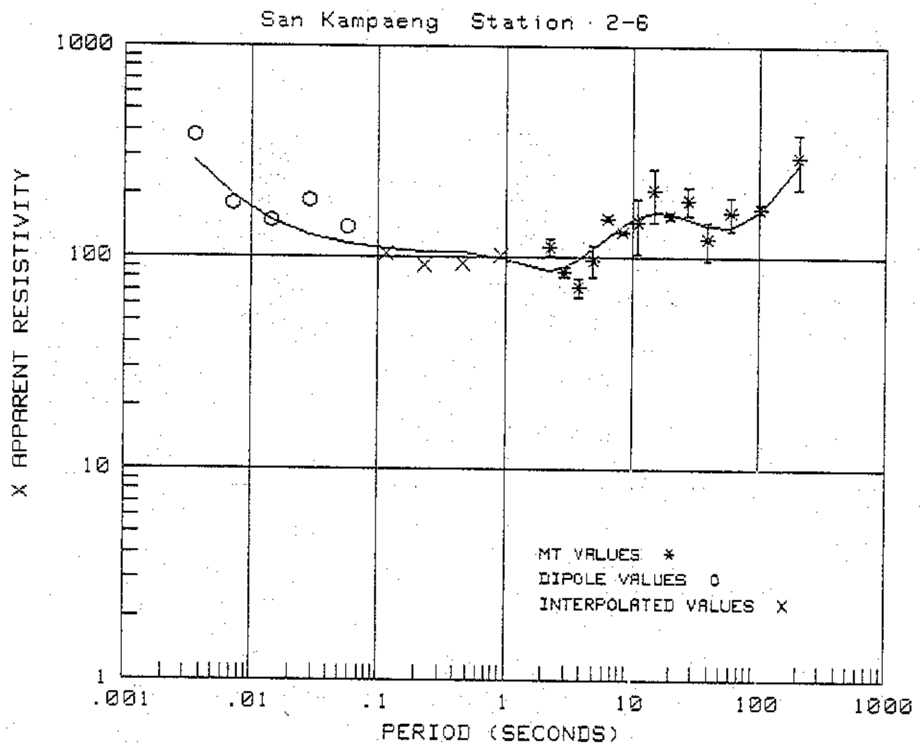

AVERAGE ROTATION ANGLE= -36.0(DEGREES)
TOTAL CONDUCTANCE = 93.5 (MHOS) (FOR TOP 7 LAYERS)

LAYERED MODEL

RESISTIVITY	DEPTH(KM)	ALTITUDE(M)
		395.0 (SURFACE)
1039.5	.114	281.0
779.6	.171	224.0
649.7	.331	64.0
3.0	.339	56.0
430.8	.392	3.0
100.0	7.000	-6605.0
5.0	7.121	-6726.0
4325.0	31.000	-30605.0
32.0	38.000	-37605.0

San Kampaeng Station 2-6

MODEL DATA

PERIOD (SECONDS)	APPARENT RESISTIVITY
.0036	286.95
.0071	194.62
.0143	149.27
.0286	127.07
.0570	115.91
.1143	109.89
.2286	106.44
.4571	106.54
.9143	98.52
2.2605	86.74
2.9257	90.27
3.7926	98.09
4.9230	110.01
6.4000	125.04
8.3934	141.40
11.1304	155.41
14.8406	162.39
20.0787	160.24
27.6755	150.97
39.3840	140.76
60.2373	139.54
102.4003	167.44
204.7921	276.65

X-AXIS FIELD DATA

PERIOD (SECONDS)	APPARENT RESISTIVITY	
.0036	376.59	
.0071	178.23	
.0143	148.09	
.0286	185.40	
.0570	138.59	
.1143	103.88	
.2286	92.13	
.4571	92.63	
.9143	101.32	
2.2605	111.66 ±	10.373
2.9257	85.16 ±	4.498
3.7926	71.90 ±	7.292
4.9230	96.99 ±	17.156
6.4000	152.93 ±	4.712
8.3934	131.07 ±	1.561
11.1304	145.81 ±	41.480
14.8406	204.84 ±	57.176
20.0787	157.80 ±	5.397
27.6755	185.65 ±	28.495
39.3840	121.80 ±	25.713
60.2373	163.05 ±	28.356
102.4003	170.62 ±	8.437
204.7921	295.29 ±	84.382

Fig. II.1-27

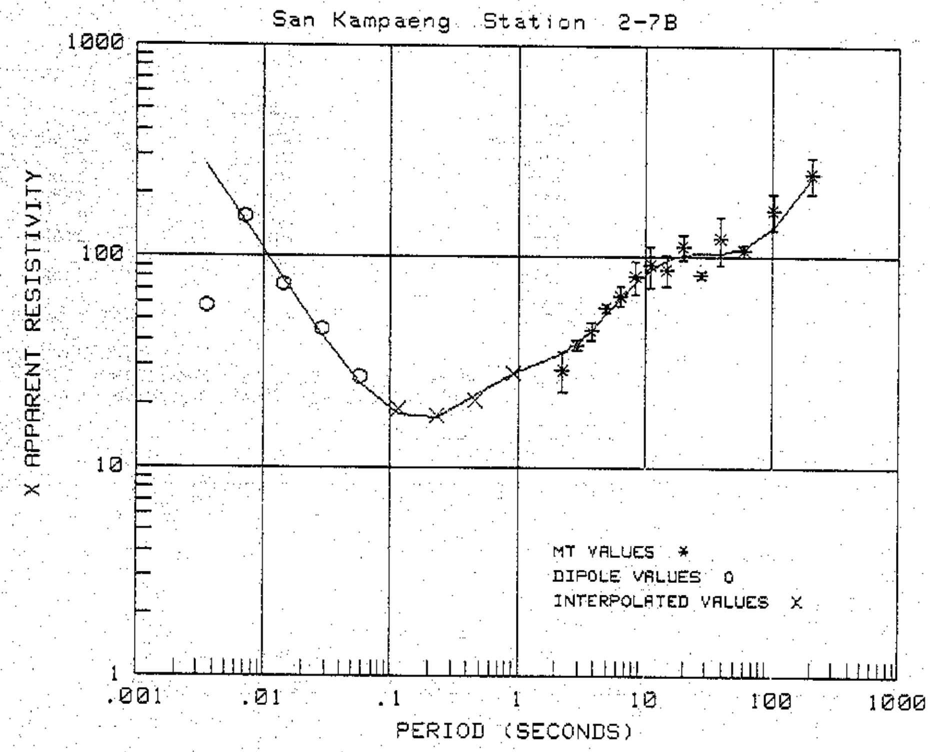

AVERAGE ROTATION ANGLE= 24.0(DEGREES)
TOTAL CONDUCTANCE = 126.0 (MHOS) (FOR TOP 6 LAYERS)

LAYERED MODEL

RESISTIVITY	DEPTH(KM)	ALTITUDE(M)
		403.0 (SURFACE)
1039.5	.114	289.0
779.6	.171	232.0
649.0	.331	72.0
3.0	.460	-57.0
100.0	5.500	-5097.0
5.0	5.661	-5258.0
4436.0	30.000	-29597.0
29.0	36.000	-35597.0

San Kampaeng Station 2-7B

MODEL DATA

PERIOD (SECONDS)	APPARENT RESISTIVITY
.0036	270.60
.0071	146.18
.0143	77.67
.0286	41.87
.0570	24.71
.1143	17.88
.2286	17.36
.4571	21.63
.9143	27.44
2.2605	34.54
2.9257	38.66
3.7926	44.63
4.9230	52.66
6.4000	62.68
8.3934	74.40
11.1304	86.46
14.8406	96.28
20.0787	101.89
27.6755	103.02
39.3840	102.93
60.2373	109.44
102.4003	139.78
204.7921	240.03

X-AXIS FIELD DATA

PERIOD (SECONDS)	APPARENT RESISTIVITY
.0036	57.96
.0071	154.38
.0143	72.85
.0286	45.31
.0570	26.52
.1143	18.83
.2286	17.70
.4571	20.52
.9143	27.39
2.2605	28.55 ± 6.140
2.9257	37.48 ± 2.089
3.7926	43.83 ± 4.490
4.9230	56.69 ± 2.285
6.4000	65.07 ± 6.647
8.3934	80.29 ± 14.406
11.1304	90.54 ± 20.006
14.8406	86.79 ± 14.542
20.0787	110.79 ± 14.857
27.6755	81.87 ± 2.406
39.3840	122.85 ± 30.693
60.2373	107.15 ± 6.526
102.4003	166.81 ± 33.052
204.7921	246.64 ± 47.756

Fig II.1-28

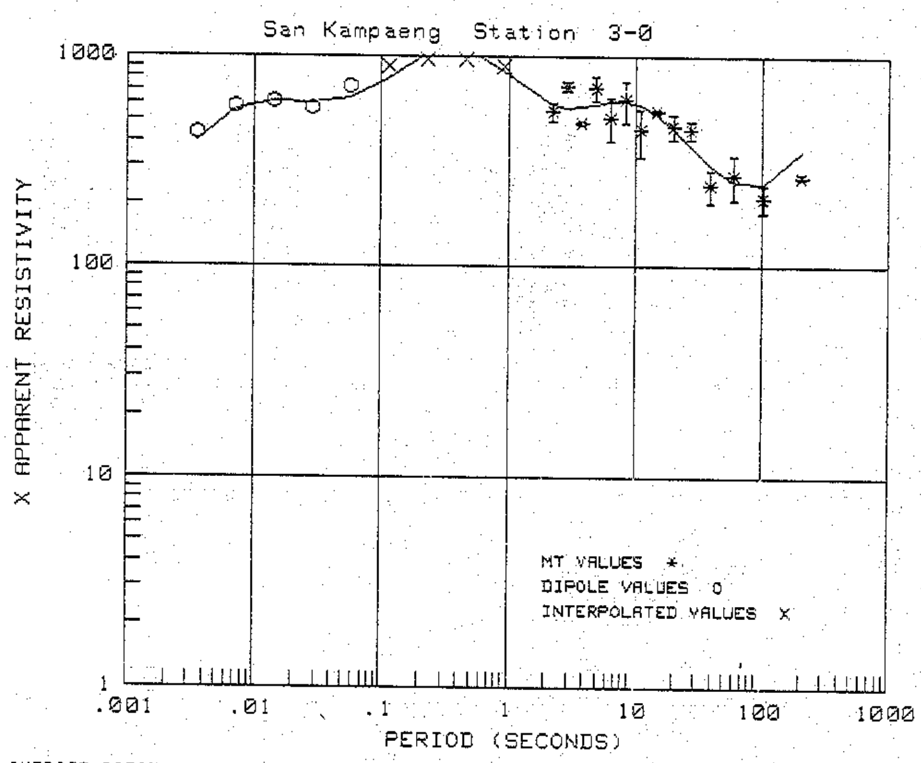

AVERAGE ROTATION ANGLE= 31.0(DEGREES)
TOTAL CONDUCTANCE = 42.7 (MHOS) (FOR TOP 7 LAYERS)

LAYERED MODEL

RESISTIVITY	DEPTH(KM)	ALTITUDE(M)
		350.0 (SURFACE)
397.0	.445	-95.0
1697.8	1.350	-1000.0
1488.8	1.828	-1478.0
3.0	1.834	-1484.0
5000.0	4.000	-3650.0
1500.0	12.000	-11650.0
5.0	12.165	-11815.0
5650.0	38.000	-37650.0
49.0	50.000	-49650.0

MODEL DATA

PERIOD (SECONDS)	APPARENT RESISTIVITY
.0036	397.00
.0071	558.77
.0143	615.60
.0286	607.21
.0570	639.15
.1143	783.82
.2286	1042.44
.4571	1107.27
.9143	849.90
2.2605	590.26
2.9257	573.96
3.7926	578.66
4.9230	595.91
6.4000	612.79
8.3934	614.07
11.1304	586.51
14.8406	529.44
20.0787	452.73
27.6755	372.59
39.3840	302.59
60.2373	253.43
102.4003	249.74
204.7921	352.96

San Kampaeng Station 3-0

X-AXIS FIELD DATA

PERIOD (SECONDS)	APPARENT RESISTIVITY
.0036	435.83
.0071	580.07
.0143	610.87
.0286	575.07
.0570	727.72
.1143	892.37
.2286	969.90
.4571	963.42
.9143	900.87
2.2605	548.53 ± 51.860
2.9257	724.05 ± 41.755
3.7926	485.64 ± 10.482
4.9230	706.61 ± 95.566
6.4000	515.81 ± 120.644
8.3934	618.69 ± 138.024
11.1304	446.86 ± 114.194
14.8406	546.56 ± 9.745
20.0787	466.59 ± 60.873
27.6755	447.48 ± 44.122
39.3840	243.79 ± 44.368
60.2373	272.55 ± 64.175
102.4003	211.33 ± 31.385
204.7921	268.25 ± 7.652

Fig. II.1.29

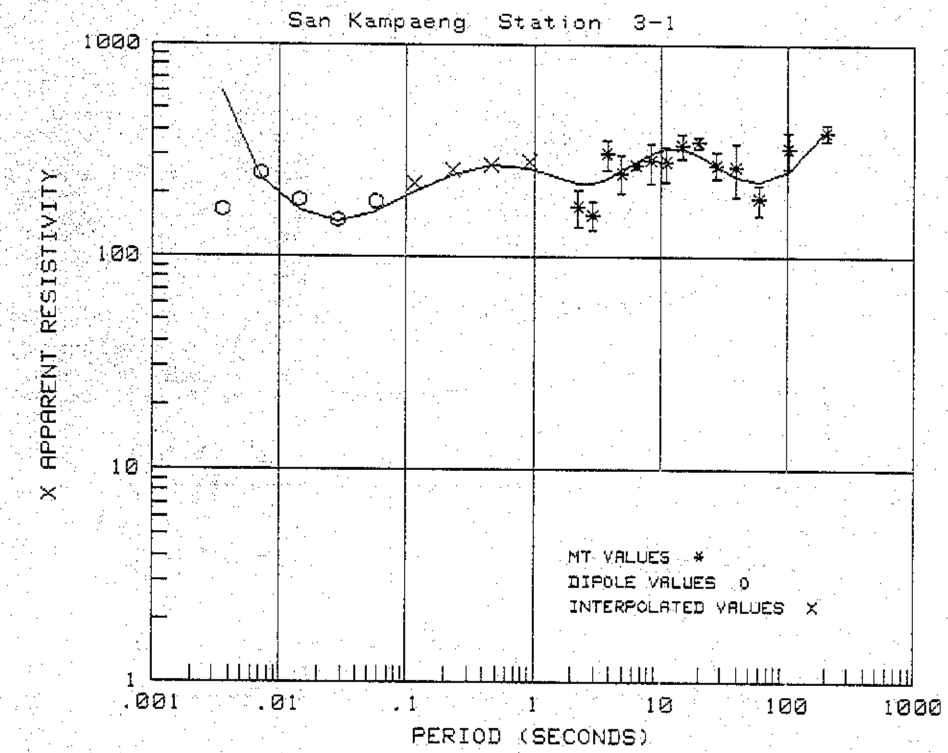

AVERAGE ROTATION ANGLE= -57.0(DEGREES)
TOTAL CONDUCTANCE = 64.4 (MHOS) (FOR TOP 7 LAYERS)

LAYERED MODEL

RESISTIVITY	DEPTH(KM)	ALTITUDE(M)
		362.0 (SURFACE)
603.6	.124	238.0
266.9	.378	-16.0
234.1	.512	-150.0
3.0	.524	-162.0
517.4	3.714	-3352.0
215.6	10.500	-10138.0
5.0	10.605	-10243.0
5210.0	38.000	-37638.0
46.0	47.000	-46638.0

MODEL DATA

PERIOD (SECONDS)	APPARENT RESISTIVITY
.0036	603.60
.0071	234.44
.0143	165.87
.0286	145.54
.0570	162.22
.1143	202.41
.2286	243.00
.4571	272.54
.9143	260.86
2.2605	220.10
2.9257	223.44
3.7926	236.27
4.9230	257.43
6.4000	283.45
8.3934	308.71
11.1304	324.38
14.8406	322.52
20.0787	302.26
27.6755	270.79
39.3840	240.08
60.2373	224.90
102.4003	254.64
204.7921	404.12

San Kampaeng Station 3-1

X-AXIS FIELD DATA

PERIOD (SECONDS)	APPARENT RESISTIVITY
.0036	165.59
.0071	246.82
.0143	186.66
.0286	149.21
.0570	181.13
.1143	223.72
.2286	254.74
.4571	273.04
.9143	281.13
2.2605	171.92 ± 34.221
2.9257	158.72 ± 24.516
3.7926	305.72 ± 49.779
4.9230	249.75 ± 51.086
6.4000	270.63 ± 10.172
8.3934	284.31 ± 61.182
11.1304	279.05 ± 53.711
14.8406	337.00 ± 43.968
20.0787	346.41 ± 22.429
27.6755	272.33 ± 38.342
39.3840	267.04 ± 76.420
60.2373	188.96 ± 30.601
102.4003	326.79 ± 65.450
204.7921	391.38 ± 36.349

Fig. II.1-30

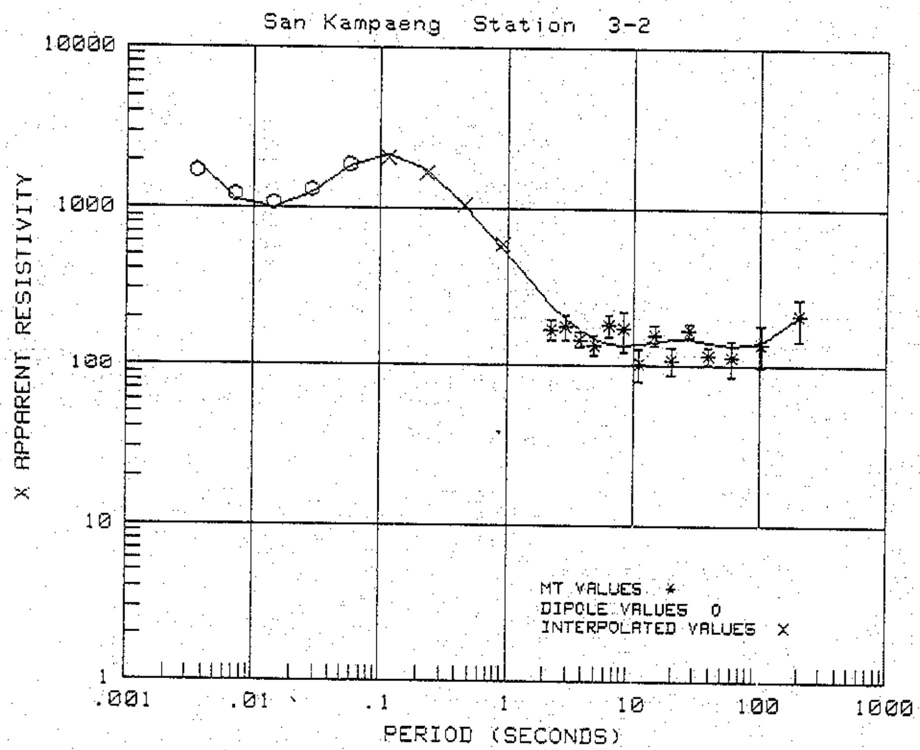

AVERAGE ROTATION ANGLE= -60.0(DEGREES)
TOTAL CONDUCTANCE = 135.0 (MHOS) (FOR TOP 6 LAYERS)

LAYERED MODEL

RESISTIVITY	DEPTH(KM)	ALTITUDE(M)
		375.0 (SURFACE)
1954.6	.262	113.0
1991.7	.788	-413.0
1021.0	1.067	-692.0
3.0	1.070	-695.0
5829.3	7.879	-7504.0
5.0	8.540	-8165.0
5346.0	39.000	-38625.0
42.0	49.000	-48625.0

San Kampaeng Station 3-2

MODEL DATA

PERIOD (SECONDS)	APPARENT RESISTIVITY
.0036	1954.60
.0071	1140.98
.0143	1011.92
.0286	1265.33
.0570	1834.22
.1143	2189.53
.2286	1745.33
.4571	1032.95
.9143	548.02
2.2605	243.62
2.9257	200.02
3.7926	169.24
4.9230	149.27
6.4000	138.44
8.3934	135.15
11.1304	137.88
14.8406	143.69
20.0787	148.50
27.6755	148.15
39.3840	141.58
60.2373	133.83
102.4003	141.83
204.7921	207.36

X-AXIS FIELD DATA

PERIOD (SECONDS)	APPARENT RESISTIVITY
.0036	1720.82
.0071	1228.23
.0143	1089.29
.0286	1326.47
.0570	1882.64
.1143	2053.57
.2286	1656.41
.4571	1065.34
.9143	587.20
2.2605	170.19 ± 24.330
2.9257	176.48 ± 32.430
3.7926	146.64 ± 15.557
4.9230	136.73 ± 20.332
6.4000	180.59 ± 27.841
8.3934	171.25 ± 48.860
11.1304	103.60 ± 23.970
14.8406	157.33 ± 22.107
20.0787	109.36 ± 21.657
27.6755	168.93 ± 15.660
39.3840	117.79 ± 15.220
60.2373	115.17 ± 29.937
102.4003	138.64 ± 40.502
204.7921	206.94 ± 62.224

Fig. II.1-31

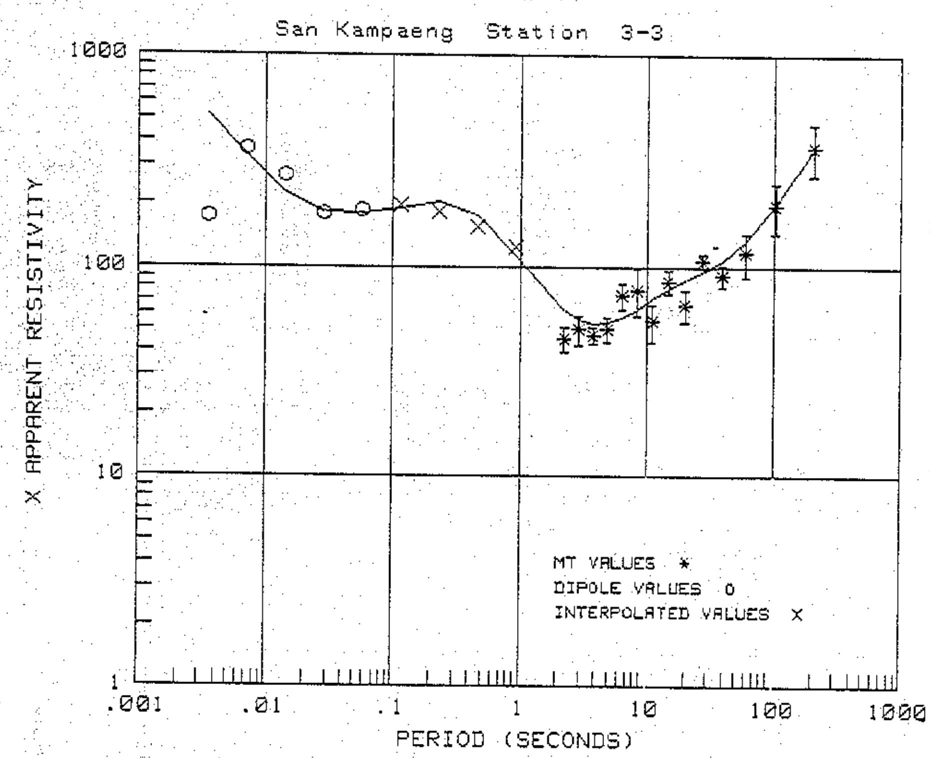

AVERAGE ROTATION ANGLE= -19.0(DEGREES)
TOTAL CONDUCTANCE = 149.7 (MHOS) (FOR TOP 7 LAYERS)

LAYERED MODEL

RESISTIVITY	DEPTH(KM)	ALTITUDE(M)
		375.0 (SURFACE)
1100.0	.146	229.0
369.0	.444	-69.0
323.6	.602	-227.0
3.0	.615	-240.0
356.0	2.000	-1625.0
100.0	4.000	-3625.0
5.0	4.600	-4225.0
5028.0	38.000	-37625.0
45.0	43.000	-42625.0

MODEL DATA

PERIOD (SECONDS)	APPARENT RESISTIVITY
.0036	520.95
.0071	336.65
.0143	223.66
.0286	181.65
.0570	177.77
.1143	188.60
.2286	202.72
.4571	174.25
.9143	113.25
2.2605	62.06
2.9257	56.07
3.7926	53.43
4.9230	53.90
6.4000	57.17
8.3934	62.96
11.1304	70.59
14.8406	78.75
20.0787	86.69
27.6755	94.97
39.3840	107.26
60.2373	133.70
102.4003	198.10
204.7921	371.27

San Kampaeng Station 3-3

X-AXIS FIELD DATA

PERIOD (SECONDS)	APPARENT RESISTIVITY
.0036	171.72
.0071	360.06
.0143	271.16
.0286	177.93
.0570	186.87
.1143	196.38
.2286	182.93
.4571	155.67
.9143	124.56
2.2605	45.06 ± 5.856
2.9257	50.07 ± 8.364
3.7926	46.94 ± 4.527
4.9230	49.78 ± 6.729
6.4000	73.00 ± 10.231
8.3934	78.25 ± 20.295
11.1304	54.64 ± 11.492
14.8406	85.54 ± 10.927
20.0787	65.91 ± 11.867
27.6755	107.08 ± 9.024
39.3840	90.88 ± 10.675
60.2373	116.75 ± 27.590
102.4003	194.05 ± 51.536
204.7921	370.58 ± 101.300

Fig. II.1-32

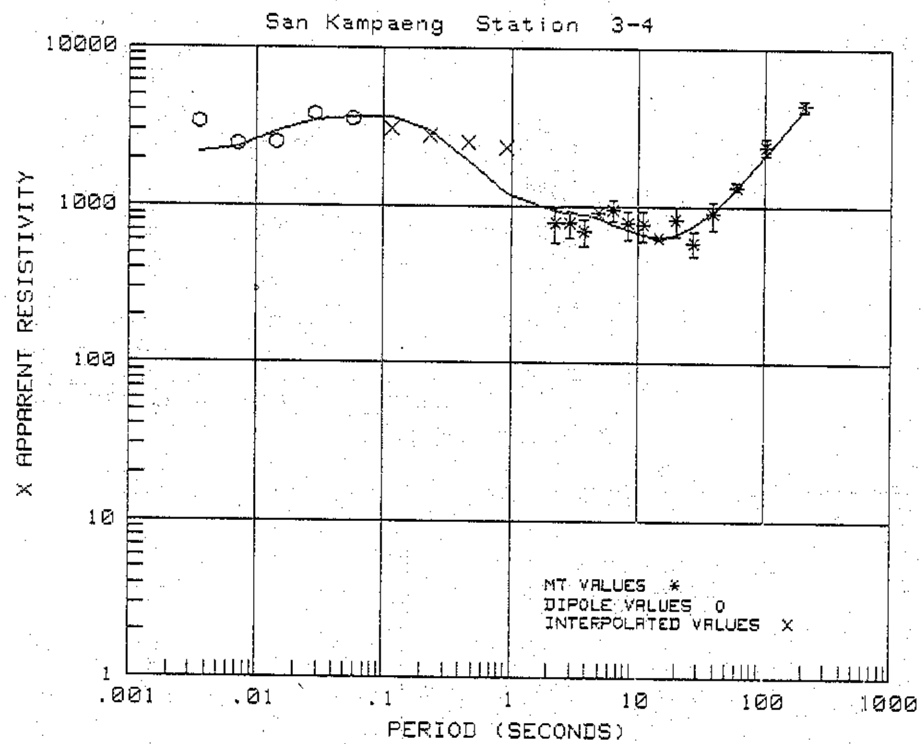

AVERAGE ROTATION ANGLE= -57.0(DEGREES)
TOTAL CONDUCTANCE = 25.8 (MHOS) (FOR TOP 7 LAYERS)

LAYERED MODEL

RESISTIVITY	DEPTH(KM)	ALTITUDE(M)
		410.0 (SURFACE)
15052.4	.191	219.0
5047.4	.582	-172.0
4427.2	.788	-378.0
4.0	.790	-380.0
10000.0	4.800	-4390.0
1500.0	12.000	-11590.0
5.0	12.100	-11690.0
5324.0	39.000	-38590.0
42.0	41.000	-40590.0

San Kampaeng Station 3-4

MODEL DATA

PERIOD (SECONDS)	APPARENT RESISTIVITY
.0036	2196.79
.0071	2333.24
.0143	2935.00
.0286	3441.55
.0570	3579.72
.1143	3606.15
.2286	2968.64
.4571	1918.02
.9143	1223.67
2.2605	943.69
2.9257	920.38
3.7926	888.66
4.9230	839.47
6.4000	776.55
8.3934	711.48
11.1304	660.96
14.8406	641.73
20.0787	667.36
27.6755	756.05
39.3840	941.96
60.2373	1324.89
102.4003	2155.48
204.7921	4233.76

X-AXIS FIELD DATA

PERIOD (SECONDS)	APPARENT RESISTIVITY
.0036	3349.13
.0071	2440.75
.0143	2529.59
.0286	3757.57
.0570	3578.52
.1143	3077.21
.2286	2748.61
.4571	2525.07
.9143	2362.75
2.2605	787.08 ± 197.861
2.9257	785.64 ± 150.367
3.7926	696.47 ± 130.625
4.9230	911.38 ± 9.001
6.4000	956.16 ± 143.571
8.3934	781.10 ± 154.501
11.1304	764.89 ± 160.915
14.8406	637.60 ± 11.821
20.0787	830.49 ± 183.599
27.6755	592.52 ± 103.393
39.3840	908.93 ± 185.050
60.2373	1354.16 ± 81.108
102.4003	2423.32 ± 290.356
204.7921	4374.59 ± 338.582

Fig. II.1-33

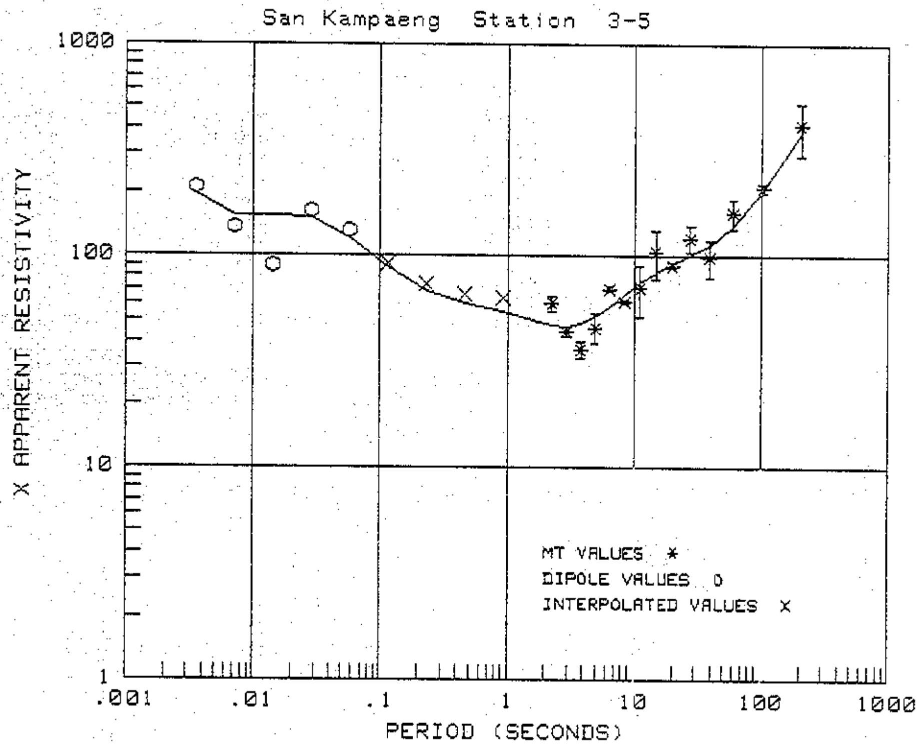

AVERAGE ROTATION ANGLE= -61.0(DEGREES)
TOTAL CONDUCTANCE = 148.9 (MHOS) (FOR TOP 7 LAYERS)

LAYERED MODEL

RESISTIVITY	DEPTH(KM)	ALTITUDE(M)
		395.0 (SURFACE)
318.7	.316	79.0
4.0	.330	65.0
1500.0	1.036	-641.0
3.0	1.085	-690.0
55.0	6.000	-5605.0
147.0	10.000	-9605.0
5.0	10.055	-9660.0
5100.0	38.000	-37605.0
46.0	43.000	-42605.0

MODEL DATA

PERIOD (SECONDS)	APPARENT RESISTIVITY
.0036	194.31
.0071	153.43
.0143	155.19
.0286	150.86
.0570	119.44
.1143	87.67
.2286	68.80
.4571	59.68
.9143	54.49
2.2605	47.18
2.9257	46.81
3.7926	48.31
4.9230	52.00
6.4000	57.86
8.3934	65.75
11.1304	74.87
14.8406	83.72
20.0787	91.63
27.6755	99.52
39.3840	111.58
60.2373	138.47
102.4003	204.82
204.7921	383.72

San Kampaeng Station 3-5

X-AXIS FIELD DATA

PERIOD (SECONDS)	APPARENT RESISTIVITY	
.0036	211.23	
.0071	136.66	
.0143	90.12	
.0286	162.64	
.0570	132.06	
.1143	92.08	
.2286	74.01	
.4571	66.11	
.9143	63.35	
2.2605	59.84	± 5.188
2.9257	44.34	± 2.186
3.7926	36.28	± 3.434
4.9230	46.25	± 7.636
6.4000	69.91	± 2.010
8.3934	61.26	± .681
11.1304	70.56	± 18.697
14.8406	104.15	± 27.133
20.0787	90.32	± 2.883
27.6755	120.85	± 17.313
39.3840	97.55	± 19.220
60.2373	160.24	± 26.010
102.4003	208.46	± 9.620
204.7921	407.85	± 108.777

Fig. II.1-34

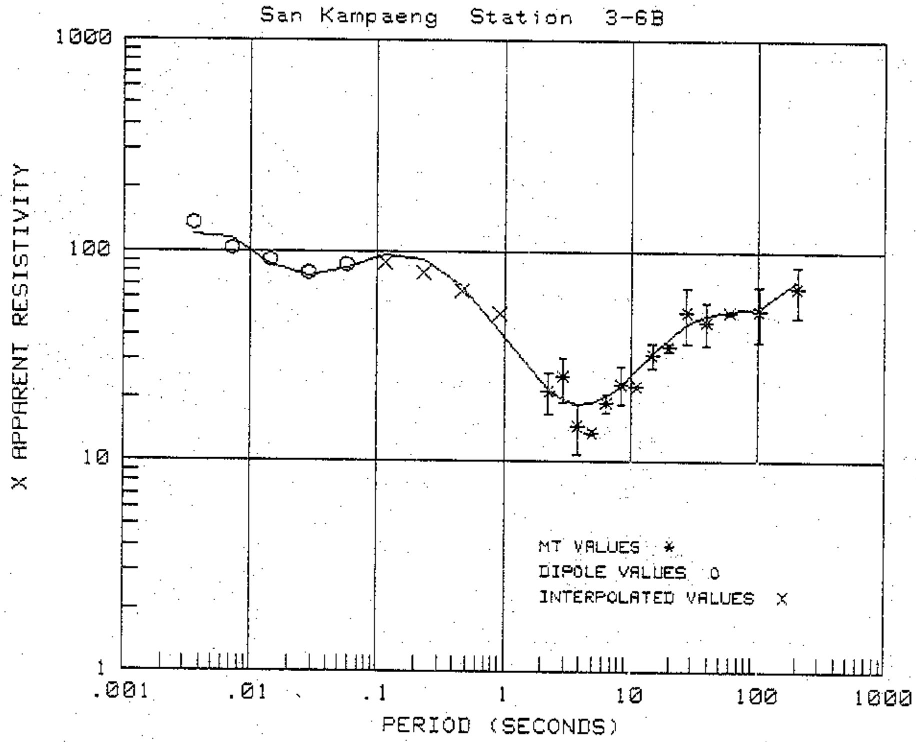

AVERAGE ROTATION ANGLE= 39.0(DEGREES)
TOTAL CONDUCTANCE = 254.3 (MHOS) (FOR TOP 7 LAYERS)

LAYERED MODEL

RESISTIVITY	DEPTH(KM)	ALTITUDE(M)
		405.0 (SURFACE)
118.9	.095	310.0
154.6	.288	117.0
135.6	.390	15.0
3.0	.406	-1.0
163.0	1.500	-1095.0
40.0	2.000	-1595.0
5.0	3.135	-2730.0
4600.0	30.000	-29595.0
25.0	40.000	-39595.0

San Kampaeng Station 3-6B

MODEL DATA

PERIOD (SECONDS)	APPARENT RESISTIVITY
.0036	118.90
.0071	115.33
.0143	86.32
.0286	76.52
.0570	84.16
.1143	96.56
.2286	92.06
.4571	68.21
.9143	41.48
2.2605	21.98
2.9257	19.70
3.7926	18.66
4.9230	18.81
6.4000	20.15
8.3934	22.79
11.1304	26.87
14.8406	32.23
20.0787	38.60
27.6755	44.96
39.3840	49.71
60.2373	51.81
102.4003	54.46
204.7921	73.07

X-AXIS FIELD DATA

PERIOD (SECONDS)	APPARENT RESISTIVITY		
.0036	135.50		
.0071	103.15		
.0143	91.44		
.0286	79.56		
.0570	86.25		
.1143	88.32		
.2286	79.62		
.4571	65.24		
.9143	50.08		
2.2605	21.28	±	4.774
2.9257	24.99	±	5.993
3.7926	14.61	±	3.856
4.9230	13.72	±	.344
6.4000	18.81	±	1.909
8.3934	23.15	±	4.759
11.1304	22.60	±	.868
14.8406	31.77	±	4.321
20.0787	34.68	±	1.432
27.6755	51.33	±	15.295
39.3840	46.03	±	10.533
60.2373	51.27	±	1.215
102.4003	52.46	±	15.276
204.7921	66.53	±	18.084

Fig. II.1-35

San Kampaeng Station 4-0

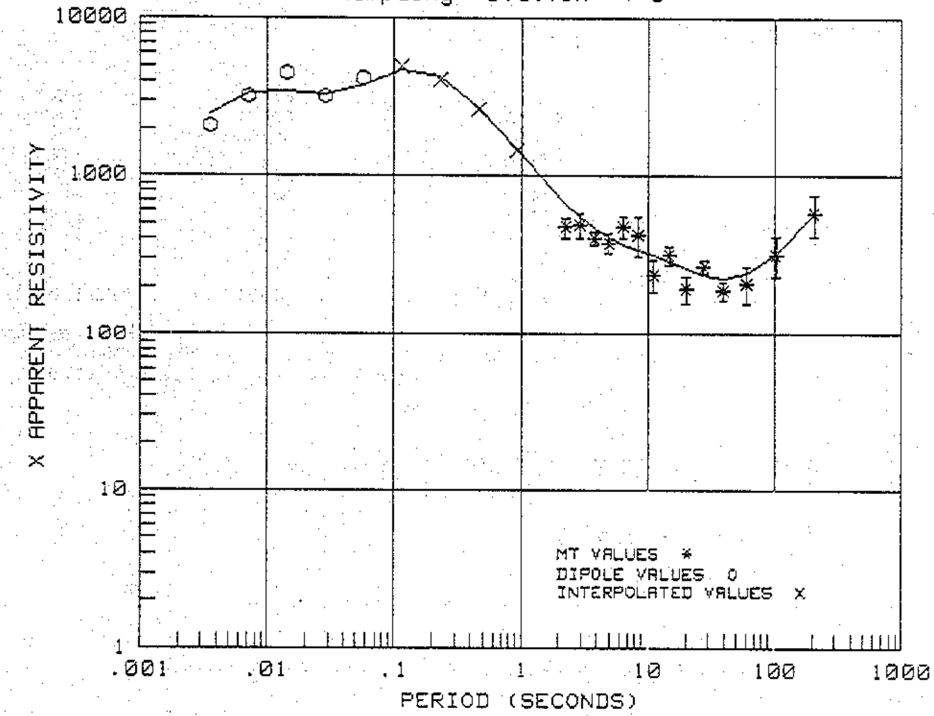

AVERAGE ROTATION ANGLE= 40.0(DEGREES)
TOTAL CONDUCTANCE = 89.0 (MHOS) (FOR TOP 5 LAYERS)

LAYERED MODEL

RESISTIVITY	DEPTH(KM)	ALTITUDE(M)
		375.0 (SURFACE)
974.5	.386	-11.0
24363.3	3.532	-3157.0
3.0	3.536	-3161.0
91362.3	13.244	-12869.0
5.0	13.679	-13304.0
5348.0	39.000	-38625.0
49.0	45.000	-44625.0

San Kampaeng Station 4-0

MODEL DATA

PERIOD (SECONDS)	APPARENT RESISTIVITY
.0036	2440.26
.0071	3391.99
.0143	3435.81
.0286	3249.72
.0570	3831.68
.1143	4725.13
.2286	4263.53
.4571	2715.64
.9143	1478.21
2.2605	666.57
2.9257	549.11
3.7926	464.78
4.9230	406.50
6.4000	366.97
8.3934	337.95
11.1304	312.35
14.8406	286.12
20.0787	258.93
27.6755	236.14
39.3840	226.11
60.2373	243.85
102.4003	325.75
204.7921	579.40

X-AXIS FIELD DATA

PERIOD (SECONDS)	APPARENT RESISTIVITY
.0036	2096.40
.0071	3218.88
.0143	4534.71
.0286	3189.69
.0570	4183.46
.1143	4919.85
.2286	4107.43
.4571	2652.41
.9143	1438.27
2.2605	471.75 ± 65.396
2.9257	486.45 ± 86.679
3.7926	404.59 ± 41.623
4.9230	373.39 ± 53.840
6.4000	475.32 ± 71.060
8.3934	425.48 ± 117.718
11.1304	237.05 ± 53.184
14.8406	312.45 ± 42.573
20.0787	192.75 ± 37.015
27.6755	268.27 ± 24.115
39.3840	189.27 ± 23.715
60.2373	210.87 ± 53.154
102.4003	318.66 ± 90.270
204.7921	578.26 ± 168.606

Fig. II.1-36

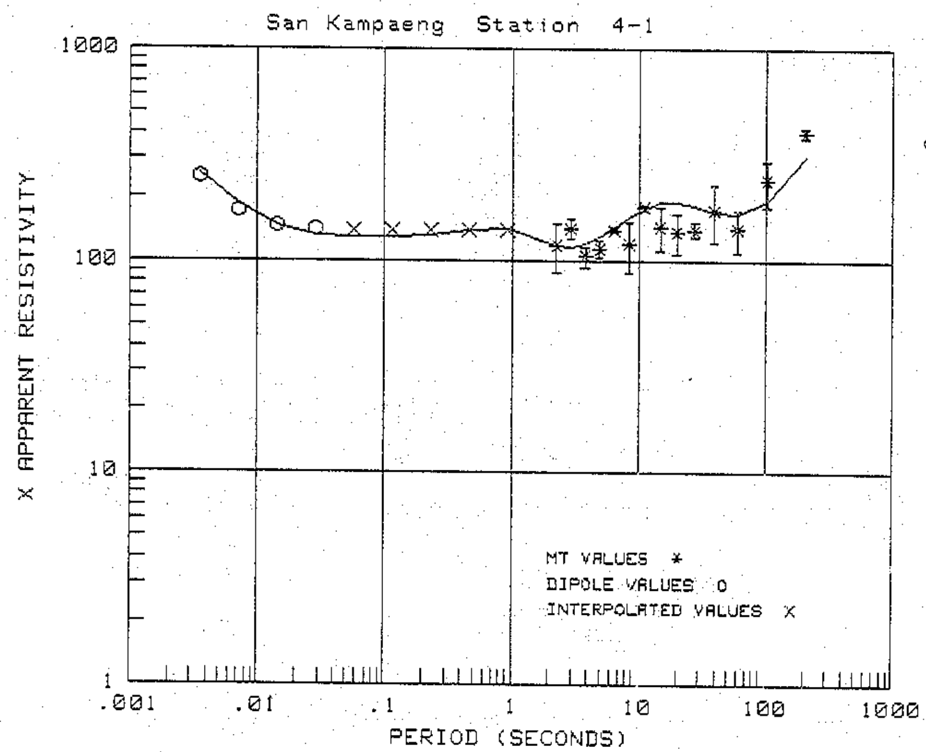

AVERAGE ROTATION ANGLE= 53.0(DEGREES)
TOTAL CONDUCTANCE = 94.6 (MHOS), (FOR TOP 7 LAYERS)
LAYERED MODEL

RESISTIVITY	DEPTH(KM)	ALTITUDE(M)
		385.0 (SURFACE)
500.0	.137	248.0
300.0	.205	180.0
150.0	.397	-12.0
3.0	.404	-19.0
621.1	.471	-86.0
144.2	8.405	-8020.0
5.0	8.582	-8197.0
5216.0	36.000	-35615.0
44.0	45.000	-44615.0

MODEL DATA

PERIOD (SECONDS)	APPARENT RESISTIVITY
.0036	257.00
.0071	184.09
.0143	146.87
.0286	132.09
.0570	128.61
.1143	129.89
.2286	132.12
.4571	139.27
.9143	140.14
2.2605	117.85
2.9257	116.44
3.7926	120.05
4.9230	129.00
6.4000	142.71
8.3934	159.81
11.1304	176.83
14.8406	188.21
20.0787	189.91
27.6755	181.81
39.3840	169.69
60.2373	164.82
102.4003	190.68
204.7921	305.69

San Kampaeng Station 4-1

X-AXIS FIELD DATA

PERIOD (SECONDS)	APPARENT RESISTIVITY		
.0036	246.83		
.0071	173.00		
.0143	146.47		
.0286	140.63		
.0570	138.60		
.1143	137.62		
.2286	137.44		
.4571	137.83		
.9143	138.60		
2.2605	118.64	±	31.015
2.9257	141.85	±	16.106
3.7926	104.79	±	11.637
4.9230	114.25	±	9.841
6.4000	139.72	±	2.795
8.3934	119.27	±	31.377
11.1304	177.54	±	5.580
14.8406	144.47	±	32.623
20.0787	136.42	±	29.544
27.6755	139.49	±	10.924
39.3840	173.62	±	51.793
60.2373	140.51	±	31.723
102.4003	236.70	±	56.741
204.7921	397.00	±	24.684

Fig. II.1-37

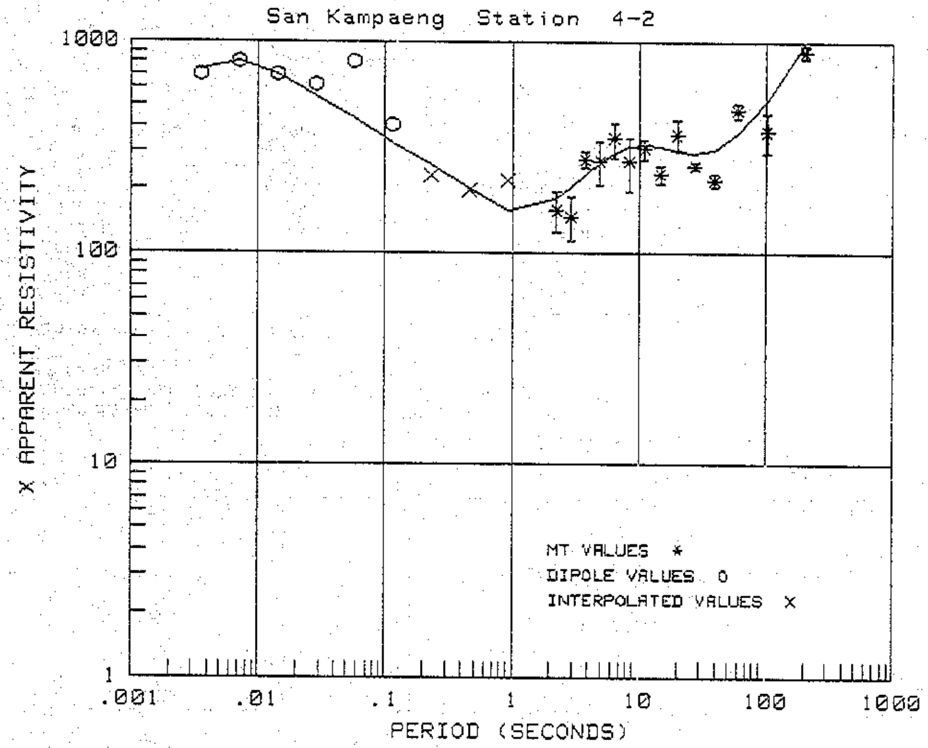

AVERAGE ROTATION ANGLE= 66.0(DEGREES)
TOTAL CONDUCTANCE = 49.5 (MHOS) (FOR TOP 8 LAYERS)

LAYERED MODEL

RESISTIVITY	DEPTH(KM)	ALTITUDE(M)
		385.0 (SURFACE)
478.9	.296	89.0
1488.6	.895	-510.0
1305.0	1.210	-825.0
3.0	1.213	-828.0
159.6	2.997	-2612.0
10.0	3.050	-2665.0
200.0	6.000	-5615.0
5.0	6.080	-5695.0
5500.0	37.000	-36615.0
46.0	42.000	-41615.0

San Kampaeng Station 4-2

MODEL DATA

PERIOD (SECONDS)	APPARENT RESISTIVITY
.0036	732.98
.0071	802.18
.0143	701.23
.0286	552.03
.0570	431.17
.1143	329.09
.2286	260.60
.4571	200.35
.9143	156.92
2.2605	178.56
2.9257	203.19
3.7926	234.30
4.9230	268.32
6.4000	299.37
8.3934	320.93
11.1304	327.25
14.8406	319.11
20.0787	304.66
27.6755	296.20
39.3840	308.27
60.2373	366.73
102.4003	532.52
204.7921	991.37

X-AXIS FIELD DATA

PERIOD (SECONDS)	APPARENT RESISTIVITY
.0036	696.71
.0071	802.98
.0143	692.11
.0286	626.11
.0570	881.30
.1143	404.12
.2286	229.90
.4571	195.06
.9143	219.23
2.2605	158.47 ± 34.597
2.9257	147.27 ± 33.139
3.7926	277.73 ± 24.622
4.9230	272.78 ± 67.022
6.4000	347.67 ± 66.505
8.3934	271.58 ± 79.868
11.1304	318.64 ± 34.025
14.8406	233.93 ± 23.935
20.0787	364.44 ± 58.538
27.6755	258.09 ± 9.484
39.3840	218.71 ± 16.070
60.2373	474.20 ± 37.047
102.4003	377.60 ± 81.807
204.7921	899.22 ± 60.491

Fig. II.1-38

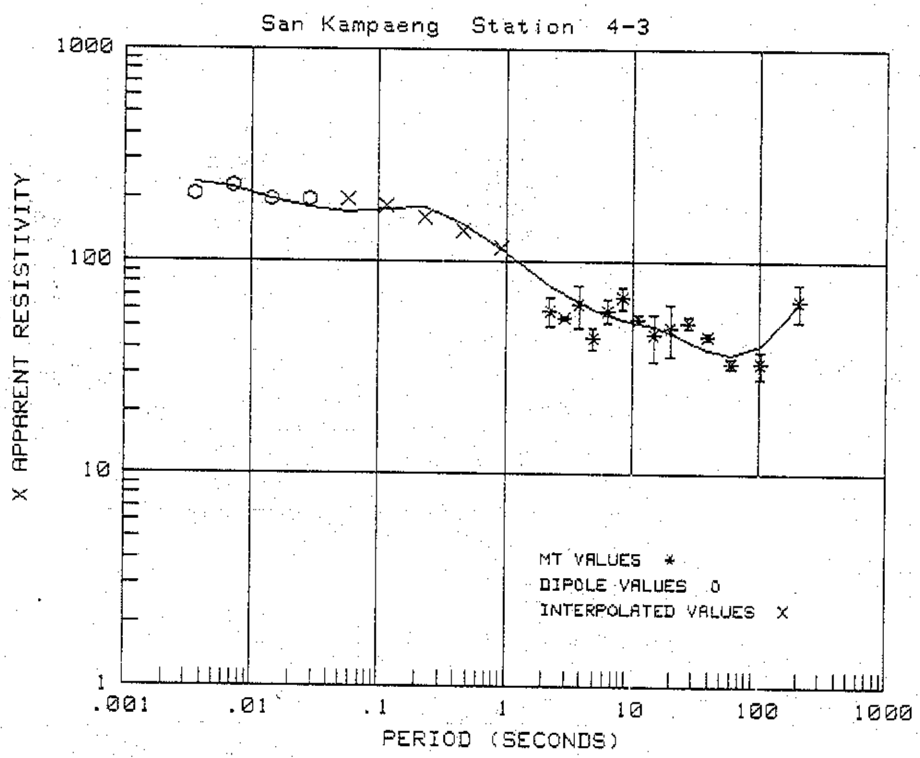

AVERAGE ROTATION ANGLE= -4.0(DEGREES)
TOTAL CONDUCTANCE = 140.2 (MHOS) (FOR TOP 9 LAYERS)

LAYERED MODEL

RESISTIVITY	DEPTH(KM)	ALTITUDE(M)
		382.0 (SURFACE)
140.8	.128	254.0
559.0	.387	-5.0
490.3	.524	-142.0
3.0	.530	-148.0
250.0	.800	-418.0
144.6	3.500	-3118.0
10.0	4.000	-3618.0
100.0	6.000	-5618.0
5.0	6.234	-5852.0
49.0	32.000	-31618.0

San Kampaeng Station 4-3

MODEL DATA

PERIOD (SECONDS)	APPARENT RESISTIVITY
.0036	233.81
.0071	220.27
.0143	197.07
.0286	179.43
.0570	168.74
.1143	175.34
.2286	177.09
.4571	148.58
.9143	113.47
2.2605	78.22
2.9257	71.05
3.7926	65.11
4.9230	60.36
6.4000	56.77
8.3934	54.16
11.1304	52.18
14.8406	50.10
20.0787	47.09
27.6755	43.01
39.3840	38.81
60.2373	36.57
102.4003	41.07
204.7921	64.48

X-AXIS FIELD DATA

PERIOD (SECONDS)	APPARENT RESISTIVITY	
.0036	206.77	
.0071	227.51	
.0143	196.72	
.0286	195.40	
.0570	193.87	
.1143	180.84	
.2286	160.75	
.4571	137.94	
.9143	115.68	
2.2605	59.42	± 8.984
2.9257	55.18	± 1.092
3.7926	63.69	± 14.018
4.9230	44.12	± 5.400
6.4000	59.30	± 7.620
8.3934	68.58	± 7.913
11.1304	54.32	± 2.683
14.8406	45.48	± 11.016
20.0787	49.67	± 13.410
27.6755	52.51	± 3.388
39.3840	44.67	± 1.627
60.2373	33.83	± 2.052
102.4003	33.44	± 4.905
204.7921	65.48	± 12.840

Fig. II.1-39

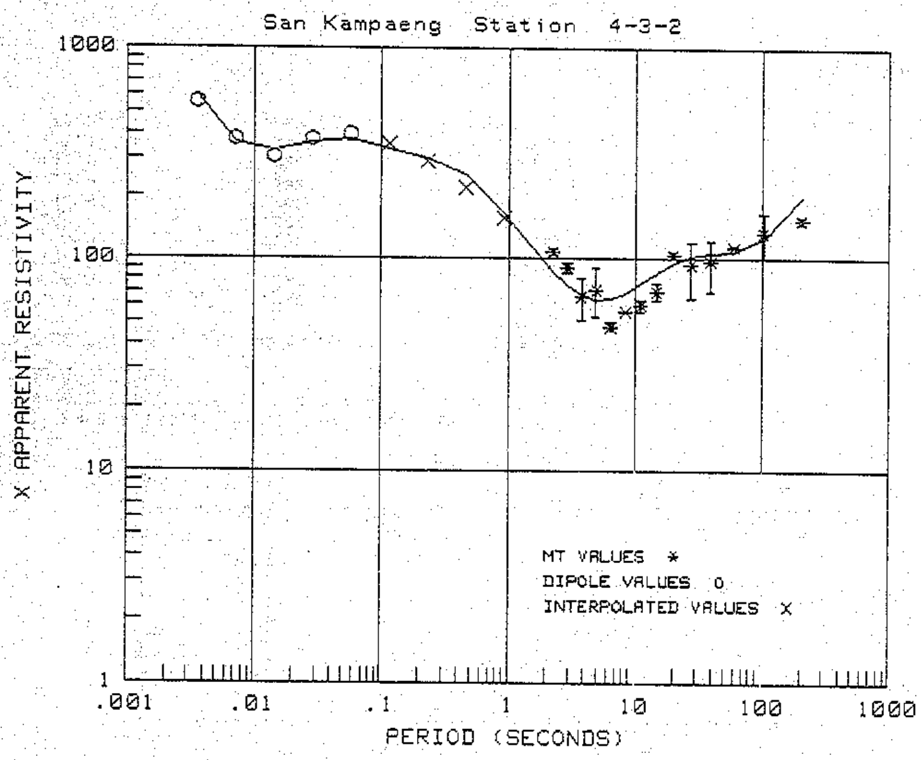

AVERAGE ROTATION ANGLE= -77.0(DEGREES)
TOTAL CONDUCTANCE = 159.1 (MHOS) (FOR TOP 7 LAYERS)

LAYERED MODEL

RESISTIVITY	DEPTH(KM)	ALTITUDE(M)
		381.0 (SURFACE)
599.5	.145	236.0
610.9	.436	-55.0
313.1	.591	-210.0
3.0	.597	-216.0
1500.0	2.000	-1619.0
100.0	5.000	-4619.0
5.0	5.625	-5244.0
5430.0	38.000	-37619.0
47.0	48.000	-47619.0

San Kampaeng Station 4-3-2

MODEL DATA

PERIOD (SECONDS)	APPARENT RESISTIVITY
.0036	599.50
.0071	359.11
.0143	329.13
.0286	361.33
.0570	375.46
.1143	339.07
.2286	303.40
.4571	252.63
.9143	166.89
2.2605	85.89
2.9257	74.17
3.7926	66.88
4.9230	63.71
6.4000	64.33
8.3934	68.55
11.1304	76.01
14.8406	85.40
20.0787	94.79
27.6755	101.56
39.3840	104.70
60.2373	108.14
102.4003	126.55
204.7921	200.33

X-AXIS FIELD DATA

PERIOD (SECONDS)	APPARENT RESISTIVITY	
.0036	560.75	
.0071	373.54	
.0143	310.31	
.0286	373.58	
.0570	393.20	
.1143	355.01	
.2286	289.98	
.4571	219.62	
.9143	157.88	
2.2605	107.74	± 3.107
2.9257	89.60	± 4.745
3.7926	65.70	± 14.500
4.9230	70.95	± 18.326
6.4000	47.79	± 2.271
8.3934	55.81	± .222
11.1304	59.73	± 3.989
14.8406	70.21	± 6.428
20.0787	103.69	± 3.712
27.6755	92.32	± 27.444
39.3840	95.92	± 26.776
60.2373	114.36	± 1.737
102.4003	132.99	± 32.738
204.7921	154.97	± 6.026

Fig. II.1-40

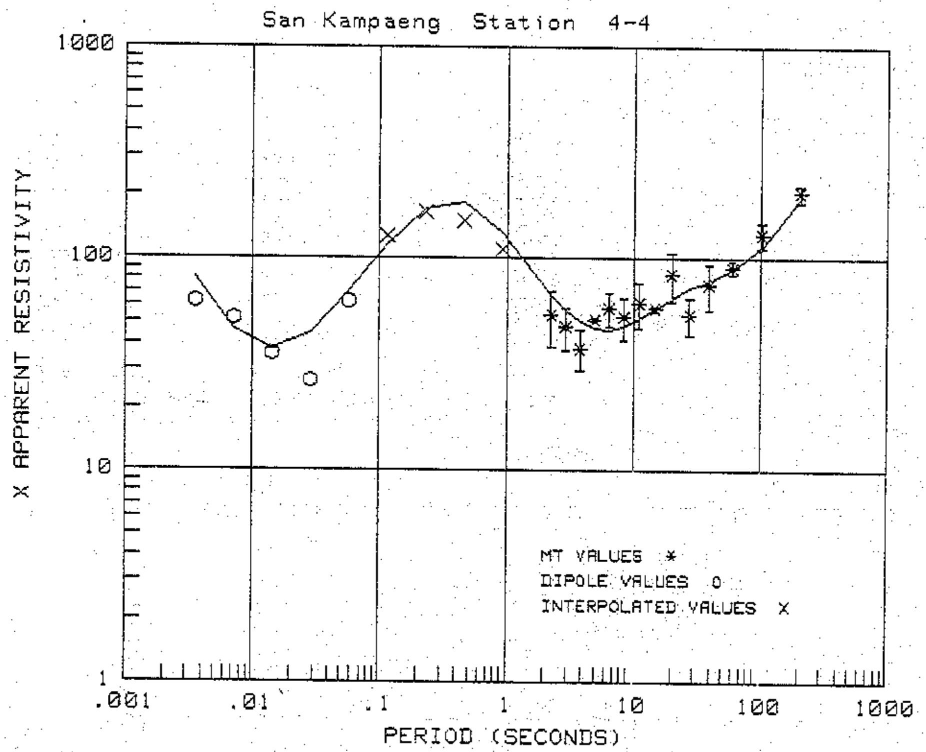

AVERAGE ROTATION ANGLE= -37.0(DEGREES)
TOTAL CONDUCTANCE = 197.5 (MHOS) (FOR TOP 7 LAYERS)

LAYERED MODEL

RESISTIVITY	DEPTH(KM)	ALTITUDE(M)
		410.0 (SURFACE)
80.0	.121	289.0
30.0	.370	40.0
200.0	.501	-91.0
3.0	.502	-92.0
3000.0	3.400	-2990.0
35.0	4.300	-3890.0
5.0	5.100	-4690.0
5620.0	39.000	-38590.0
46.0	47.000	-46590.0

San Kampaeng Station 4-4

MODEL DATA

PERIOD (SECONDS)	APPARENT RESISTIVITY
.0036	80.00
.0071	45.75
.0143	37.80
.0286	44.60
.0570	69.54
.1143	115.44
.2286	169.61
.4571	180.84
.9143	130.37
2.2605	67.15
2.9257	57.05
3.7926	50.27
4.9230	46.57
6.4000	45.71
8.3934	47.53
11.1304	51.88
14.8406	58.11
20.0787	65.26
27.6755	72.02
39.3840	78.20
60.2373	87.67
102.4003	113.43
204.7921	193.82

X-AXIS FIELD DATA

PERIOD (SECONDS)	APPARENT RESISTIVITY	
.0036	62.67	
.0071	51.66	
.0143	35.54	
.0286	26.77	
.0570	62.20	
.1143	125.99	
.2286	162.15	
.4571	148.73	
.9143	108.66	
2.2605	54.29	± 15.748
2.9257	47.41	± 10.470
3.7926	37.72	± 8.164
4.9230	51.17	± .583
6.4000	57.91	± 10.033
8.3934	52.89	± 12.072
11.1304	61.30	± 14.879
14.8406	57.67	± 1.234
20.0787	83.67	± 21.342
27.6755	54.05	± 10.882
39.3840	75.04	± 17.627
60.2373	89.90	± 6.213
102.4003	129.70	± 17.931
204.7921	201.26	± 17.973

Fig. II.1-41

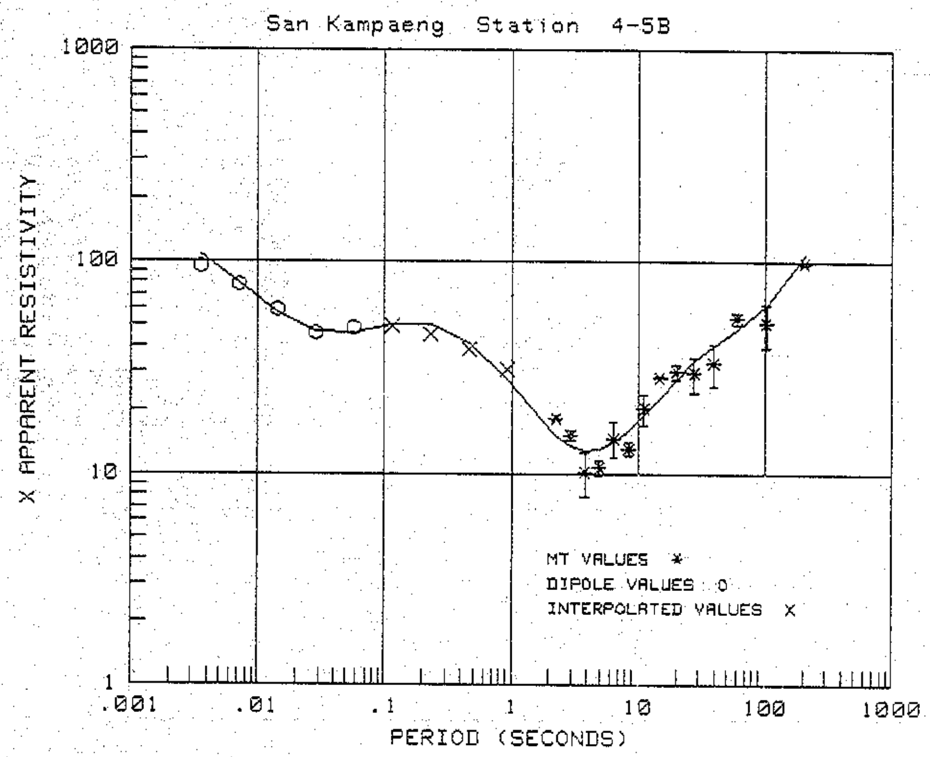

AVERAGE ROTATION ANGLE= -57.0(DEGREES)
TOTAL CONDUCTANCE = 300.0 (MHOS) (FOR TOP 7 LAYERS)

LAYERED MODEL

RESISTIVITY	DEPTH(KM)	ALTITUDE(M)
		408.0 (SURFACE)
107.4	.076	332.0
85.9	.228	180.0
64.4	.312	96.0
3.0	.332	76.0
64.4	1.201	-793.0
25.6	1.601	-1193.0
5.0	2.903	-2495.0
5273.0	37.500	-37092.0
42.0	46.000	-45592.0

MODEL DATA

PERIOD (SECONDS)	APPARENT RESISTIVITY
.0036	107.40
.0071	78.56
.0143	56.86
.0286	46.52
.0570	46.03
.1143	50.47
.2286	50.18
.4571	41.19
.9143	27.48
2.2605	15.17
2.9257	13.63
3.7926	12.93
4.9230	13.05
6.4000	14.01
8.3934	15.89
11.1304	18.82
14.8406	22.78
20.0787	27.75
27.6755	33.40
39.3840	39.50
60.2373	47.27
102.4003	62.72
204.7921	107.04

San Kampaeng Station 4-5B

X-AXIS FIELD DATA

PERIOD (SECONDS)	APPARENT RESISTIVITY
.0036	94.40
.0071	77.90
.0143	58.87
.0286	45.73
.0570	48.00
.1143	49.15
.2286	45.20
.4571	38.33
.9143	30.77
2.2605	18.34 ± .393
2.9257	15.18 ± .902
3.7926	10.19 ± 2.373
4.9230	10.75 ± .861
6.4000	14.70 ± 2.748
8.3934	13.15 ± .851
11.1304	20.24 ± 3.190
14.8406	28.29 ± .115
20.0787	30.06 ± 2.685
27.6755	29.44 ± 5.692
39.3840	33.09 ± 7.264
60.2373	53.76 ± 3.195
102.4003	50.74 ± 12.011
204.7921	98.56 ± 2.288

Fig. II.1-42

plotted on the ρ_a-T curve, (Fig. II.1-10 ~ Fig. II.1-42).

3-2-3 Error bar

Error bar is determined as the product of calculated value of apparent resistivity and multiple coherency determined by the following formula.

$$\text{multiple coherency} = \frac{[E^Q\ E^*]}{[(E^Q\ E^{Q*})(E\ E^*)]}$$

The E is the electric field calculated by the basic formula of analysis of the impedance tensor obtained as shown in 3-2-2. The multiple coherency is the coherency between the measured electric field and the calculated electric field. This value expresses the relation between the electric field and the magnetic field which are measured. In case this value is 1, it can be said that the calculated impedance expresses the relation between electric field and magnetic field completely. On the other hand, in case this value is 0, the calculated impedance expresses nothing about the above relation. In the present survey, if the value of multiple coherency is less than 0.9, such data are not employed.

3-2-4 Total conductance value

The total conductance value, listed next to the average rotation angle, is calculated, after the depth analysis by the inversion program, by the following formula.

$$Ct = \sum_{i=1}^{n} (\Delta Hi/\rho i)$$

Here symbols stand for

- Ct : total conductance (mho)
- ΔHi : thickness of i layer (m)
- ρi : resistivity of i layer (ohm-m)

4. Results of analysis

4-1 Apparent resistivity isocontours

4-1-1 Apparent resistivity isocontours (Period 0.1143 sec) (PL. II.2.1-1)

This plan is expressing the distribution of the apparent resistivity in comparatively shallow part (shallower than 600 m in average) as the frequency is relatively high.

Three low resistivity zones are recognized in this surveyed area; around the respective sounding points of 0-1, 2-2 and 2-7. Fairly high resistivities are revealed in the other parts of the surveyed area. Extension in NW-SE direction is recognized except in the northern part.

4-1-2 Apparent resistivity isocontours (Period 11.1304 sec) (PL. II.2.1-2)

This plan is expressing the distribution of the apparent resistivity along the main direction obtained by the rotation of the coordinate axes by the MT method.

The shape and the distribution of this apparent resistivity isoconters are roughly similar to the distribution of the apparent resistivity (PL. II.2.1-1) drawn from the results of the CSAMT method.

Large conductive zone is recognized around the sounding point 2-2, which is same in the PL. II.2.1-1. In the eastern part (including the sounding points of 3-6, and 4-5), larger conductive zone is recognized. In Fig. II.2.1-1, the sounding point 2-7 is in the center of the conductive layer, but in this plan, the point 2-7 is not found in the center, because the eastern part is correspondent to the larger conductive zone.

4-1-3 Apparent resistivity (Period 39.384 sec) PL. II.2.1-3)

The trend of the apparent resistivity isocontours in this plan reveal quite similar pattern as shown in PL. II.2.1-1. However, the high apparent resistivity zone found in the northeastern part of the surveyed area in PL. II.2.1-2 is not recognized in this plan.

4-2 Results obtained from the one-dimensional model analysis

4-2-1 Basic interpretation of depth and standard classification of resistivity

One-dimensional model analysis was executed at every sounding point, based on the apparent resistivity curve drawn from the actually measured values. This analysis was to compare the apparent resistivity curve of the measured values to that of the theoretical values obtained from assumption of layer model. If the above two curves are not coincident, the comparison was repeated until they get certain coincidence each other, by varying layer model automatically. The underground layer model was determined, after this process, as shown in the results of the data processing. Resistivity of each layer is represented by average of the values of resistivity at each point. In this survey the following table of standard resistivity was applied (Table II.2.1-3).

Table II.2.1-3 Standard classification of resistivity

Average resistivity (ohm-m)	Corresponding layer
876.0	Ra
3.0	Ca
1,098.0	Rb
5.0	Cb
4,551.0	Rc
38.0	Cc
High resistivity	Basement

Here R represents such layers as having high resistivity while C represents conductive layers.

The analysis was completed here on the basis of the assumption of one-dimensional model, as the first step of the geological interpretation. In the paragraph 4-3, another analysis was executed on the basis of the comprehension by two-dimensional model, upon the consideration of geothermal patterns (for example, highly conductive fractures to work as geothermal reservoir).

4-2-2 Total conductance (PL. II.2.1-4)

The values of the total conductance in this plan are those obtained from the sum of the conductance values of the respective layers in the shallower part than the Rc layer, based on the interpretation by the one-dimensional model.

There are two conductive zones in this plan. The one is a small anomaly containing the sounding point 2-2, while the other is an anomaly found in the southeastern part of the surveyed area containing the sounding points 4-5 and 3-6. In the other part of the surveyed area, conductance value is low, generally.

4-2-3 Structure isocontours for the top of conductive formation (shallow and deep) (PL. II.2.1-5,6)

The boundary between the Ra layer and the Ca layer of average 3 ohm-m, and the top of the Cb layer of average 5 ohm-m are expressed in elevation (m) above sea level.

The Ca layer (conductive layer in shallow part) is distributed around the sounding point 2-2, and the thickness is less than 400 meters. In PL. II.2.1-6, a zone of the deepest top is recognized in the northern part of the surveyed area, while in the other parts, the tops are shallower than 0 meter above sea level.

The Cb layer is distributed in deeper part than the Ca layer, and the thickness of the Cb layer is generally more than that of the Cb layer. The plan of the Top of Deep Conductive Formation is expressing similar pattern as seen in the Total Conductance distribution map. Especially, in the areas revealing high conductance value anticlines are recognized in this illustration. Viewing from this fact, it is thought that the increase of thickness of layers has some influence to the conductance anomalies, partly, although the undulation of the top of the conductive layers is responsible for them. This result came from the one-dimensional profile analysis, and is confirmed by the two-dimensional profile analysis.

4-2-4 Isopachs of the overburden overlying highly conductive formation (PL. II.2.1-7)

Variation of thickness of the overburden with high resistivity overlying the conductive layer Cb is expressed here (The thickness of the Cb layer is thought to be negligible compared to the depth of the top of the Cb layer). It is remarkable that there are two small areas (including the sounding points of 2-2, 2-3, 3-6 and 4-5) divided by the isopach of 3,000 meters.

As there are big differences of elevation of the surface in this surveyed area, it is more effective for the preparation of subset map to employ this isopach map rather than the Structure Isocontour map for the top of the conductive formation. By the subset map (PL. II.2.1-9), conductive anomalies expressed in the Total Conductance (PL. II.2.1-4) and shallow anomalies are compared whether they can be compatible. For this purpose, the Isopaches of the overburden overlying highly conductive formation are divided into the following three groups, basically.

D_1 : the group in which the range of the thickness ΔH is less than 1,000 meters.

D_2 : the group in which the range of the thickness ΔH is between 1,000 and 3,000 meters.

D_3 : the group in which the range of the thickness ΔH is over 3,000 meters.

4-2-5 Top of electric basement (PL. II.2.1-8)

Depth of the top of the electric basement, that is, the top of the high resistivity layer Rb or Rc is expressed by the results of the one-dimensional model analysis stated in the paragraph 4-2-1. It is remarkable in this map that there are two areas where anticlines are distributed; the area around the sounding point 2-2 and the area including the points of 3-6 and 4-5, and that there are two areas where synclines are distributed; the area including the points of 2-0, 3-0, 3-1 and 4-0 and the area around 3-4. There are faults between each of the two anticlinal zones and the synclinal zone.

4-3 Subset map and two-dimensional analysis

4-3-1 Classification of total conductance

Based on the Total conductance distribution map (PL. II.2.1-4) mentioned in the paragraph 4-2-2, the total conductance values are divided into the following three groups.

TC_1 : the group in which total conductance values are less than 100 mho
TC_2 : the group in which total conductance values are between 100 and 200 mho
TC_3 : the group in which total conductance values are over 200 mho

These three groups are used as the fundamental conception, together with the groups of D_1, D_2 and D_3 of the thickness of the high resistivity overburden, determined in the paragraph of 4-2-4.

The distribution of the conductance values in such groups as TC_1, TC_2 and TC_3 is shown in Table II.2.1-4.

Table II.2.1-4 Average conductance values

Classification of conductance values	Average conductance value (mho)	Sounding point	
		Number	Composition (%)
TC_1	70	14	42.4
TC_2	135	15	45.4
TC_3	261	4	12.2

4-3-2 Subset map (PL. II.2.1-9)

Combining three groups of the total conductance values with another three groups of the thickness of the high resistivity overburden, the following 9 subsets are determined.

Subset A_1 ; D_1 and TC_1
Subset B_1 ; D_1 and TC_2
Subset C_1 ; D_1 and TC_3
Subset A_2 ; D_2 and TC_1
Subset B_2 ; D_2 and TC_2
Subset C_2 ; D_2 and TC_3
Subset A_3 ; D_3 and TC_1
Subset B_3 ; D_3 and TC_2
Subset C_3 ; D_3 and TC_3

Of them, the subset A_1 is not applicable to this surveyed area. Excluding this subset A_1, basic explanation is given here on the other 8 subsets.

(1) Subset B_1 and C_1

The maximum assumed thickness of the high resistivity overburden of these two subsets of B_1 and C_1 is 1,000 meters, which expresses that they are extremely shallow conductive layers.

It is estimated that the average conductance value of the subset B_1 is 135 mhos and the average thickness of the conductive layers is 675 meters. As this average thickness is comparatively large, it is highly possible that fractures are contained in these shallow conductive layers.

The average conductance value of the subset C_1 is 261 mhos and the average thickness of the conductive layers is approximately 1,305 meters. It is thought that there would be favorable fractures in the layers.

In these subsets B_1 and C_1, there are several points where it is difficult to assume one-dimensional model. Therefore the followings are noted.

In the area where conductive layers are distributed in a shallow part and the topographical variation is rather abrupt, there is a possibility that local high conductance anomalies would appear, reflecting the existence of the conductive layer in a shallow part. Accordingly, it is thought to be highly possible that hydrothermal solution is contained in the subsets of B_1 and C_1, but the calculated average of the thickness is, in some cases, different from the actual value, especially when the subject sounding point is located at the outcrop of the conductive layer and when the topographical variation is quite abrupt around the sounding point.

(2) Subset A_2, B_2 and C_2

These three subsets of A_2, B_2 and C_2 are those where conductive layer is overlaid by the comparatively thick overburden of high resistivity (1,000 ~ 3,000 m). Because local conductive anomalies are not recognized to appear by outcrops of local conductive layers, they are not influenced so much by the undulation of conductive layers as the subsets B_1 and C_1. Accordingly, there is almost no restriction as seen in the subsets B_1 and C_1.

The average conductance of the subset A_2 is 70 mho and the average thickness is about 350 meters. These figures are thought to reveal that there is little possibility for the favorable geothermal reservoir to exist in the subsets of B_2 and C_2.

(3) Subset A_3, B_3 and C_3

The matters mentioned as for the subsets A_2, B_2 and C_2 are applicable to these subsets of A_3, B_3 and C_3, and the subsets B_3 and C_3 are thought to compose favorable areas for development, generally.

The purpose of the subset maps is to help and guide selection and classification of favorable area.

The subsets of C_1, C_2, C_3, B_1, B_2 and B_3 are such areas to be recommended as the favorable area for geothemal reservoir (though subsets C_1 and B_1 have some restrictions as aforementioned).

4-3-3 Two-dimensional model analysis

The profile 1 and 2, which are obtained by the two dimensional analysis, are shown in Fig. II.2.1-10,11. Also, the locations of the profiles are shown on PL. II.2.1-10. On the profiles, are displayed surface, conductive layer, top of high resistivity layer and top of the basement (in most cases, Rc layer). Furthermore, in some cases, several layers are added to them, for their congruence to both of the theoretical and the measured conductance values.

The present two-dimensional model analysis was executed along the two profiles. The profiles and corresponding two-dimensional models are shown on the same figures.

The two-dimensional model analysis was executed for the purpose to determine the depth of the reservoirs where favorable fractures exist and the depth of the conductive layers, in the area where conductive anomalies were recognized on the Total conductance distribution map (PL. II.2.1-4). In order to obtain theoretical values of conductance in the main direction on the assumption of a resistivity distribution, a model program to calculate amplitude in the electromagnetic field which is lead from the two-dimensional structure was employed.

Actual geological structure can be treated as three-dimensional structure. Therefore, in the two-dimensional model analysis, conductance value was taken to be constant along the perpendicular directon to the Y'OZ plane.

The most effective way to apply the two-dimensional model is to select such area where the variation of the conductance values is quite rapid on the Total conductance distribution map. This variation is also coincident with the contrast of the resistivity. In this two-dimensional model analysis, the model was determined so that the theoretical conductance values in the direction of OY' axis could be as close as possible to the conductance value obtained from the measured value, by repeating the model calculations.

It is noted that columnar symmetrical structure is assumed, as a precondition, on the geological structure in the surveyed area. However, real geological structure does not have such ideal condition necessarily in the volcanic area, and it was tried to point out the degree of influence by the variation of the two-dimensional model caused by the distribution of total conductance in the direction of OY' axis.

By the results of these analysis, several interesting conclusion have been obtained concerning the locations of fracture zones which are capable of being geothermal reservoir.

Of the symbols used in the two-dimensional model, such symbols as Ra, Rb, Rc, Ca, Cb, Cc were determined in the paragraph 4-2-1. Two more symbols of F and EB were used there. The symbol F stands for fracture zone, indicating extremely conductive narrow shape. Its resistivity was assumed to be 0.1 ohm-m. The other symbol EB stands for electric basement with extremely high resistivity. Its resistivity was assumed to be 10,000 ohm-m.

Under the restriction concerning the two-dimensional model analysis, the fracture zone (F) was traced to be vertical or horizontal.

(1) Profile 1 (Fig. II.2.1-10)

The theoretical conductance curve which is well correspondent to the measured conductance values is shown at the top of the Fig. II.2.1-10. It is obvious that the fractures exist below the sounding point 4-5, which is located in the narrow subset between the subset C_3 and the subset C_1.

To compare this result with the Electric Basement (PL. II.2.1-8), highly conductive fractures are distributed along the side of the anticline axis found in the southeastern margin of the surveyed area.

As this model and the following model are concerning the layers shallower than the Rc layer, the Cc layer which is seated in extremely deep part and which would be a heavy charge to the model program, was not taken into consideration.

However, as afore-mentioned, it was necessary to assume several characteristic layers which were not listed in the table of the standard classification of resistivity (Table II.2.1-3).

That is, a conductive layer Cb-c was assumed to be at the depth of 6,000 meters. The thickness of this layer is 500 meters and its resistivity is 25 ohm-m. Also, it was necessary to assume the high resistivity overburden of Ra-a layer in addition to the Ra layer. The resistivity of This Ra-a layer is from 60 to 150 ohm-meter.

(2) Profile 2. (Fig. II.2.1-11)

It can be said that the basic geological structure is almost same as the shown on the profile 1. Fractures exist below the point 2-2. The calculated values and the measured values of conductance are well coincident, and fractures are recognized at the depth of 1,000 meters. In addition to the characteristic layers which were mentioned in the paragraph stating about profile 1, two more layers were necessary; the Cb-b layer of the resistivity of 16 ohm-m to 20 ohm-m, and the Ra-b layer of the resistivity of 30 ohm-m to 50 ohm-m. Apparently, it is out of the conception of the table of the standard classification of resistivity (Table II.2.1-3) to establish such assumed layers as Ra-a, Ra-b, Cb-b and Cb-c, but the reason is that the table of standard classification of resistivity had been prepared on the basis of the values at 33 sounding points, registering high resistivity generally, except for the points 2-2, 3-6 and 4-5.

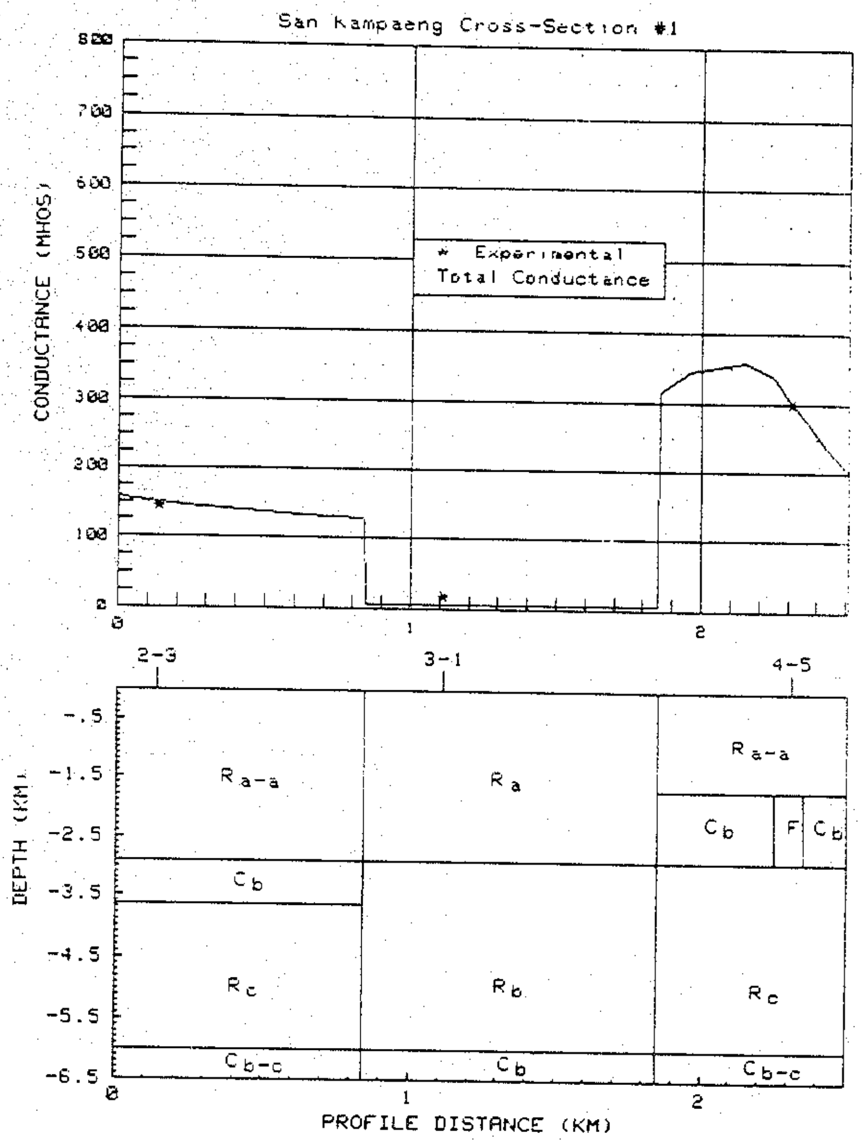

Fig. II.2.1-10 Two-dimensional model analysis (Section 1)

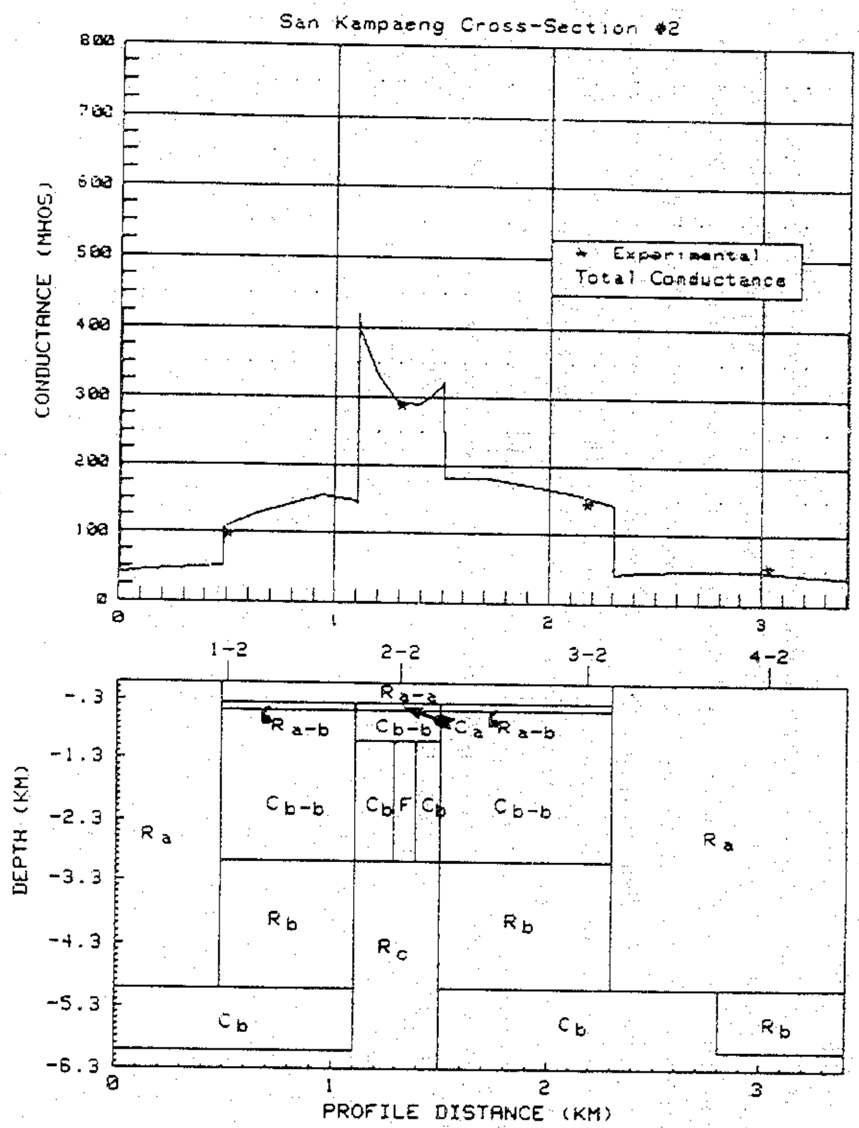

Fig. II.2.1-11 Two-dimensional model analysis (Section 2)

5. Summary

5-1 Method of the survey

The deep electric survey was carried out for the purpose to obtain informations on the geothermal reservoirs through the vertical and horizontal distribution of the resistivities in the surveyed area by measuring ratios of the electric field to the magnetic field.

Total 33 sounding points were established on the grid of the spacing of 800 meters.

The survey was composed of magnetotelluric method (MT) and vertical electromagnetic sounding method (CSAMT). The former is to measure components of natural electric field and magnetic field with the frequency domain of 1 Hz ~ 0.01 Hz (period 1 sec ~ 100 sec), while the latter is to measure such electric field and magnetic field as induced by artificial magnetic field with the frequency domain of 280 Hz ~ 1 Hz.

The basic formula to calculate apparent resistivities from the measured values of the electric field and magnetic field is common to these two methods of the survey.

$$\rho a = 0.2\,T\,[E/H]^2$$

Here ρa : apparent resistivity (ohm-m)

T : period (sec)

E : electric field (mV/km)

H : magnetic field (γ)

The results of the data treatment obtained through the MT method and the CSAMT method are summarized in the apprent resistivity curves, which express the relation of the period to the apparent resistivities. Various analysis were executed by the apparent resistivity curves.

5-2 Analysis results

5-2-1 Apparent resistivity isocontours (PL. II.2.1-1,2,3)

These plans are expressing the distribution of the apparent resistivities against the frequency or periods of 8 Hz (11 sec) and 75 Hz (39 sec) on the apparent resistivity curves. By the characteristics of the electromagnetic waves, the longer the period is (39 sec in this analysis), the deeper part the underground structure is reflected to. On the contrary, the higher the frequency is (8,75 Hz in this analysis), the shallower resistivity structure is revealed.

It is obvious from these maps that the values of the resistivity in this surveyed area are fairly high. The low resistivity areas common to the maps of PL. II.2.1-1,2,3 are the area around the sounding point 2-2, where the present geothermal indications are distributed and the area including the sounding points of 2-7, 3-6 and 4-5 in the southeastern part of the surveyed area. This anomaly found in the southeastern part is thought to occupy pretty big area, but as the location is along the margin of the surveyed area, the extension is uncertain.

5-2-2 Total conductance (PL. II.2.1-4)

The values of the total conductance in the plan are those obtained from the sum, according to the following formula, of the conductance values of the respective layers in the shallower part than the electric basement (Rb layer, Rc layer) which is obtained from the results of the one-dimensional model analysis on the resistivity curves.

$$TC = \sum_{i=1}^{n} \frac{hi}{\rho i}$$

Here TC : total conductance (mho)

hi : thickness of i layer (m)

ρi : resistivity of i layer (ohm-m)

By the distribution of the total conductance values, anomalies of the layeres in the shallower part than the electric basement are clarified.

As seen in the apparent resistivity Isocontours maps, two conductive anomalies are recognized in this plan. However, it is remarkable that the values of the total conductance are low as a whole, and that it has a little contrast. These facts are thought to reveal that the high resistivity layers are predominantly distributed in the surveyed area.

5-2-3 Structure isocontours for the top of conductive formation (shallow and deep) (PL. II.2.1-5,6)

These plans express the forms of the top of the conductive layers found by the results of the one-dimensional model analysis. As there are conductive layers in the shallow part as well as in the deep part in this surveyed area, two structure isocontour maps for the top of the conductive formations were prepared in each of these parts.

In the structure isocontour map for the top of the shallow conductive layers, the shallowest part is recognized around the sounding point 2-2, where the depth is 0 to 400 meters above sea level. The most of the other parts are included in the area delineated by the isocontour of 0 meter above sea level, and no remarkable undulation is recognized.

The pattern shown in the structure isocontour map for the top of the conductive layer is similar to that displayed in the Total conductance distribution map. The areas where high conductance values are exhibited are correspondent to anticline structure in this map. This undulation is as steep as −3,000 meters to −9,000 meters. Therefore, the assumption of the horizontal multi-layered structure, the precondition of the one-dimensional model analysis, can not be applicable. The profile analysis was executed by the program with the assumption of two dimensional model.

5-2-4 Isopachs of the overburden overlying conductive formation (PL. II.2.1-7)

Variation of the thickness of the overburden overlying the conductive layers is expressed in this map. For the preparation of the subset maps, values of the thickness are divided into the following three groups.

D_1 : the group in which the range of the thickness ΔH is less than 1,000 meters

D_2 : the group in which the range of the thickness ΔH is between 1,000 and 3,000 meters

D_3 : the group in which the range of the thickness ΔH is over 3,000 meters

5-2-5 Electric basement (PL. II.2.1-8)

Depth of the top of the Rb layer or Rc layer, which was taken as the basement in the calculation of the total conductance values, is expressed in this plan, in meters above sea level.

This plan reveals similar pattern to the structure isocontour map for the top of deep conductive formation (PL. II.2.1-6). This fact is revealing that the undulation of the deep conductive layer is correspondent to that of the basement.

However, in the central part of the anticlinal zone or of the synclinal zone, the depth is different, which is suggesting the difference of the thickness of the conductive layers. Also, viewing from the fact that there is fair amount of difference of the level between the anticlinal zone and the synclinal zone, existence of a fault is estimated there.

5-2-6 Subset maps (PL. II.2.1-9)

Total conductance values are divided into the following three groups, for the preparation of this map.

TC_1 : the group in which total conductance values are less than 100 mhos.
TC_2 : the group in which total conductance values are between 100 and 200 mhos.
TC_3 : the group in which total conductance values are over 200 mhos.

Combining three groups of the total conductance values with another three groups of the thickness of the overburden down to the deep conductive formation, the following 9 subsets are determined.

Subset A_1 ; D_1 and TC_1
Subset B_1 ; D_1 and TC_2
Subset C_1 ; D_1 and TC_3
Subset A_2 ; D_2 and TC_1
Subset B_2 ; D_2 and TC_2
Subset C_2 ; D_2 and TC_3
Subset A_3 ; D_3 and TC_1
Subset B_3 ; D_3 and TC_2
Subset C_3 ; D_3 and TC_3

Of the above subset dividion, it is hardly thought that favorable geothermal reservoirs would exist in the subsets A_1, A_2 and A_3, as their total conductance values are low. Also, as the depths of the subsets B_3 and C_3 are fairly deep, it is difficult to take them as the objects for geothermal development, even if there would be some geothermal reservoirs.

5-2-7 Two dimensional model analysis

This analysis was executed for the purpose to determine the depth of the layers containing favorable fractures and the conductive layers in the areas where conductive anomalies were recognized on the Total conductance map.

The two-dimensional analysis was actually performed with two survey lines (PL. II.2.1-10). The results are shown in Fig. II.2.1-10,11. Fracture zones were recognized in two localities; around the sounding point of 4-5 and that of 2-2.